In Situ Leaf Growth Measurements Using Digital Image Analysis

A thesis submitted to Auckland University of Technology
In fulfilment of the requirements of the degree of
Doctor of Philosophy (PhD)
in Environmental Science, by

Jonas Hilty

Institute for Applied Ecology New Zealand
School of Science
Faculty of Health and Environmental Sciences
Auckland University of Technology
New Zealand
2019

Abstract

Plant growth is a broad topic that is of interest in many different research fields from the basics of plant functioning, to agricultural research, and ecology. In this thesis, I first distinguish different aspects of plant growth, and discuss how they are coupled across spatiotemporal scales. I then focus on short term eudicot leaf growth measurements, as this is a topic that is relatively sparsely explored in the literature, despite its importance for plant resource use efficiency and performance. There are methodological challenges to measure leaf expansion, particularly in situ because of adverse environmental conditions. I adopted an existing leaf growth measurement method based on leaf fixation and marker tracking for long term outdoor measurements, and I explored the viability of a custom made stereo vision system for the same task. Using marker tracking, I observed a consistent diel growth pattern with considerable leaf area shrinkage in the morning, re-expansion in the afternoon, and growth at night in the mangrove *Avicennia marina*. Using stereo vision, I achieved a high correlation of leaf area measurements with a ground truth from scanned leaves, but the accuracy was comparatively low. The marker tracking worked well in the most adverse environment and is a suitable low cost method for in situ leaf growth measurements.

Keywords: auxanometer, diel growth cycle, instantaneous leaf growth measurement, image analysis, leaf expansion, leaf shrinkage, plant growth definitions, stereo vision

Table of Contents

List of Figures

iv

List of Tables

Attestation of Authorship

I hereby declare that this submission is my own work and that, to the best of my knowledge and belief, it contains no material previously published or written by another person (except where explicitly defined in the acknowledgements), nor material which to a substantial extent has been submitted for the award of any other degree or diploma of a university or other institution of higher learning.

<div align="right">

Jonas Hilty
Auckland
30 April 2019

</div>

Co-Authorship Declaration

Plant growth: the What, the How, and the Why. Invited Tansley Review for *New Phytologist*

Author	Contribution	Share [%]	Signature
Jonas Hilty	Concept, writing, figures	80	
Sebastian Leuzinger	Concept, writing	10	
Bertrand Muller	Writing, review	5	
Florent Pantin	Writing, review	5	

Co-Authorship Declaration

Author	Contribution	Share [%]	Signature
Jonas Hilty	Study design, instrument design, field experiment, image analysis software, data analysis, writing	90	
Sebastian Leuzinger	Study design, field experiment, writing	5	
Chris Pook	Instrument design, review	5	

Acknowledgements

List of Symbols

Basic quantities

Symbol	Unit	Unit Name	Description
t			time point; calendar date
t	s	second	time duration
	min	minute	
	h	hour	
	d	day	
T	°C	degree Celsius	temperature
A	mm^2		area
V	mm^3		volume
λ	nm		wavelength
E	W m^{-2}		irradiance; radiant flux per area
N	kg m s^{-2}	Newton	force

Chemical elements

Symbol	Description
C	carbon
N	nitrogen
P	phosphorus

Environmental quantities

Symbol	Unit	Description
H_{rel}		relative humidity in percent
P_{sat}	kPa	saturation pressure of water
P_{vpd}	kPa	vapour-pressure deficit
D	m	water depth

Hydraulics

Symbol	Unit	Description
P	MPa	turgor pressure
ε	MPa	elastic modulus
θ	MPa^{-1}	cell wall extensibility
d_{lwd}		relative leaf water deficit
c_{tgr}		normalised turgor change

Model parameters

Symbol	Unit	Description
Y		System variable
g	model dependent	growth rate
g_{agr}	mm^2 h^{-1}	absolute growth rate
$g_{\text{rgr}_{\text{exp}}}$	h^{-1}	relative growth rate, exponential
$g_{\text{rgr}_{\text{lin}}}$	h^{-1}	relative growth rate, linear
c_{rac}		relative area change
t_T	°C d; °C h	thermal time

Statistics

Symbol	Description
μ	mean
σ	standard deviation
σ^2	variance
R^2	coefficient of determination
p	probability value of statistical test
n	sample size
F	F-value
t	t-value
ε	error term

Stereo vision; geometry

Symbol	Unit	Description
f	mm	focal length
b	mm	baseline distance
d	pixel	disparity; pixel distance
s	mm (pixel)$^{-1}$	sensor pixel size
(X, Y, Z)	mm	real world pixel coordinates
v		vertex; point in space

Image operations

Symbol	Unit	Description
I		image
R		image component, region
W		filter kernel
$E(R)$		Ellipse fitting to image region R
$\mathcal{A}(R)$	pixel	Pixel area of image region R
r	pixel in^{-1}	image resolution; dots per inch

Chapter 1

Introduction

"Photographic registration will probably be largely employed in the future, for series of pictures may be obtained which when placed in a kinematograph show the phases of several days' or weeks' growth in a minute or so" (Pfeffer, 1903, p. 23).

"The current availability and comparatively low cost of integrative computer graphics equipment should greatly ease the formerly laborious job of analyzing plant growth patterns from the time lapse photographs of marked plants" (Silk & Erickson, 1979, p. 500).

The idea to use photographs to quantify plant growth is not new by any means. In the last two decades this research field has seen rapid progress driven by the development in computer hardware, image sensors, and computer vision algorithms. Nevertheless, many aspects of plant growth remain under-explored, among them is the quantification of short-term leaf growth, particularly under natural conditions.

1.1. Motivation

Measuring leaf growth is crucial for understanding the influence of environmental and ontogenetic drivers on plant resource efficiency and performance (Walter, Silk & Schurr, 2009). The development of plant organs requires the availability of carbohydrates for building material and as an energy source, as well as favourable hydraulic conditions to drive expansion (Pantin, Simonneau & Muller, 2012). Other important environmental factors that can drive or limit plant growth are temperature, and nutrient availability (Körner, 2015). This multitude of environmental influences on plant

growth leads to a high phenotypic plasticity in many plants, which makes it hard to disentangle genetic and environmental effects on growth (Tardieu, Cabrera-Bosquet, Pridmore & Bennett, 2017). Today, the analysis of the genome is a standard process, while the quantification of the phenotype and of plant of growth is far more challenging (Walter, Liebisch & Hund, 2015). Furthermore, the manifestation of growth processes also depends on the timescale of the measurement. Because of such challenges it is necessary to clearly distinguish different growth processes, and to select a method that best describes the investigated process. This is the focus of Chapter 2. In this section I give a more general overview of leaf growth drivers, and of shoot growth measurement methods.

Ontogenetic and environmental influence on leaf growth

The spatial expansion pattern of monocotyledon and eudicotyledon leaves is distinctly different. Monocot leaves have a one-dimensional expansion pattern with a growth zone consisting of a basal meristem followed by an expansion zone, while in eudicots cell proliferation and expansion occur in the whole lamina (Granier & Tardieu, 2009). In monocots, the number of meristem cells is the main determinant of leaf growth (Gazquez & Beemster, 2017). In eudicot leaves no similar analysis is possible, because growth is not evenly distributed in different leaf zones, and exit from proliferation usually (but not always) occurs in a tip-base gradient (Granier & Tardieu, 2009). Factors that theoretically could influence eudicot leaf size include the number of cells in the primordium, the duration and rate of cell proliferation, the duration and rate of cell expansion (including endoreduplication), and the extent of meristemoid division (Gonzalez, Vanhaeren & Inzé, 2012; see Section 2.2 for more details) . In the next section I present evidence from the well studied species maize (*Zea mays*) and sunflower (*Helianthus annuus*) as case studies how ontogenetic and environmental factors impact long-term leaf growth (at timescales of one day or longer).

Long-term leaf growth

Final leaf area is dependent on plant ontogeny. It is a function of leaf position and follows a bell shaped curve in maize (Chenu, Rey, Dauzat, Guilioni & Lecoeur, 2008) and sunflower (Dosio et al., 2003). Both species show an S-shaped development of leaf length or area for individual leaves (Muller, Reymond & Tardieu, 2001; Dosio et al., 2003). For a given leaf position the growth duration is constant when expressed in thermal time, and when growth is not limited by other factors (Muller et al., 2001; Dosio et al., 2003). Thermal time is the temperature integral above a species dependant threshold with regards to time (see Chapter 2, Table 3).

The exact shapes of the leaf development curves demonstrate the difference between monocot and eudicot growth forms. In maize, early leaf elongation is almost exponential, although a detailed analysis shows that relative growth rates slightly decrease at first, before they increase to a maximum. This is followed by a short period of truly linear growth when the division and elongation zone are at their maximum size, before growth ceases (Muller et al., 2001). In sunflower, there is no linear leaf growth phase. Instead, there are two exponential growth phases, followed by an exponential decrease of the relative growth rate (Dosio et al., 2003). The first exponential phase is in the very early stage of leaf development when the leaf area is below 1 mm^2. The second exponential phase is first driven by an exponential increase in the number of cells, and a small increase in cell size (Tardieu, Granier & Muller, 1999). Then, the cell division rate decreases, while the leaf area continues to grow at the same rate for a short period, driven by a steep increase in cell expansion.

A decrease in soil water content leads to a decreased leaf length, respectively area, in both maize and sunflower. In maize the shorter leaf length results from a reduced number of cells, which is caused by a reduction in both cell division rate, and meristem size, while the final cell length remains

unchanged (Sprangers, Avramova & Beemster, 2016). In sunflower, the timing of the water deficit determines the mechanism of leaf area reduction. An early deficit leads to a reduction of cell number but not cell size, while a late water deficit does not affect cell number, but reduces cell size (Granier & Tardieu, 1999a). Because of the base-tip gradient in leaf development, one water deficit period can have different effects in different parts of the same leaf. The duration of the leaf development expressed in thermal time is unaffected by water deficits, but cell division or expansion rates are reduced (Granier & Tardieu, 1999a).

In maize, a short period of intense shading during the exponential growth phase reduced the final leaf length. The shading caused an immediate decrease in leaf elongation rates, which was partly compensated by a longer development time (Muller et al., 2001). Similarly, in sunflower a shading treatment starting during the exponential growth phase reduced the final leaf area by reducing cell division rates and final cell number. When the shading started during later leaf development, the final leaf area was unaffected (Granier & Tardieu, 1999a). The growth duration in thermal time was increased when the shading started at the leaf initiation, but it remained unaffected when the treatment started later during leaf development. The reduction of the whole plant available photosynthetic radiation by either shading, or by partly covering leaves resulted in similar leaf development patterns, suggesting an involvement of carbon metabolism in the decrease of leaf growth rates. The final cell area was not affected by shading, except for the most intense treatment, which lead to an increase in cell area, while the final cell number remained low.

A reduction in available nitrogen lead to a reduced leaf length in maize for leaf position seven or higher (Vos, Putten & Birch, 2005). In sunflower, nitrogen limitation lead to a uniform decrease in leaf area independent of leaf position (Trápani & Hall, 1996). Inter-plant competition lead to a decrease in leaf area above a certain leaf position in maize (Maddonni, Otegui

& Cirilo, 2001) and sunflower (Dosio et al., 2003).

From the above examples the following general picture emerges. First, the duration of leaf development is constant when expressed in thermal time, but shading treatments can increase the duration of leaf development. Second, soil water deficits lead to a decrease in cell division or expansion rates. In maize the mature cell size is not affected by water deficits, while in sunflower cell size can be reduced. Third, shading can reduce the final leaf area by reducing cell division rates. Fourth, nutrient limitation leads to whole plant leaf area reduction. Similar patterns have also been reported for *Arabidopsis thaliana* in terms of thermal time (Granier et al., 2002), water stress (Skirycz et al., 2010), and shading (Cookson, Van Lijsebettens & Granier, 2005).

A feature that cannot be measured by observing leaf area growth is the specific leaf area (SLA, m^2 kg^{-1}) expressed as leaf area per unit dry weight of leaf tissue. To approximate SLA development, it would be necessary to obtain information about leaf thickness and density in addition to the area. In general, SLA strongly depends on light intensity and temperature, with low light leading to higher SLAs, and low temperature leading to lower SLAs (thicker leaves; Poorter, Niinemets, Poorter, Wright & Villar, 2009).

Short-term leaf growth

The knowledge of the influence of environmental factors on short-term leaf growth at sub-daily timescales is limited. The best studied species are among cereal crops where it was generally found that monocot leaf growth is driven by soil and air temperature (Walter et al., 2009). Eudicot leaf growth, on the other hand, is subject to strong endogenous controls. For example, in *Arabidopsis thaliana* and *Ricinus communis* a distinct diel growth patterns exist even when plants are grown in continuous light, suggesting that the timing of growth is influenced by the circadian clock (Poire et al., 2010). Additionally, there was no influence of short-term temperature fluc-

tuations on leaf growth in several eudicot species when the daily mean temperature was kept the same (Poire et al., 2010).

It has been suggested that there are two types of short-term eudicot leaf growth patterns (Walter et al., 2009; Ruts, Matsubara, Wiese-Klinkenberg & Walter, 2012): type 1 plants that show the highest leaf growth rates at dawn just after the onset of light, and type 2 plants that show the highest growth rates at dusk. For example, in *Arabidopsis thaliana* leaf growth is peaking shortly after the transition from night to day (Wiese, Christ, Virnich, Schurr & Walter, 2007; Dornbusch, Michaud, Xenarios & Fankhauser, 2014). Furthermore, this peak persists if the night length is manipulated (Dornbusch et al., 2014). Therefore, *A. thaliana* would be classified as type 1 plant (Walter et al., 2009).

Leaf growth measurements on *Arabidopsis thaliana* showed an interesting shift in leaf expansion rates during its development (Pantin, Simonneau, Rolland, Dauzat & Muller, 2011). In the first few days after emergence the growth rate was higher during the day while in older leaves the growth rate was higher at night. This might reflect a switch from metabolic limitations restricting growth at night in young leaves to hydraulic limitations restricting growth at day in older leaves. In mutants without starch production or with impaired starch degradation the nocturnal growth reduction was much stronger than in the wild type. Therefore, the lack of starch at night seems to impair leaf growth in young leaves. This is in line with the general observation that in *A. thaliana* starch pools are depleted almost linearly during night time to optimise growth (Stitt & Zeeman, 2012).

Hydraulic growth limitation occurred in older *A. thaliana* leaves, and relative growth rates at day were lower than at night. Evidence suggested that growth was reduced during the day because water was lost by transpiration which limited the potential for cell expansion. This hypothesis was supported by the observation that under water stress *A. thaliana* showed higher growth rates at night even in young leaves, and the amplitude between di-

urnal and nocturnal growth was increased. A similar pattern was also observed in a mutant with higher stomatal conductance but similar net photosynthesis compared to the wild type. In Section 2.2 I give a detailed explanation on how hydraulics can limit tissue expansion.

Overview of shoot and leaf growth measurement methods

Plant growth can be defined as an increase in biomass (structural growth), or plant size (expansive growth; Pantin et al., 2012; Chapter 2) . Dry biomass can only be measured post harvesting, which has the disadvantage that the same individual can only be measured once, and therefore growth patterns can only be derived from mean values of different individuals, as opposed to observing the same plant over time. Furthermore, harvesting is highly labour intensive. Therefore, automated non-invasive methods for measuring plant growth are desirable.

The simplest non-automated method for recording expansive growth is repeated measurements with a ruler, which is also labour intensive and not very precise. Historically, precision was improved by observing the plant through a "horizontal microscope" as described by Pfeffer (1903, p. 20). An early example of an automated growth meter (auxanometer) is the recording of shoot elongation on a rotating cylinder (Pfeffer, 1903). Other classical instruments to measure elongation are the interferometer based on two interfering light rays of which one is displaced by a mirror connected to the plant (reviewed by Ruge, Whaley & Ziegler, 1961), or the linear variable differential transformer (LVDT; Hsiao, Acevedo & Henderson, 1970).

Auxanometer and LVDT both require the application of force by fixing the plant through a cord to a weight to record changes in position. Obvious shortcomings of this setting are that applied tensile forces may influence the growth and that it is not suitable to attach a weight to small plant organs (Pfeffer, 1881). Furthermore, there may be thermal expansion of the cord, although this is described as "insignificant" in comparison to the total

growth (Hsiao et al., 1970, p. 591). The method of applying a force to the leaf tip to measure its elongation is still applied for measuring leaf elongation in the field (Nagelmüller, Kirchgessner, Yates, Hiltpold & Walter, 2016). Based on this principle, leaf elongation was measured by visually tracking beads connected to the leaf.

Leaf area was traditionally measured by tracing the shape directly to paper or by using light and diazo paper (H. T. Brown & Escombe, 1905). Later photoelectric devices were developed to measure the area of harvested leaves (reviewed by Ruge et al., 1961). This technology resembles the use of scanners which today is a very simple method for measuring leaf area (e.g. O'Neal, Landis & Isaacs, 2002). A notable historic study that used manual ruler measurements was conducted by Gregory (1921) who applied ellipse or hexagon models to calculate leaf area. Additionally, for some monocotyledon species there exist well-established statistical correlations to calculate the leaf area from length and maximal width (reviewed by Ruge et al., 1961).

Another method to describe and measure plant growth is the analysis of photographs, an idea already implemented by Pfeffer (1900) who set up a device to acquire time lapse series of growing plants and algae. Pfeffer's aim was to demonstrate plant movements during his lectures but later the method was also used to measure growth by manually analysing images (reviewed by Ruge et al., 1961). While this method used to be expensive and labour intensive, today it is possible to automatically and non-invasively measure plant growth using relatively cheap devices. An extensive review of early computer vision applications in plant science was given by Price and Osborne (1990). Plant growth can be estimated from digital images and statistical correlations (Eguchi & Matsui, 1977), a method still widely applied today. To my knowledge the first study directly and automatically measuring plant growth using image analysis was presented by Jaffe, Wakefield, Telewski, Gulley and Biro (1985) recording the elongation of maize seedlings.

Classic plant or leaf growth measurement methods like the auxanometer or LVDT only collect information about elongation and are not able to measure leaf area increase or to detect where within the organ the growth takes place. In monocots, leaf growth takes place at the base of the leaf and is largely one-dimensional, therefore this is not much of a limitation. In eudicots, it has long been observed that leaf growth is often not uniformly distributed and that "various parts of the lamina expand at different rates, depending upon their distance from the tip and age of the leaf" (Maksymowych, 1973, p. 41). By using digital image analysis and optical flow estimations (Barron & Liptay, 1994, 1997) it becomes possible to distinguish growth in different areas of a leaf at a high temporal resolution (Schmundt, Stitt, Jahne & Schurr, 1998). Optical flow tracks the same point in a series of pictures over time. Some species lack distinctive features at the leaf surface, and ink dots have often been applied to simplify the tracking (e.g. Das Gupta & Nath, 2015; Granier & Tardieu, 1998b; Remmler & Rolland-Lagan, 2012). This approach is similar to a classical study using small holes and red lead as markers (Hales, 1727).

Despite the potential of image analysis in plant quantification, there still remain many challenges of which one is the measurement of leaf growth (Minervini, Scharr & Tsaftaris, 2015). Complicated leaf shapes or wavy surfaces can make computer-vision-based growth measurements difficult. Today, the most widely used semi-automated method to measure eudicot leaf growth requires the fixation of a leaf to keep it in a plane (Schmundt et al., 1998). Since the fixation prevents movements, it becomes possible to estimate relative leaf growth by tracking the perceived leaf area in time-lapse pictures from a camera that is set up parallel to the leaf surface. This task can be simplified by automatically tracking markers at the leaf fixation point (expansive growth; Mielewczik, Friedli, Kirchgessner & Walter, 2013; Chapter 3) . However, just like it is the case for the one-dimensional auxanometer or LVDT, the fixation may influence growth since it applies

tension to the leaf and prevents it from moving. Schmundt et al. (1998) compared their image-based growth analysis to simultaneous measurements with an LVDT and found that the measured growth was similar but that the image analysis was less noisy.

Since the application of tensile forces potentially impacts leaf growth, the choice of the weight needs to be determined carefully. Surprisingly, this issue is only briefly discussed in the literature. In their pioneering study Jaffe et al. (1985) applied different forces to corn seedlings and observed their growth pattern compared to an undisturbed control. Low forces slightly increased growth between ca. 0.5 and 3.5 hours after application, while higher forces slightly decreased growth. Later, the difference in growth rates was reduced but did not completely disappear. While the growth rate was similar with no applied force and $1.14\,N$, the growth was higher at forces of $0.38\,N$ or $0.76\,N$ (no difference between the two latter treatments).

In contrast, *Ricinus communis* leaves showed decreased growth rates for low forces and increased growth rates for high forces compared to an unconstrained control (Walter, Feil & Schurr, 2002). In old leaves experiencing mechanical stress the starch concentration at day was significantly higher than in the control which indicates a disturbance of the carbohydrate metabolism. In their experiments on maize leaves Hsiao et al. (1970) simply compared the growth rate with the applied force of $0.04\,N$ to the one with twice the force and found no difference. Further, they observed that the leaf was shrinking after cutting off the roots despite the applied tension indicating that the force by itself did not cause growth. In *Laurus nobilis*, leaves lateral mechanical stress shifted the direction of growth in the treated area (Bar-Sinai et al., 2016). These examples show that mechanical stress can influence leaf growth and that there is no linear relationship between the applied force and changes in growth rate. Therefore, no general conclusion on the best force to be used in such experiments can be drawn. Instead, for any species the appropriate force needs to be determined before the experiment.

Leaf fixation restricts movements that are present in many species. In *Ricinus communis* low tensile forces lead to a lower growth rate during night-time compared to the control (Walter et al., 2002). Under undisturbed condition *Ricinus communis* leaves show strong movements during the night. Therefore, it was speculated that the restriction of leaf movements reduces the leaf growth rate at times when strong movements would occur (Walter et al., 2002). The application of stronger forces lead to a re-establishment of similar growth rates in fixed and undisturbed leaves. In a study using a laser scanner to determine leaf length and inclination angle of *Arabidopsis thaliana*, it was found that leaf elongation and movements are coupled (Dornbusch et al., 2014). Such examples suggest that the application of mechanical force to measure leaf growth is rather questionable for species that show strong leaf movements.

Image analysis and phenotyping

As shown by the quotes in the Chapter abstract, the use of image analysis and computer vision for plant growth measurements has long been predicted (Pfeffer, 1903; Silk & Erickson, 1979). In recent years, various plant phenotyping methods emerged that allow the measurement of plant traits in a semi-automated manner for hundreds of plants based on spectral characteristics (Fiorani & Schurr, 2013; Gibbs et al., 2016). Among these traits, growth is central since it often characterises plant sensitivity to stresses (Tardieu et al., 2017). Probably the simplest approximation for plant growth using image analysis is the increase of the shoot area as observed by one camera. This requires that the growth mainly occurs in a plane so that the distance between the camera and the object remains the same. If this is not the case, plant parts that are close to the camera appear bigger which impairs the result.

It is also required to accurately segment the plant from the background. In controlled conditions this can easily be achieved by having a back-

ground colour that is distinctly different from the greenish plant parts. This simple approach was implemented by many researchers (Arvidsson, Perez-Rodriguez & Mueller-Roeber, 2011; De Vylder, Vandenbussche, Hu, Philips & Van der Straeten, 2012; Jansen et al., 2009; Leister, Varotto, Pesaresi, Niwergall & Salamini, 1999; Tisné et al., 2013; Walter et al., 2007; X. Zhang, Hause & Borevitz, 2012; Dobrescu, Scorza, Tsaftaris & McCormick, 2017; Minervini, Giuffrida, Perata & Tsaftaris, 2017; Tomé et al., 2017; Faragó, Sass, Valkai, Andrási & Szabados, 2018; Vasseur, Bresson, Wang, Schwab & Weigel, 2018) for analysing *Arabidopsis thaliana* or *Nicotiana tabacum* growth using top view images. The rosette shapes of young *Arabidopsis thaliana* and to some degree *Nicotiana tabacum* plants fulfil the requirement that growth mainly takes place in a plane. However, plant leaves show oscillating movements which can be observed by using a similar top view imaging setup and by tracking leaf tips in older (32 days) *Arabidopsis thaliana* (Bours, Muthuraman, Bouwmeester & van der Krol, 2012). The most challenging tasks in this approach are background removal (Minervini, Abdelsamea & Tsaftaris, 2014), and segmentation of individual leaves (Scharr et al., 2015; Giuffrida, Doerner & Tsaftaris, 2018).

This method provides an approximation of relative shoot growth. To include plant features such as dry weight, statistical correlations with the observed plant area in the image need to be established by harvesting the plant and manually measure the features. For herbaceous grasses it is possible to predict fresh and dry biomass using side view images (Tackenberg, 2007). Therefore, this approach is the most widely used method for the observation of monocot crops in automated plant phenotyping systems (Fahlgren et al., 2015; Hartmann, Czauderna, Hoffmann, Stein & Schreiber, 2011; Klukas, Chen & Pape, 2014; Knecht, Campbell, Caprez, Swanson & Walia, 2016; W. N. Yang et al., 2014). One example is the commercial *Scanalyzer* system (LemnaTec GmbH) in which plant pots are kept on a conveyer belt and are frequently moved to an imaging chamber where top and side view

images are taken. It is also possible to establish phenotyping systems in agricultural fields, albeit at high costs and with considerable technological effort (Kirchgessner et al., 2016).

Three-dimensional leaf reconstruction

Since plant leaves sometimes have complex three-dimensional (3D) shapes and show movements throughout the day, a system that captures 3D information of the leaf surface is preferred. There are several such methods available that already have been tested on plants. Here, I give an overview on some of these methods and briefly discuss their advantages and disadvantages. Generally, 3D imaging approaches can be categorised into active and passive methods, where active methods require laser emittance, or the projection of a light pattern, and passive methods rely on ambient light, or require illumination.

One active method is laser scanning. This term may refer to different technologies; here I will use it to refer to laser triangulation. Another laser-based technollogy called time of flight is presented below. Simply speaking, in laser triangulation the distance to the object is calculated by projecting a laser spot or line and measuring its reflectance angle in a receiving sensor. Laser triangulation has a high accuracy and precision for plant growth measurements but it is only suitable for close range measurements (Paulus, Schumann, Kuhlmann & Leon, 2014). In that study, measurements were conducted manually once a day, but automated measurements of whole plants are possible using robots (Chaudhury & Barron, 2018). There are also commercial systems available that are specifically designed for measuring plants, for example *Phenospex PlantEye*, or *LemnaTec PhenoCenter*. The *LemnaTec* system is described in Dornbusch et al. (2012) for measuring leaf elongation and movements of *Arabidopsis thaliana*. The *Phenospex PlantEye* system is suitable for field applications for both monocot (Vadez et al., 2015) and eudicot plants (Kjaer & Ottosen, 2015). It also includes an automated

calculation of total visible leaf area. However, the laser scan line moves during the measurement which disturbs the result in case of plant movements due to wind.

Time of flight (ToF) cameras estimate the distance to an object based on the measured return time of a laser signal; they give an image with a depth value for each pixel. Time of flight is a class of lidar (light detection and ranging), a technology that is often used for broad-scale canopy characterisation; see Section 2.3. It is generally suitable for imaging leaves, but in direct sunlight the depth measurement may be noisy (Kazmi, Foix, Alenya & Andersen, 2014). Furthermore, ToF sensors have a low pixel resolution which may impair the accuracy of the measurement. This can be overcome by combining the depth image with high-resolution colour images (Alenya, Dellen & Torras, 2011; Uchiyama et al., 2017). One advantage of ToF is the availability of low cost consumer grade devices such as the Microsoft Kinect v2, or the Intel RealSense SR300. Some ToF application examples include plant volume estimation (Andujar, Dorado, Fernandez-Quintanilla & Ribeiro, 2016), stalk thickness estimation (Batz, Méndez-Dorado & Thomasson, 2016), or weed detection (Gai, Tang & Steward, 2015). Further, ToF has been used for plant shoot reconstruction (McCormick, Truong & Mullet, 2016), and for measuring total leaf area growth (Hu, Wang, Xiang, Wu & Jiang, 2018). Song, Glasbey, Polder and van der Heijden (2014) used information from ToF and from stereo vision (described below) for individual leaf area calculation.

The last active method I discuss here is structured light. In such a system a defined light pattern is projected and the geometry of the object is calculated from the shift of the pattern. This technology is used in the Microsoft Kinect v1 which can be used for plant imaging and leaf segmentation (Chene et al., 2012), but it is not suitable for leaf area measurements due to the low image resolution (Paulus, Behmann, Mahlein, Plumer & Kuhlmann, 2014). With higher resolution, structured light systems allow accurate leaf

area estimations (Bellasio, Olejnickova, Tesar, Sebela & Nedbal, 2012) and the characterisation of growth processes (Li et al., 2013). The Microsoft Kinect v1 sensor also works for measurements in the field although there is the potential of sunlight interfering with the projected light pattern (Andujar, Fernandez-Quintanilla & Dorado, 2015).

Two widely used passive methods are stereo vision and structure from motion. In a stereo vision system, two cameras with fixed positions relative to each other are used to calculate the distance of an object to the camera. Matching points in corresponding pictures from the two cameras are detected and used for the calculation, see Chapter 4. Therefore, for every pixel that is matched in both images, real world coordinates are available. However, some plant leaves lack a distinct texture which makes this matching challenging. Furthermore, if images are acquired in direct sunlight, sensor saturation may occur which also impairs the matching (Kazmi et al., 2014). Stereo vision can be used to measure leaf angles (Biskup, Scharr, Schurr & Rascher, 2007; Muller-Linow, Pinto-Espinosa, Scharr & Rascher, 2015), leaf cover area (Lati, Filin & Eizenberg, 2013) or the leaf area index (LAI; Leemans, Dumont & Destain, 2013). However, LAI estimations become imprecise in case of occlusion due to overlapping leaves. The area of fully visible leaves can be accurately reconstructed (Xiong et al., 2017). T. T. Nguyen, Slaughter, Maloof and Sinha (2016) used an extensive setup consisting of five stereo camera pairs, a rotating turntable and the projection of a random light pattern to reconstruct whole plant geometry and growth. Finally, Aksoy et al. (2015) used stereo vision for leaf detection and estimate to leaf growth by applying an ellipse model.

Structure from motion (SfM) uses multiple pictures from different viewpoints to calculate a 3D model of the object (Snavely, Seitz & Szeliski, 2008). Real world dimensions need to be added to the model by defining the coordinates of reference points in the scene. Plant models generated by SfM can then be segmented into different organs (Pound, French, Fozard,

Murchie & Pridmore, 2016) and properties such as leaf area or stem height can be calculated (Paproki, Sirault, Berry, Furbank & Fripp, 2012). Structure from motion is also suitable for crop monitoring in the field (Jay, Rabatel, Hadoux, Moura & Gorretta, 2015). There are commercial SfM software packages available which makes the reconstruction of one scene fairly simple. However, for an automated plant growth analysis a more complicated image analysis workflow is required (Duan et al., 2016). Structure from motion is a good method for generating whole plant models but it requires a lot of input images. Image acquisition therefore requires some time or a system that automatically captures pictures from different viewpoints. Also, the post processing can take a long time for complicated plant structures (Pound et al., 2016).

Other methods for three dimensional reconstruction that have not yet been applied broadly are light-field photography (Apelt, Breuer, Nikoloski, Stitt & Kragler, 2015), shape from silhouette (Golbach, Kootstra, Damjanovic, Otten & van de Zedde, 2015), or photometric stereo (Smith, Zhang, Hansen, Hales & Smith, 2018).

1.2. Contributions

"Plant growth" is an umbrella term that refers to different processes, and the development of a single leaf may be of limited relevance for the whole plant. Therefore, I first take a step back in Chapter 2 to discuss different aspects of plant growth, and how growth definitions shift depending on the spatiotemporal focus of analysis. I continue with an overview of growth measurement methods from cell to system, and conclude with a discussion why plant growth measurements are important in the first place.

In Chapters 3 and 4, I focus on outdoor leaf growth measurements. Most studies are conducted in growth chambers or greenhouses, and there is a lack of knowledge of leaf development in situ. For large plants such as trees,

experiments under controlled conditions are hardly possible, but methods for direct measurements of individual leaves are sparse.

In Chapter 3, I adopted the leaf fixation method (Mielewczik et al., 2013) for long-term outdoor measurements. To my knowledge, this is the first study measuring leaf area growth in situ on a mature tree. Although a similar method has been used in the greenhouse for measuring leaf growth of young *Populus deltoides* (Walter et al., 2005; Matsubara et al., 2006), and there is also a method for in situ palm frond elongation measurements (Zhen, Tripler, Peng & Lazarovitch, 2017).

Because leaf fixation and the application of tensile forces can alter growth, a contactless method would be preferable. In Chapter 4, I explored the suitability of stereo vision for this task. Outdoor measurements are generally challenging for vision-based methods, because of direct sunlight, wind, and rain. I built a custom made device in order to minimise such effects. I found that stereo vision is a suitable technology for in situ leaf area measurements, but the measurement error was relatively large.

Chapter 2

Plant Growth: the What, the How, and the Why

Plant growth is a widely used term that can have different meanings depending on the context and the spatiotemporal scale of analysis. In this chapter, I first answer the question what is plant growth? I then review different methods for how plant growth can be measured and analysed at different organisational and temporal levels. I conclude by discussing why gaining a better understanding of plant growth is essential in particular to disentangle genetic and environmental effects on the phenotype.

This Chapter has been submitted to *New Phytologist* as an invited Tansley Review. It is co-authored by Sebastian Leuzinger, Bertrand Muller, and Florent Pantin.

2.1. Introduction

One of the first modern attempts to study plant growth can be found in the seminal book "Vegetable Staticks" of the botanist Stephen Hales (1727). Hales designed methods to locate and quantify internode and leaf blade growth. Over the following century, it was understood that growth depends on the fixation of carbon from the atmosphere (de Saussure, 1804), and on nutrient uptake from the soil (Sprengel, 1828; von Liebig, 1840). The observation and measurement of plant growth has a long tradition in agriculture (e.g. Kreusler, 1878) and forestry (e.g. Weber, 1891), but also in the study

of plant physiology (Pfeffer, 1881). However, many aspects of growth still remain obscure.

Inherent challenges of growth studies are the observation and quantification of processes that spatially span several orders of magnitude from cell to plant and community, and temporally range from immediate stress reactions to centuries for ecosystem succession. Furthermore, strong environmental effects on growth induce feedbacks between development, physiology, and microclimate, which make it hard to isolate individual processes. This difficulty can (and must) be overcome by clearly defining frames of analyses, i.e. a robust definition of growth variables, and ideally formalisms accounting for the impact of the environment.

Despite the interest in measuring and predicting growth, there is no single definition of "plant growth", as a multitude of processes can be summarised under this term. At the smallest scale, growth is related to the functioning of meristems and consequently cessation of meristem growth is often followed by cessation of organ growth (Granier & Tardieu, 1998b; Moreno-Ortega, Fort, Muller & Guédon, 2017). Consistent with this, there are often strong correlations between cell number and organ size (Cookson et al., 2005; Gazquez & Beemster, 2017). However, there also exist large periods during which organs grow without cell proliferation. For example, in the sunflower leaf the total number of cells is reached when the leaf area is approximately 25% of its final size (Granier & Tardieu, 1998b). The leaf keeps expanding for about another week and the final area is highly variable depending on environmental conditions (Granier & Tardieu, 1999b). In this example, growth is defined as organ expansion. In another sense, plant growth is the accumulation of biomass, resulting from the balance between carbon assimilation and carbon loss through respiration, exudation, shedding, or herbivory.

In this paper, I distinguish these different viewpoints on growth, and I discuss how and to what degree the various underlying processes are

coupled at different spatiotemporal scales. I then review various methods to measure growth, as particular methods often implicitly target certain aspects of plant growth but not others. While growth regulation at the molecular level is beyond the scope of this review, I believe that a precise definition of the various facets of "plant growth" is the first step in the analysis of growth processes and their underlying genetic and environmental drivers.

Following the bon mot to see the forest for the trees, I discuss growth concepts at different levels from cells to, organs, plants, and ecosystems, and at different temporal scales from hours to centuries. I take this hierarchical approach, because growth activities manifest differently at different scales, despite all resulting from similar processes at the cell level. Each unit does not exist in isolation, but in relation to plant internal controls and external environmental constraints. For example, a cell of a developing eudicot leaf will undergo proliferation, expansion, or no growth depending on the location in the leaf, the leaf and plant ontogeny, as well as the plant's environmental conditions such as temperature, soil water potential, or shading from competing plants. At the same time, the growth of one particular leaf could coincide with plant net defoliation due to litterfall. In this case we would observe biomass growth at the leaf level, but no growth or even biomass loss at the plant or ecosystem level. Such simple examples demonstrate the need to define reference metrics to analyse plant growth (Leuzinger & Hättenschwiler, 2013). I present a general growth concept for plants (viridiplantae) in the next subsection, but implicitly focus on seed plants for the rest of the paper.

2.2. The What. A clarification of various growth concepts

Different aspects of plant growth

I define "growth" in a strict sense as an *irreversible increase* in cell number, structural biomass, or plant volume (Table 1, Figure 1). I adopt the terminology *structural growth* to refer to an irreversible increase in structural biomass, that is biomass fixed into plant structures such as cellulose, lipids, or proteins (Figure 1a,b,c,e). Alternatively, biomass can be present in the form of secondary metabolites, or as storage compounds referred to as non-structural carbohydrates (NSC; Figure 1h). I also adopt the term *expansive growth* to refer to an irreversible increase in fresh volume (Figure 1a,c,d; Pantin et al., 2012). The irreversible nature of expansion is linked to the plastic deformation of cell walls, as opposed to their elastic deformation (Cosgrove, 1993) resulting in reversible elastic cell swelling, or shrinkage (Figure 1i). Plant volume is the space occupied by plant tissue; it is the sum of all cell volume and intercellular space. Expansive growth is the irreversible increase in plant volume as a result of cell (and airspace) expansion that can occur during or after the cell cycle (Green, 1976). Growth sensu lato is often related to cell production (Figure 1a,b), which is essential for later cell differentiation (Figure 1f). According to the strict definition, the loss of cells through shedding of plant parts is not part of growth (Figure 1g).

In a broader sense, "growth" can be defined as biomass or volume *change*. This definition does not distinguish between different biomass types or functions, and it allows for "negative growth". In this sense, biomass change is the mass balance between material "acquisition" through photosynthesis and nutrient uptake, and losses from respiration, exudation, shedding, herbivory, etc. Similarly, volume change is the difference between organ expansion and losses of plant parts. Throughout the rest of this chapter

Table 1. Definition of terms used

Plant	Land plants and green algae; viridiplantae
Plant growth	Irreversible increase in cell number, structural biomass, or volume of a plant; change in plant biomass, or volume
Structural growth	Irreversible increase in structural biomass
Expansive growth	Irreversible increase in cell, organ, or plant size
Cell production	The increase in cell number as the result of a mitotic or meiotic cell cycle
Cell proliferation	Increase in cell number and concurrent increase in total tissue size
Cell partitioning	Cell production without an increase in total volume
Endoreduplication	DNA replication without increase in cell number
Structural biomass	Structural components of plant tissues (cellulose, lignin, cell membrane lipids, proteins, nucleic acids, etc.)
Non-structural carbohydrates (NSC)	Insoluble polymers (e.g. starch, fructans) or soluble oligomers (hexoses, sucrose, sugar-alcools, etc.) that are used as short-term or long-term stores
Net primary production (NPP)	The integral of gross primary production minus autotrophic respiration during a given time on a given area, expressed in biomass, carbon mass, or energy
Size	Length, area, or volume

the term "growth" without specification refers to either of the growth processes, or their combination.

Cell production and cell cycle

Cells are the fundamental building blocks of all life, and their multiplication through the cell cycle always requires structural growth for DNA and cell wall synthesis (Figure 1a,b). Usually, there is also expansive growth during the cell cycle, so that the combined volume of the daughter cells is larger than the initial volume of the mother cell. The term *cell division* could
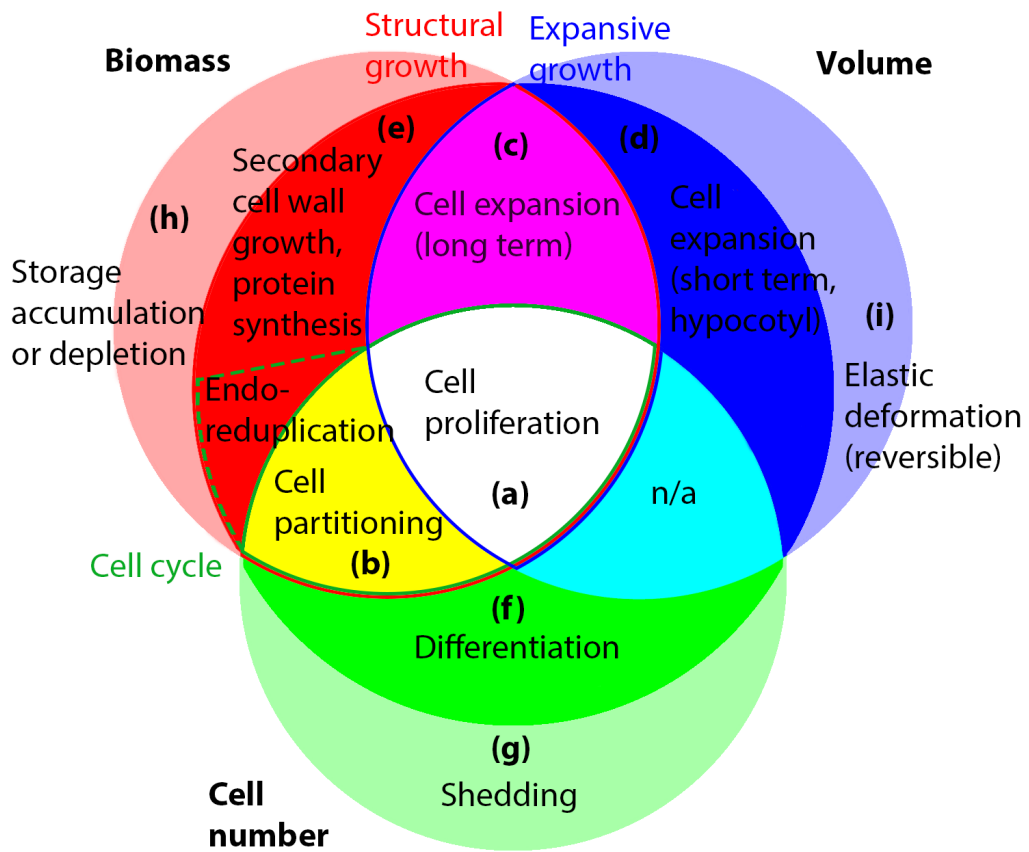
Figure 1. Different aspects of plant growth and their coupling. Growth can be described as an irreversible increase in cell number, structural biomass, or plant volume. The irreversible increase in structural biomass is called structural growth; the irreversible increase in volume is called expansive growth. The increase in cell number through the cell cycle is always part of structural growth, as it requires DNA and cell wall synthesis. (a) Cell proliferation is the process of increasing in cell numbers, while maintaining an average cell size. Therefore, proliferation includes all three aspects of growth. (b) A cell cycle without an increase in total size is called cell partitioning. (c) Cell expansion is the irreversible increase in cell size under turgor pressure (expansive growth), which requires cell wall synthesis to maintain stability (structural growth). (d) In hypocotyls, cell wall synthesis and cell expansion are regulated by different mechanisms which implies that cell expansion can occur without structural growth for short times (Ivakov et al., 2017). (e) Secondary cell wall growth, protein synthesis, and endoreduplication are structural growth processes without notable changes in volume (although ploidy correlates with cell size). (f) Cell differentiation, and (g) shedding, as well as (h) the accumulation and depletion of storage components, and (i) elastic deformation are not directly part of growth sensu stricto.

refer either to the whole cell cycle, or only to the mitotic phase. Therefore, I favour the term cell proliferation to describe this case of an increase in cell number and tissue volume (Figure 1a). Usually, the mean cell size is maintained during proliferation. In the shoot apical meristem this may be achieved by coordinating the regulation of the cell cycle duration, the cell growth rate, or both depending on the cell area at birth (Serrano-Mislata, Schiessl & Sablowski, 2015; Willis et al., 2016; Jones et al., 2017). Cell proliferation also includes cases where the individual cell size is decreasing but the total tissue size is increasing, for example during early *Arabidopsis thaliana* embryo development (Yoshida et al., 2014), or in root tips (Erickson & Sax, 1956; Moreno-Ortega et al., 2017). On the other hand, a cell cycle without any increase in total size, for example zygote cleavage, is called cell partitioning (after Green, 1976, Figure 1b). Finally, a special case of the cell cycle is endoreduplication, the replication of DNA not followed by mitosis. The resulting high-ploidy cells are generally also larger in size (Sugimoto-Shirasu & Roberts, 2003).

Expansive growth

Cell volume *change* strongly depends on turgor pressure and results from two different processes, elastic cell deformation, and irreversible cell wall extension (Figure 1c,d), as formulated in the Lockhart equation (Lockhart, 1965; Ortega, 1985):

$$\frac{dV}{V dt} = \frac{1}{\varepsilon}\frac{dP}{dt} + \theta \cdot max\left(P - P_c, 0\right) \ , \tag{1}$$

where V [µm^3] is the cell volume, P [MPa] is the turgor pressure, P_c [MPa] is the critical turgor pressure, or yield stress, ε [MPa] is the cell elastic modulus, and θ [MPa^{-1}] is the cell wall extensibility. Relative cell volume change results from elastic swelling or shrinkage, or from irreversible cell expansion, with both components depending on turgor. This poses a challenge

for the study of expansive growth. For single cells it is possible to experimentally distinguish elastic deformation and expansion (Proseus, Ortega & Boyer, 1999), while for tissue expansion it is assumed that there are only limited growth activities during periods of elastic shrinkage (Zweifel, Haeni, Buchmann & Eugster, 2016). Turgor pressure by itself does not lead to expansive growth, as it first requires cell wall loosening (Cosgrove, 2016).

Bioamss change and structural growth

Biomass *change* is the mass balance between biomass formation and biomass losses. A large part of total biomass is stored as compounds that form the structure of plants: cellulose and lignin in the cell walls, lipids in the membranes, and proteins within the cell. Another part of total biomass is stored in the form of NSC (sugars and starch) as a buffer against diel (Stitt & Zeeman, 2012), seasonal (Klein, Vitasse & Hoch, 2016), or disturbance-based fluctuations in carbohydrate assimilation. Because NSC reserves can be depleted (negative biomass change) their accumulation falls outside the definition of structural growth (Figure 1h). Similarly, the production, accumulation, and release of secondary metabolites are also not part of structural growth (Fig. 1h).

The introduced constraint that structural growth is irreversible allows a clear theoretical definition, but there are also some ambiguities. For instance, membrane lipids and proteins generally show a much shorter lifespan than the lignocellulosic compounds within a given cell, e.g. in the xylem where the cytoplasmic content rapidly disappears for the cell to be functional just through its empty walls. Similarly, nutrient remobilisation is not accounted for as negative growth, but it can contribute to structural growth in another plant part. Therefore, in terms of structural growth, the irreversibility refers to chemical-functional characteristics and time frames.

For the growth of seeds, fruits, or storage organs the construction of cells is part of structural growth, but the accumulation of sugars or starch is not.

Such cases are accounted for by the broader "growth" definition *biomass change*. Similarly, the loss of plant parts through shedding, litterfall, or herbivory is not part of structural growth, although it is a biomass loss which may affect growth potential. When NSC reserves are depleted to support structural growth, the two "growth" concepts may have different signs. For example, a sprouting potato has a (positive) structural growth, while the biomass change is negative because of respiration losses.

Frame of analysis

Growth analysis requires the definition of the analysed system, of the system variable, and of reference metrics (Table 2). The system under consideration can be any of the hierarchical levels cell, organ, plant, or community (Figure 2). The system variable is typically a metric for one of the two main aspects of growth: biomass or volume; see Table 2. Alternatively, it can express a count or an index, e.g. the number of cells, or leaf area index (LAI; Watson, 1958). The definition and selection of reference metrics such as *per unit surface area*, or *per individual* is critically important, as its choice can cause a sign reversal while interpreting results (Leuzinger & Hättenschwiler, 2013). In growth analysis, *per time duration* is a required reference metric, and it typically varies from hours to years, depending on the analysed system. Again, changing the temporal reference metric can change the interpretation of results fundamentally. For example, alpine meadows have the same net primary production (NPP) as tropical rainforests when only analysed for the growing season, but vastly different NPP over the whole year (Körner, 2003a).

To account for the temperature dependence of growth it can be useful to introduce thermal time instead of chronological time (Gallagher, 1979; Granier & Tardieu, 1998a). Rates of different plant development processes are dependent on temperature and follow species specific negatively skewed Arrhenius-type bell curves (Parent, Turc, Gibon, Stitt & Tardieu,

2010; Parent & Tardieu, 2012). When the temperature increases above an optimum, development rates decrease rapidly. Below the optimum, there is an ideal range in which rates increase quasi-linearly with temperature, and thermal time is the integral of temperature above a species-specific lower threshold (Table 3).

For the quantitative description of growth, we are interested in the size of a system variable Y at any time, as well as its change with respect to time. Growth analysis requires at least two measurements of Y at different points in time. Given enough measurements, we may be able to formulate a growth model $Y = f(t)$ to predict Y as a function of time, or thermal time. The absolute growth rate (AGR) is the derivative $dY/dt = f'(t)$, and absolute growth is the integral of the absolute growth rate during a given time period. The analysis of relative growth rates (RGR $= dY/(Y\,dt)$) is often more meaningful than the analysis of absolute growth rates, because it controls for the quantity of Y. Relative growth rates can be calculated using exponential (Blackman, 1919), or linear models (West, Briggs & Kidd, 1920), see Table 3. The predicted RGR can substantially differ between the two models, except for very small ΔY when the enumerator approaches zero. Very small Δt usually coincide with small ΔY and therefore indirectly lead to the same result. However, for plant growth analyses both exponential and linear models are usually too simplistic and may only be suitable during certain developmental stages. For the analysis over a plant's life cycle, nonlinear models such as logistic models are more appropriate to describe growth (Paine et al., 2012).

Table 2. Different metrics for growth analysis and associated methods

System variable	Method
Mass	
– Fresh mass [kg]	Lysimeter, harvesting
– Biomass (dry) [kg]	Harvesting
– Structural biomass [kg]	Harvesting and chemical analysis
– Carbon mass, other element's mass [kg]	Harvesting and chemical analysis
– Fixed energy; calorific value [kJ]	Calorimeter
– "Useful" biomass [kg]	
– Carbon flux [kg]	Eddy covariance
Size	
– One dimension (1D) [m]	
○ Leaf, root, stem length	Meter, auxanometer, image analysis
○ Stem radius, diameter change	Dendrometer
○ Canopy height	Airborne or space-borne lidar, or image analysis
– Two dimensions (2D) [m^2]	
○ Cell area (projected)	Microscope
○ Leaf area (one sided, projected)	Harvesting, image analysis
– Three dimensions (3D) [m^3]	
○ Cell, organ, plant volume	Confocal microscopy, X-ray
○ Shoot architecture, root convex hull; space "covered"	Image analysis, terrestrial lidar
Indices	
– Cell, organ, plant count	
– Leaf area index (LAI) [m^2 m^{-2}]	Ceptometer, hemispherical photography
– Greenness; Normalised difference vegetation index (NDVI), enhanced vegetation index (EVI)	Remote sensing (near surface, airborne, space-borne)
Reference metric	
– Time [h], [d], [wk], [yr]	
– Thermal time [°C h], [°C d]	
– Land surface area [m^2]	
– System variable (relative growth)	
– Higher hierarchy, individual	

Growth analysis requires the definition of the system variable (main metric) and of one or multiple reference metrics. Time is always a reference metric. At the landscape-scale, land surface area is also a mandatory reference metric (except for indices).

Table 3. Mathematical formulas

	Formula	Definition
Model	$Y = f(t)$	Development of system variable Y (see Table 2) as a function of time t
Absolute growth rate (AGR)	$\begin{aligned} g_{AGR} &= \frac{dY}{d\boldsymbol{t}} = f'(t) \\ g_{AGR} &= \frac{\Delta Y}{\Delta \boldsymbol{t}} \end{aligned}$	Change in Y per time
Absolute growth	$\begin{aligned} \Delta Y &= \int_{t_{i-1}}^{t_i} f'(t)\, d\boldsymbol{t} \\ &= f(t_i) - f(t_{i-1}), \\ & \Delta Y > 0 \end{aligned}$	Absolute change of Y between two points in time
Relative growth rate (RGR), exponential	$g_{RGR_{exp}} = \frac{\ln\left(\frac{Y_i}{Y_{i-1}}\right)}{\Delta \boldsymbol{t}}$	Change in Y per time, relative to Y
Relative growth rate (RGR), linear	$g_{RGR_{lin}} = \frac{Y_i - Y_{i-1}}{\frac{1}{2}(Y_i + Y_{i-1}) \cdot \Delta \boldsymbol{t}}$	Change in Y per time, relative to mean Y
Thermal time	$\begin{aligned} t_T &= \int (T(\boldsymbol{t}) - T_0) d\boldsymbol{t} \\ &\approx \sum \Delta \boldsymbol{t} \cdot (\overline{T} - T_0), \\ & T \varepsilon T_{opt} \end{aligned}$	"Physiological time"; Mean temperature $\overline{T}$ above species specific threshold temperature T_0 multiplied by time duration $\Delta \boldsymbol{t}$ (usually expressed in hours, or days), given T is in the optimal temperature range T_{opt}
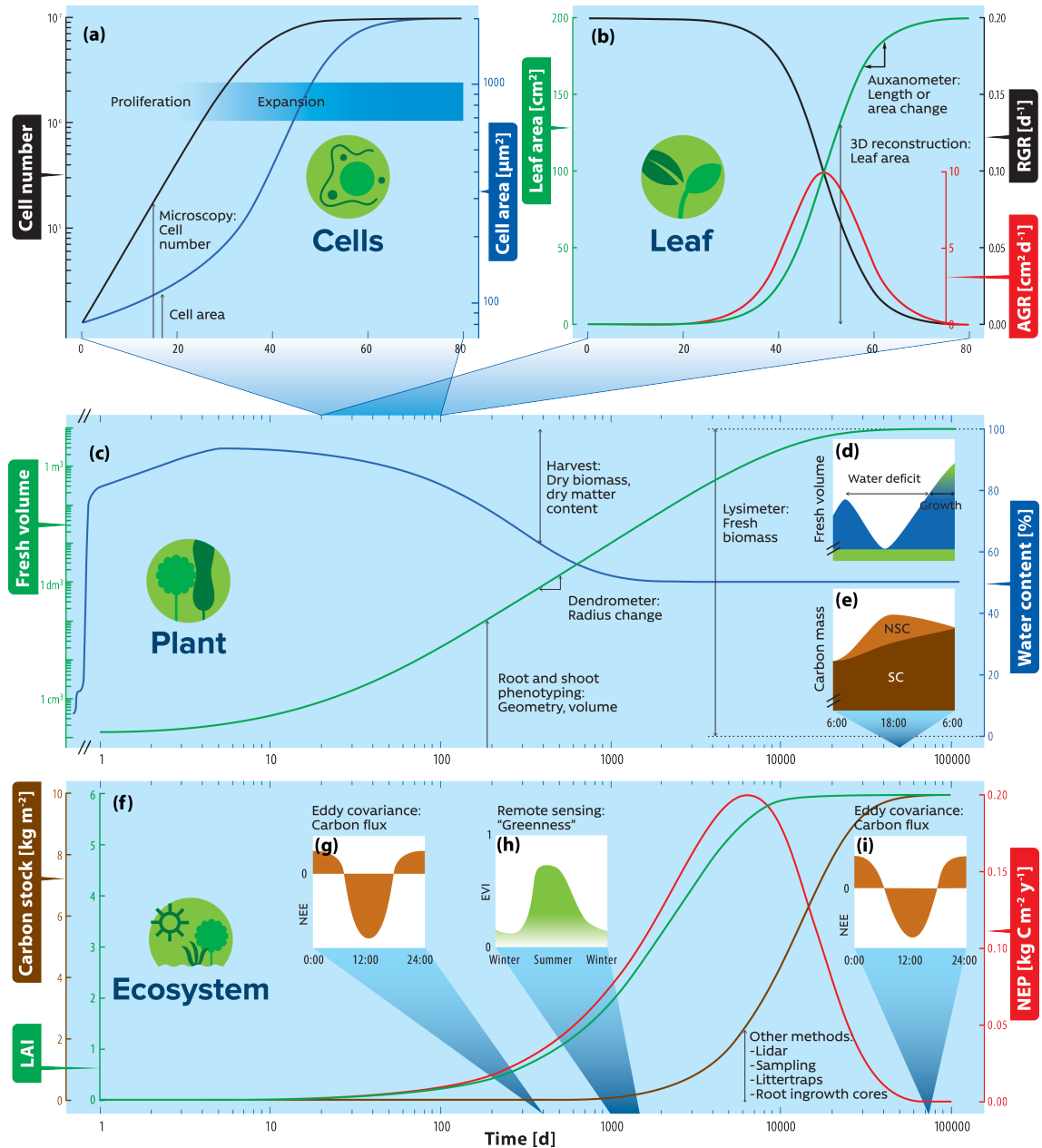
Figure 2. A summary of growth processes across spatiotemporal scales, growth metrics, and measurement methods. (a,b) Eudicot leaf area growth modelled by a logistic function. (a) Development of cell number (black), and cell area (blue) visualising the transition from proliferation to cell expansion driven leaf expansion. (b) Leaf area development in green as an example for organ expansion, corresponding relative growth rate (RGR) in black, and absolute growth rate (AGR) in red. (c) Tree volume growth modelled by a von Bertalanffy function in green; estimated water content in blue. Data for seedling hydration during the first five days from soybean (Wahab, 1971). Later, water content is exponentially decreasing towards 50%. (d) Stylised diel fluctuation of fresh volume, and (e) carbon mass (NSC: Non-structural carbohydrates; SC: structural carbohydrates). (f) Ecosystem primary succession modelled by a Chapman-Richards function. Total standing carbon mass per area in black, and corresponding net ecosystem production (NEP) in red. The development of the leaf area index (LAI) has been modelled independently based on a simple asymptotic curve. (g,i) Stylised diel curves of net ecosystem exchange (NEE) carbon fluxes for an early and late stage of succession (different scales). (h) Stylised yearly course of the enhanced vegetation index (EVI) for a deciduous forest. Arrows and corresponding labels indicate different methods for growth measurement, or approximation.

For the spatiotemporal analysis of tissue expansion, it is necessary to introduce metrics that account for regional variation across the tissue. Botanical pioneers have proposed to treat the tissue as a mechanical continuum, allowing the development of kinematic frameworks similar to the ones used in fluid dynamics (Silk & Erickson, 1979; Goodall & Green, 1986). Two alternative approaches are distinguished: the Eulerian and the Lagrangian specifications of growth. While both approaches require tracking the position of landmarks in the growing tissue over time (Section 2.3), their respective usefulness depends on how growth organises across the tissue. On the one hand, the Eulerian or spatial approach generates a velocity vector field that describes the displacement of points relative to a fixed coordinate system. It is particularly suitable for organs with a one-dimensional expansion pattern such as roots (Beemster & Baskin, 1998), or monocot leaves (Muller et al., 2001). In such systems expansive growth can be expressed as a function of the distance to the meristem. The Lagrangian or material approach, on the other hand, follows the displacement of given elements through space and time so that the coordinate system is attached to the tracked points and deforms with growth. This approach describes the local growth properties of a physical region in terms of growth rate, anisotropy, direction, and rotation rate, four types of parameters that can be encapsulated within the growth tensor (Hejnowicz & Romberger, 1984). It is particularly suitable for eudicot leaves (Figure 2a,b) where the size and location of the expansion and proliferation zone changes during development, with variation depending on the species (Walter et al., 2009; Das Gupta & Nath, 2015) and the tissue layer (Alvarez, Furumizu, Efroni, Eshed & Bowman, 2016; Fox et al., 2018).

While the Eulerian and Lagrangian frameworks are useful to quantify the spatiotemporal changes in tissue shape, they may also be used to dissect the contributions of cell division and expansion to tissue growth rate (reviewed in Fiorani & Beemster, 2006). They also help in interpreting the

spatiotemporal changes in concentration of any molecule observed along a growing zone, by enabling the computation of biosynthesis and deposition rates (e.g. Merret et al., 2010; Silk & Bogeat-Triboulot, 2014). However, these frameworks do not inform us directly about the mechanisms underlying the establishment of regional differences that originate tissue morphogenesis, since the biological specification of particular regions does not result from Eulerian and Lagrangian processes. As argued by Coen, Rolland-Lagan, Matthews, Bangham and Prusinkiewicz (2004), mechanistic frameworks of tissue morphogenesis should account for mutual interactions between tissue patterning and growth.

Coupling and uncoupling of growth processes

Structural growth is mainly associated with carbon and metabolic processes, while expansive growth is mainly associated with water and hydraulic processes. The ratio between structural growth rate and expansive growth rate determines tissue density, and the ratio between cell proliferation rate and cell expansion rate determines cell density. Over long timescales all aspects of growth have to be coordinated to a certain degree, as there must be upper and lower boundaries to cell and tissue density that limit the accumulation of matter without expansion, or expansion without structural growth.

The duality of structural and expansive growth becomes apparent when analysing cell expansion. Structural growth requires carbohydrates, which are assimilated during daytime, while expansive growth requires turgor pressure, which usually is higher at night time when water loss through transpiration is minimal. This temporal variation in growth conditions requires a complex coordination of cell wall synthesis and expansion (Verbančič, Lunn, Stitt & Persson, 2018). In *Arabidopsis thaliana* hypocotyls, cell expansion and cell wall synthesis are regulated by different mechanisms, which suggests that for short timescales cells can expand without cell

wall synthesis (Ivakov et al., 2017). After expansion, structural growth can take place without (notable) volume change through secondary cell wall growth, or protein synthesis. For whole organs, similar mechanisms apply, and growth can be limited by either carbohydrate supply, or hydraulics (Pantin et al., 2011; Pantin et al., 2012). The detailed (and separate) analysis of these processes is critical as one will likely be more limiting for growth at any given time, thus driving the overall progress of growth (Fatichi, Pappas, Zscheischler & Leuzinger, 2019).

A special case of tissue expansion is "stored growth" which is observed at the transition from water stress to hydration. During water stress tissue expansion is low or zero, but immediately after hydration there is a short growth spurt, before expansion drops to a steady state level. This phenomena has been described for maize leaves (Acevedo, Hsiao & Henderson, 1971), and stems of different tree species (Zweifel et al., 2016). It suggests that the potential for cell wall extension "accumulates" during water stress. Two possible mechanisms for this phenomenon are ongoing cell wall loosening without subsequent expansion, or the provision of new material, as it has been shown for calcium pectate in *Chara corallina* (Proseus & Boyer, 2008).

The total number of cells in a given species and organ is much more variable than the mature size of its cells. A striking example is the comparison of bonsai trees to trees of similar genomes but with unrestricted growth, which showed little differences in leaf cell size, while the total leaf area differed by a factor of five to fifty depending on the species (Körner, Pelaez & John, 1989). This implies that for leaves final cell size is under strong genetic control, and that long-term expansive growth coincides with an augmented cell proliferation.

Structural equation modelling in *Arabidopsis* suggests that epidermal cell area, cell division, cell expansion, and endoreduplication are controlled at the leaf level, rather than cellular processes determining organ properties

(Tisné et al., 2008; Massonnet et al., 2011). Such "organ-level regulation" mechanism could account for the phenomenon of "compensation", according to which a change in leaf cell number appears to be (partly) balanced by a change in cell size (Tsukaya, 2008; Hisanaga, Kawade & Tsukaya, 2015). A mechanistic model of the *Arabidopsis* leaf suggests that cell growth and division are controlled by spatiotemporal regulators that partly overlap, generating correlations between division and expansion variables (Fox et al., 2018). Changing parameters in this model predicted compensation phenotypes as an emergent property, without invoking a compensating mechanism at the organ level. Thus, shared spatiotemporal regulators are likely to generate coordination between cell expansion and proliferation, resulting in a constrained phenotypic space for cell number, cell size, cell ploidy and organ size.

For the growth of individual plants I consider the development from seed to death, which covers a huge temporal range from one growing season for annual plants, to millennia for some trees (Figure 2c). This entails that different aspects of growth are in focus depending on the plant's life form and the applied research question. Often, plant growth is approximated from measurements at the organ level such as stem diameter for trees, or total leaf area for herbaceous plants (see Section 2.3). Because a large part of plant volume is made up of water, these are metrics for expansive growth. Plant water content ranges from about 50% for fresh wood to almost 95% for lettuce leaves, while seeds have a water content of around 10% (Sonnewald, 2013). (In forestry the general metric for this is moisture content, which is water mass per dry mass.) As plant water content, respectively dry matter content, changes over a plant's life cycle (Figure 2c), so does the relation between expansive and structural growth. Seeds have a low water content, and germination starts with hydration, followed by the onset of metabolism, and ends with further water uptake and cell expansion of early seedling growth (Nonogaki, Bassel & Bewley, 2010). During

the first few days after hypocotyl emergence the water content increases to more than 90%. Before the unfolding of cotyledons all material and energy for expansive and structural growth has to be accessed from storage components (negative biomass change). Leaf water content varies over a wide range from ca. 50% to 85% depending on the plant growth form (Shipley & Vu, 2002). Throughout the life cycle plant water content is expected to decrease in line with the share of leaves in total plant mass. For woody plants the water content also decreases with a higher heartwood to sapwood ratio in mature wood.

Biomass allocation

Functional growth analysis allows the study of resource allocation and plant performance in a given environment. Briggs, Kidd and West (1920) observed a close resemblance of the development of biomass-based relative growth rates (RGR, kg kg^{-1} d^{-1}) with the leaf area per plant mass (leaf area ratio, LAR, m^2 kg^{-1}) of maize. This suggests that biomass allocation between leaves, and other plant parts determines the whole plant biomass growth rate, which means that the net assimilation rate (NAR; plant mass increase per leaf area per time, kg m^{-2} d^{-1}) stays roughly constant over the plant's life cycle. This can be expressed in the growth formula $\mathrm{RGR} = \mathrm{NAR} \cdot \mathrm{LAR}$, which states that structural growth is exponential as long as NAR and LAR stay constant. Biomass allocation to different plant parts depends on environmental factors, particularly nutrient availability, water availability, and temperature (Poorter et al., 2012). However, allocation alone does not determine LAR, because the leaf mass per leaf area also depends on light intensity and temperature (Poorter et al., 2009).

Growth at the community and ecosystem level

The analysis of plant growth fundamentally changes when the analysis focuses on communities rather than individual plants, which requires the additional reference metric *per area* (Table 2). Individual plants may grow slower, or reach smaller final sizes because of competition for resources (Weiner, 1990). On the other hand, complementarity effects in space or time, as well as positive species interactions can lead to higher production per unit ground area in systems with higher diversity compared to the average production of the same species growing in monocultures (Cardinale et al., 2007).

At the ecosystem level, plant growth during a given period per unit ground area is measured by the net primary production (NPP, kg m^{-2} y^{-1}). Depending on the research question NPP is expressed in total plant biomass, carbon mass, or occasionally as calorific value ("fixed energy"; kJ m^{-2} y^{-1}). When expressed in carbon mass, NPP is the difference between all plant carbon uptake (gross primary production, GPP) and autotrophic respiration (Lieth & Whittaker, 1975). The subtraction of heterotrophic respiration results in the net ecosystem production (NEP), the change in the ecosystem carbon pool (Figure 2f; Woodwell & Whittaker, 1968). Net primary production can also be expressed as total biomass change plus the sum of all biomass losses from litterfall, etc. during a given time period.

For mature ecosystems it is expected that the long-term mean carbon pools stay approximately constant. Therefore, the term "growth" is avoided for the analysis of ecosystem carbon pools, and it is only used when the mean carbon pool changes as a result of changing environmental conditions (Schimel, 1995). In managed systems, such as forestry and agriculture, the variable of interest is not the total biomass, but the "useful" biomass, or yield. Conceptually, this is similar to the biomass change of the desired plant part such as stems or grains, with the considered time period being

one harvest cycle. (If the biomass losses are zero, yield is similar to NPP.)

2.3.   The How. Growth measurement methods

In this section I present different methods for measuring growth at different spatiotemporal scales (Figure 2), and discuss in which frameworks they can be useful.

Saptiotemporal analysis of tissue and organ growth

Quantifying where and when growth occurs in a tissue or an organ is the first step towards understanding the establishment of its shape. One approach is to study the relationship between cell proliferation and growth (Figure 2a), and many kinematic studies have reported joint estimates of cell division and expansion rates since the pioneering work of Erickson and Sax (1956). However, only recently has live confocal microscopy enabled the direct imaging of cell production and tissue growth over several cell generations in multicellular tissues. It has been achieved in *Arabidopsis*, on a shoot apical meristem (Willis et al., 2016), a sepal (Hervieux et al., 2016; Hong et al., 2016), and an entire leaf (Fox et al., 2018). While many researchers interested in morphogenesis are also interested in cell proliferation, most methods employed to quantify spatiotemporal patterns of growth actually do not rely on cellular variables. The general principle is to identify or generate landmarks on the growing tissue, and to track them over time using a microscope or a camera. Natural landmarks may be tracked such as cell vertices (Kuchen et al., 2012), trichomes (Lipowczan, Piekarska-Stachowiak, Elsner & Pietrakowski, 2013), or vein junctions (Taylor et al., 2003). Any identifiable feature can be used to automatically track entire leaves at late stages of development by optical flow analysis (Schmundt et al., 1998). For early stages of development, confocal microscopy coupled to image analysis software is most suitable (Barbier de Reuille et al., 2015; Bassel & Smith, 2016),

but this technique requires plants to be stained or genetically transformed so that cells can be properly imaged. Landmarks may also be artificially added on the surface using ink spots (e.g. Granier & Tardieu, 1998b; Das Gupta & Nath, 2015), or fluorescent particles (Remmler & Rolland-Lagan, 2012). Alternatively, clonal or sector analysis may be used to compare the rate and direction of growth across different regions of an organ. The principle is to genetically mark individual cells at an early stage, and to visualize their lineage at a later stage. This can be achieved by chimeric, heat-shock induction of antocyanins (Rolland-Lagan, Bangham & Coen, 2003), or fluorescent proteins (Kuchen et al., 2012) in adapted genetic backgrounds.

Saptiotemporal analysis of tissue and organ growth

Leaves

Expansive leaf growth is typically approximated from leaf length or area measurements, but ignoring thickness (Figure 2b). Leaf area is defined as the projected area of the fresh leaf lamina (Cornelissen et al., 2003). However, in functional growth analysis, petiole and rachis are also included for the estimation of specific leaf area. In some cases there are considerable differences between projected and real surface area, for example in buckled leaves (Nath, Crawford, Carpenter & Coen, 2003), or in cylindrical leaves such as pine needles (Grace, 1987). For harvested leaves, the area can be measured using scanners (e.g. O'Neal et al., 2002). In this case, a time-course of average leaf growth is established from multiple, destructive harvests.

To increase measurement frequency and precision, auxanometers have been developed to automatically record one-dimensional shoot or leaf elongation by tracking growth induced displacements. Early examples include the mechanical registration on a rotating cylinder (Pfeffer, 1903), or the recording of the voltage output of a linear variable differential transformer (Hsiao et al., 1970). For the measurement of two-dimensional leaf

area growth, an auxanometer (leaf area meter) has been developed that records the displacement of multiple markers using image analysis (Mielewczik et al., 2013; Chapter 3) . This type of auxanometers rely on the application of forces to keep the organ extended, so that the recorded movements truly reflect growth. This method is not suitable for small or fragile organs. Furthermore, the mechanical stress could alter growth (Walter et al., 2002), which needs to be ruled out in preliminary control experiments; see Chapter 1.

A direct measurement of individual leaf area and orientation is possible fron three dimensional reconstruction, for example using light-field cameras (Apelt et al., 2015), or commercial laser scanning systems (Dornbusch et al., 2012; Kjaer & Ottosen, 2015). A truly 3D volume measurement of single leaves (i.e. accounting for leaf thickness) can be achieved with X-rays (Pfeifer, Mielewczik, Friedli, Kirchgessner & Walter, 2018), but not with laser scanning (Dupuis, Holst & Kuhlmann, 2017).

Roots

The measurement of root architecture and growth in situ is inherently difficult. In turn, many laboratory-based methods have been developed (Zhu, Ingram, Benfey & Elich, 2011). The continuous measurement of root elongation requires cultivating the plant in a transparent growth medium. Often, root growth is limited to a plane to simplify root tip tracking (Neufeld, Durall, Rich & Tingey, 1989). Systems with automated image acquisition and analysis allow the continuous measurement of a high number of plants (Nagel et al., 2012; Wu et al., 2018). Such setups limit the size of plants that can be analysed, and may not accurately represent unrestricted growth in soil (Hargreaves, Gregory & Bengough, 2009). In the field, minirhizotron tubes allow the observation of root production and turnover (Johnson, Tingey, Phillips & Storm, 2001), with dedicated software available for image analysis (Zeng, Birchfield & Wells, 2008).

Stems

For trees, growth of the whole stem is hard to measure as it would require to accurately quantify the biomass allocation, or volume increase along the whole stem and branches. However, total stem biomass can be estimated from height and diameter based on statistical models (e.g. Repola, 2009). This approach is useful for forest inventories (see below), and could also be applied to estimate the growth of individual trees if the measurement interval is long enough to observe an effect that is above the model uncertainty. Stem volume can also be reconstructed from terrestrial lidar measurements (Raumonen et al., 2013), and biomass can be estimated based on average wood density. The absolute radius change of woody stems can be measured using band or point dendrometers (Zweifel et al., 2010). Point dendrometers with automated data logger allow a high sampling frequency, but only a limited number of measurement points per stem.

Reproductive organs

Some methods cited above also apply to reproductive organs depending on their morphology. For instance, the variations in diameter of large fruits (e.g. Higgs & Jones, 1984), or the changes in length of long styles (e.g. maize silks, Turc, Bouteillé, Fuad-Hassan, Welcker & Tardieu, 2016) can be monitored using displacement transducers at a daily or hourly timescale. At the hourly timescale, these devices record patterns of contraction and expansion; these data are useful to understand organ water relations. Nonetheless, displacement transducers are a low-throughput technology and imaging methods are being developed to monitor the development of reproductive organs at a high throughput (e.g. maize silks and ear, Brichet et al., 2017).

All organs

Finally, optical projection tomography allows visualizing detailed internal structures and gene expression patterns in any organ (Lee et al., 2006) up to the whole-plant level for small specimens (Lee et al., 2016).

Growth at the plant level

Imaging methods

In recent years, various plant phenotyping methods emerged that allow the measurement of plant traits in a semi-automated manner for hundreds of plants (Fiorani & Schurr, 2013; Gibbs et al., 2016; Tardieu et al., 2017). The rapid developments in digital photography, computer vision algorithms, deep learning, and computing power, have also made it possible to automatically and non-invasively measure shoot growth using relatively cheap devices (Tsaftaris & Noutsos, 2009; Paulus, Behmann et al., 2014; Pound et al., 2017). For herbaceous grasses it is possible to predict fresh and dry biomass using side view images (Tackenberg, 2007). Therefore, this simple approach is often used for the observation of monocot crops in phenotyping systems (e.g. Fahlgren et al., 2015; Knecht et al., 2016). Other features such as shoot height, or leaf count can also be extracted. For eudicots, the perceived shoot area as observed by one top-view camera is often directly used to approximate expansive growth (e.g. Leister et al., 1999; Dobrescu et al., 2017; Vasseur et al., 2018). This requires that the leaf expansion mainly occurs in a plane so that the distance between the camera and the object remains the same, which is the case for young *Arabidopsis thaliana* or *Nicotiana tabacum*. A better representation of shoot size can be achieved from three-dimensional reconstruction (Gibbs et al., 2016). However, a general limitation of vision-based methods is the occlusion of plant parts. Furthermore, outdoor measurements may be restricted or inaccurate due to direct sunlight, rain drops, or wind movements, depending on the method. Most

of these methods measure shoot growth, with only few studies also measure root growth simultaneously (Nagel et al., 2012; Ruts, Matsubara & Walter, 2013).

Direct determination of biomass

All methods discussed so far rely on size measurements to approximate expansive growth, or to estimate structural growth based on statistical models. The direct measurement of dry matter content, or chemical analysis (NSC, nitrogen) requires destructive harvesting. For reliable model fitting it is recommended to have a relatively high sampling rate (Paine et al., 2012). Alternatively, lysimeters combined with measurements of net water balance enable estimating a daily (dry) biomass increase on individual potted plants without destructive harvest (Halperin, Gebremedhin, Wallach & Moshelion, 2017).

Growth at the ecosystem level

At the landscape level, the ways we measure plant growth change fundamentally because the reference metric moves from individual organs of plants to a unit surface area. Apart from eddy covariance gas exchange measurements (Baldocchi et al., 2001), and perhaps large microcosm lysimeters, it is impossible to accurately track below-ground and above-ground processes simultaneously. Eddy covariance measurements track net ecosystem productivity, not plant growth directly, and their interpretation and interpolation is biased, as only homogenous, undisturbed sites are monitored (Körner, 2003c).

Aboveground biomass can be extrapolated from vegetation sampling and tree biomass allometric relationships (S. Brown, Schroeder & Birdsey, 1997), assuming constant growth patterns along the stem and branches, which may not be warranted (Chhin, Hogg, Lieffers & Huang, 2010). Similar to individual trees, biomass per unit surface area can also be estimated

from terrestrial lidar measurements, which increases the measurement precision compared to allometric equations (Calders et al., 2015). Additionally, airborne lidar measurements allow the sampling of large areas (Lim, Treitz, Wulder, St-Onge & Flood, 2003). Unless they are carried out over the same area multiple times, these methods can only be used to assess biomass stocks, rather than vegetation growth rates.

Ecosystem productivity can be estimated from remotely sensed indices such as the normalised difference vegetation index (Tucker, 1979), or the enhanced vegetation index (Huete et al., 2002). These methods are most effective at low leaf area indices, because they rely on the reflectance of light, which levels off at high LAIs (Asner, Scurlock & Hicke, 2003). Satellite-based observations have relatively low spatial and temporal resolutions. A way to overcome some of these shortcomings is vegetation monitoring using digital cameras, called near surface remote sensing ("phenocams"; Richardson et al., 2007; Sonnentag et al., 2012). Such approaches essentially measure greenness, which is only a limited approximation of plant growth. It is for example not possible to precisely predict the start of season for evergreen forests since the greenness only changes slightly over a year course (Toomey et al., 2015). Also, in short periods of drought the leaf colour remains largely unchanged while photosynthesis and growth are reduced. Litter traps are an extremely simple but effective method for estimating long-term leaf productivity, which, at constant carbon use efficiency, correlates well with stem growth.

Measuring below-ground (root) growth over large areas is very difficult. Apart from minirhizotrons (see above), ingrowth cores allow rough estimates, but are constrained to certain soil depths and difficult to extrapolate to the whole soil profile. A very tight and universal correlation between litter production, soil respiration, and root growth was found (Raich & Nadelhoffer, 1989), so that over short timescales and large areas, litterfall may be the best proxy for otherwise difficult to measure below-ground plant growth.

Again, monitoring long-term changes in soil carbon stocks is more relevant than direct estimates of below-ground growth (Scharlemann, Tanner, Hiederer & Kapos, 2014; Bailey et al., 2018). In summary, estimating plant growth at ecosystem level is very difficult, and ultimately perhaps not necessary, as changes in C pools (the net balance of all C fluxes over time) will be more important than changes in C fluxes (Leuzinger & Hättenschwiler, 2013).

2.4.   The Why. Interpretation and application of results

In the previous sections, I discussed the wealth of definitions for plant growth (the "what"), and the myriad of methods to measure it (the "how"). I showed that understanding exactly what is measured by which method and how to integrate results at various spatiotemporal scales is pivotal. In this last section, I discuss why measuring plant growth is so essential in the first place. There are three areas of research with a fundamental interest in plant growth in the widest sense: (1) basic research interested in the genetic basis and molecular regulation of plant functioning, (2) agricultural and forestry research that is ultimately interested in the quality and quantity of harvest yield of various plant organs, and (3) basic and applied ecological research, with an urge to understand the fundamental mechanisms of plant-environment interactions and productivity. The ongoing development of plant growth measurement methods makes it increasingly possible to quantify multiple growth processes simultaneously. Particularly high throughput phenotyping for agricultural research and plant breeding generates vast amounts of data that can be used for trait identification and model building (Tardieu et al., 2017). For ecosystems, it is currently not feasible to generate similar quantities of growth data for individual plants, but methods such as phenocams and eddy covariance integrate over communities at

a high temporal resolution and the combination of multiple locations allows for global extrapolations (Baldocchi et al., 2001; Richardson et al., 2007).

The multitude of growth measurement methods requires a clear description of the processes they quantify (Table 2). I feel that the applied methods often imply the definition of "growth", rather than the other way round. Because of the coupling of different growth processes, imprecise definitions may still be sufficient for certain research questions. However, particularly at sub-daily timescales it is important to distinguish between irreversible structural and expansive growth, and reversible phenomena. For the understanding of growth regulation it would be necessary to analyse processes at the sub-cell level, which is beyond the scope of this review. Therefore, Figure 1 offers a general overview, trying to tease apart the different processes and point out where they occur simultaneously. For example, cell proliferation (Figure 1a) combines DNA, protein, and cell wall synthesis with cell extension processes and other aspects of the cell cycle, such as size control. Similarly, long-term cell expansion combines cell wall synthesis and cell extension.

As pointed out in Section 2.2, most plant growth measurement methods actually describe changes in size, and may therefore not accurately represent changes in biomass or structural growth. For example, leaf area measurements cannot account for changes in leaf thickness or density. Leaf mass per area (LMA) increases with plant age in *A. thaliana* (Weraduwagel et al., 2015), and with leaf age in several evergreen species (Wright, Leishman, Read & Westoby, 2006). Furthermore, LMA strongly depends on daily photon irradiance and temperature (Poorter et al., 2009). An extreme example of uncoupling is that short term stem diameter variations negatively correlate with stand carbon flux measurements, despite strong positive correlations for monthly and yearly observations (Zweifel et al., 2010). Also, it may not be accurate to assume that the measured plant part is representative for the growth of the whole plant, as biomass allocation depends on

the environment, including plant density effects (Poorter et al., 2012). Such examples demonstrate the need for growth measurements at multiple spatiotemporal scales.

Genetic and environmental effects on growth

One aim of growth measurements is to disentangle ontogenetic from environmental effects on growth (Walter et al., 2015; Tardieu et al., 2017). Growth can be limited by the lack of resources, that is nutrients or carbohydrates, or by unfavourable growth conditions, particularly extreme temperatures, or water (soil water availability and atmospheric vapour-pressure deficit). Knowledge about environmental influences on growth can be gained from individual experiments with treatment-control comparisons, or from pooled data in the form of dose-response curves (Poorter, Niinemets, Walter, Fiorani & Schurr, 2010). To a certain degree these approaches do not account for the dynamic nature of environmental variables and growth responses. Here, continuous growth measurements can help to separate intrinsic controls and environmental factors. For example, maize leaf elongation shows immediate responses to changes in water potential of the root medium (Acevedo et al., 1971). On the other hand, *Arabidopsis* leaf expansion follows a circadian rhythm which is not affected by different (sub-daily) temperature curves, when the daily temperature sum is the same (Poire et al., 2010). Long-term observations are essential for the description of initial stress reactions and subsequent growth adjustments, such as the decrease and later (partial) compensation of leaf cell proliferation under osmotic stress (Skirycz et al., 2011). The use of thermal time is favoured over calendar time to account for the strong temperature dependence of growth processes (Parent & Tardieu, 2012).

At the cell level, the variability of environmental effects on growth becomes particularly apparent. For example, in sunflower leaves water stress causes a reduction in final cell number or in cell area depending on the time

of the water deficit (Granier & Tardieu, 1999b). Stems with seasonal growth also show a huge variation in cell size between earlywood and latewood (Cuny, Rathgeber, Frank, Fonti & Fournier, 2014), and between different environments tree diameter growth can vary as a result of increased cell size rather than cell number (Deslauriers et al., 2008). However, for some questions the cellular characteristics of a growth response are not important and the observation of the whole organ is sufficient (Granier & Tardieu, 2009). Under this premise, plant phenotyping allows for the description of various traits such as radiation use efficiency (Cabrera-Bosquet et al., 2016), or water use (Vadez et al., 2015). As it is not feasible to experimentally test for any possible environmental stress scenario, growth models have to be built based on limited data availability, and can then be tested against real world performance (Tardieu et al., 2017).

Plant growth modelling

Leaf area expansion is central in most crop models since it determines the leaf area index, and thus light capture from the Beer-Lambert analogy (Monsi & Saeki, 2005), and C fixation using the radiation use efficiency concept (Monteith, 1977). A broad distinction between model types can be made, depending on how growth in surface is formalised (Parent & Tardieu, 2014). In a first type of models (e.g. GECROS, Xinyou & Van Laar, 2005), the C fixed by the plant is then "transformed" into leaf area using specific leaf area as a parameter. Leaf expansion is thus determined by carbon assimilation and implicitly, under stressful conditions, leaf growth is reduced because photosynthesis is reduced. Several studies point to the limit of putting photosynthesis as the sole driver of leaf expansion, in particular under stressful conditions (Bogeat-Triboulot et al., 2007; Hummel et al., 2010; Tardieu, Parent, Caldeira & Welcker, 2014). The strongest evidence is probably that photosynthesis is reduced much later than growth is reduced under water stress (Muller et al., 2011). Other model types recognise that light

capture and leaf growth are two independent processes with some feed-backs. Leaf expansion is essentially driven by physical constraints, either linked to the hydraulics (Boyer & Silk, 2004), or to the mechanics of the cell wall (Cosgrove, 1993) as formalised in the Lockhart model (Eq. 1; Lock-hart, 1965). While no crop model actually uses the Lockhart equation, these models formalize climate-based limitation of leaf expansion (Jamieson, Se-menov, Brooking & Francis, 1998; Lizaso, Batchelor & Westgate, 2003). A better understanding of what are the main drivers and constraints to leaf expansion is thus crucial in order to propose relevant formalism of the pro-cesses in crop models.

Much like in the smaller-scale crop models, in terrestrial biosphere mod-els we have a choice of modelling plant growth on the basis of C source (photosynthesis), or C sink (mainly structural growth) processes. The past fifty years saw a focus on carbon source processes rather than on the pro-cesses affecting the net sink (ultimately NPP) directly. Net primary pro-ductivity is impossible to measure in its entirety in situ, while the ease of measuring C uptake at the leaf level has certainly contributed to a wide-spread perception that carbon sources control carbon sinks (Körner, 2015). To date, source-driven algorithms to estimate growth are still reflected in the architecture of almost all vegetation models (Fatichi et al., 2019). However, there have been several recent attempts of sink limited vegetation model-ling (e.g. Leuzinger, Manusch, Bugmann & Wolf, 2013; Fatichi, Leuzinger & Körner, 2014; Guillemot et al., 2017). This realisation that growth pro-cesses are often directly controlled by environmental conditions is perhaps the key reason why direct plant growth measurements are fundamentally important, and certainly an underlying motivation to write this review.

2.5. Conclusions

The study and modelling of plant growth is an increasingly important research field, particularly in a changing climate. Because of the different aspects of growth (Figure 1) and of vastly different perspectives on plant growth depending on the spatiotemporal scale (Figure 2) it is necessary to clearly define growth metrics (Table 2). Despite the ongoing methodological advances, it is extremely hard to integrate different growth aspects and scales into holistic plant growth measurements. It is only (partly) possible in a controlled glasshouse environment, and virtually impossible in situ. At the same time, scaling from organ level observations to plant or ecosystem level may not be possible, as it would require detailed knowledge of allometric relationships. Therefore, we have to be extremely cautious when using the term "growth". On the other hand, these methods allow for ever more detailed quantification of plant development, particularly in agricultural crops and the model species *Arabidopsis*.

Growth measurement in herbaceous plants is much simpler than in woody plants, because of their size and life cycle. Therefore, agricultural research and ecology are likely to face different challenges going forward. In agriculture, the focus is increasingly on the integration of growth and environmental data for model building, which requires new approaches in terms of data management and analysis (Tardieu et al., 2017). In an ecological context, direct plant growth measurements are still under-represented, mainly for logistic reasons. At this scale, coarse "opportunity for growth" models based on leaf temperature, water supply, nutrient availability, ontogeny and growing season length, may be best suited to model future plant growth. The key challenge in plant growth research remains firstly the paucity (or complete lack) of commercially available sensors to measure leaf, root, and stem growth in situ, and secondly a lack of unified concepts and definitions of plant growth. I hope that with this review I am able to shed some light

onto the hidden complexities of the term "plant growth", which appears deceivingly simple at first sight.

Chapter 3
Measurements using Marker Tracking

I measured in situ leaf growth on adult Avicennia marina mangrove trees at a 5 minute resolution. I observed a consistent diel growth pattern with considerable leaf area shrinkage in the morning, re-expansion in the afternoon, and growth at night. There was also a strong correlation between instantaneous leaf area change and turgor, suggesting that growth was driven by plant hydraulic status rather than by the rate of carbon uptake.

Prelude

Instantaneous leaf growth is rarely measured in the field. Recent exception are the tracking of leaf elongation of different grasses (Nagelmüller et al., 2016), or of palm frond elongation (Zhen et al., 2017). There are also a few classical studies, see Körner (2003a, p. 226) for an overview. To my knowledge this is the first study measuring in situ leaf area growth on a mature tree over a prolonged time period.

This chapter has been pulished: Hilty, J., Pook, C., & Leuzinger, S. (2018). Water relations determine short time leaf growth patterns in the mangrove *Avicennia marina* (Forssk.) Vierh. *Plant, Cell & Environment*, 42(2), 527-535. doi:10.1111/pce.13435, © John Wiley & Sons Ltd. I extended the methods section to include details which were too extensive for the journal article.

3.1. Introduction

Plant growth is the single most important process to sustain terrestrial life on earth. The net accumulation of phytomass can be quantified via a number of direct (dendrochronology, stem radius variation, biomass harvest, root ingrowth cores) or indirect (eddy covariance, remote sensing) methods. Most of these methods integrate growth over long time spans, and do not allow to quantify exactly when growth occurs during the day or night. Also, particularly modelling studies continue to use photosynthesis as a driver of plant growth (e.g. Mercado et al., 2018), despite evidence showing that in natural environments, other factors such as temperature, water, or nutrient availability directly limit growth long before photosynthesis is affected (Fatichi et al., 2014). The abundance of photosynthesis data and their misinterpretation as a proxy for growth exists at least partly because measurements of leaf gas exchange have become relatively straightforward, with easy to use and portable instruments. In contrast, non-destructive measurements of high-resolution leaf and plant growth are technically much more challenging, particularly in the field. Nevertheless, measuring instantaneous leaf growth is pivotal for understanding the influence of environmental and endogenous drivers on plant resource efficiency and performance (Walter et al., 2009). A fundamental understanding of the mechanism of plant growth will also inform a new generation of carbon sink driven ecosystem models (Leuzinger et al., 2013).

Leaf growth is approximated by observing leaf area over time. The development of leaf area is the result of three main processes: Cell proliferation, expansive cell growth, and elastic cell deformation (swelling and shrinkage). It is not possible to clearly distinguish between the three processes from non-destructive measurements, especially in eudicotyledons where all processes can occur simultaneously in the same region of the leaf. Therefore, net leaf area change is often equated with growth, which ignores

elastic deformation. In this chapter, I adopt the terminology from the analysis of stem radius variations, which has long dealt with similar analytical challenges, and that postulates that growth is negligible in periods of shrinkage (Zweifel et al., 2016). Periods of elastic shrinkage and swelling are called water deficit periods, and are distinguished from periods with irreversible growth.

Traditional auxanometers that automatically measure plant or leaf elongation rely on the application of a tensile force to keep the object stretched, and they record changes in the position of the tip (Hsiao et al., 1970; Pfeffer, 1903). A similar principle has also been used to measure leaf elongation of grasses in the field (Nagelmüller et al., 2016). In recent years, new methods emerged that use digital image analysis to quantify plant characteristics (Minervini et al., 2015). However, many of these methods are designed for indoor use, and do not focus on high-resolution growth measurements. Outdoor conditions are particularly challenging because direct sunlight can interfere with the sensor measurement, and electronic components require protection from rain, humidity, and overheating. A relatively simple method to measure leaf area growth of eudicotyledons is to fix a leaf in a plane, and observe it through a camera with the image plane parallel to the leaf (Schmundt et al., 1998; Walter et al., 2002). Relying on this principle, Mielewczik et al. (2013) presented a semi-automated image analysis software based on marker tracking, and they also showed the general feasibility of their method for field studies.

For eudicotyledons two different instantaneous leaf growth types have been described. One growth form shows the highest growth rates around dawn and the lowest rates around dusk, while the other form shows a reversed pattern with growth peaking around dusk (Walter et al., 2009). In contrast, leaf elongation in monocots largely follows meristem temperature, and the highest growth rates occur at midday (Walter et al., 2009). However, in *Zea mays* leaf elongation rates during daytime are lowered by evaporative

demand when expressed in thermal time (Sadok et al., 2007). Eudicotyledons show a diel leaf growth cycle that is partly controlled by the circadian clock (Poire et al., 2010; Ruts et al., 2012). A circadian regulation is thought to optimise resource use throughout the day, and to buffer against short-term environmental fluctuation that are especially pronounced for eudicot leaves (Walter et al., 2009). For example, growth does not respond to short-term temperature changes (Poire et al., 2010), and the circadian clock seems to be involved in the overnight partitioning of starch (Apelt et al., 2017). Young *Arabidopsis thaliana* leaves have lowered growth rates at night, which is associated with carbon metabolism. After a few days, this shifts to lower growth rates during daytime, when leaf expansion is limited by hydraulics (Pantin et al., 2012; Pantin et al., 2011).

Here, I present the first data on in situ leaf growth of a mature tree. I measured instantaneous leaf growth on an *Avicennia marina* subsp. *australasica* tree over several weeks using the leaf fixation method. *Avicennia marina* is highly salt tolerant, and is therefore an interesting model species to study the interplay between environmental conditions, water relations, and growth processes (Ball, 1988). My study site also has the advantage of a monospecific stand, where even mature tree crowns are easily accessible, avoiding confounding of succession and interspecific competition. My aims were (1) to test the usability of instantaneous leaf growth measurements in situ in adult trees, (2) to identify when exactly leaves grow during the day or night at a sub-hourly resolution, and (3) what environmental or plant-intrinsic parameters drive this growth.

Figure 3. Example of a picture taken by the leaf growth meter with high contrasts between sunlit and shaded areas. The bar at the bottom left gives the scale at the leaf plane.

3.2. Materials and methods

Instrument Design

I modified the method described by Mielewczik et al. (2013) for long-term outdoor use. The basic principle of this method is to fix the leaf in a frame to limit horizontal and prevent vertical movement (Figure 3). A camera was mounted with the image plane parallel to the leaf, and image time series were acquired. Leaf expansion was approximated by tracking artificial markers placed at the leaf fixation points. The development of the area spanned between the markers served as a proxy for relative leaf area change.

For the application of this method in the field I designed a compact

and weatherproof instrument, which is easy to install and allows reliable data acquisition. Pictures were taken using a Pi NoIR v2 camera controlled by a Raspberry Pi 1 B+ single board computer (Raspberry Pi Foundation, Cambridge, United Kingdom). The Pi NoiR v2 does not have an infrared filter, which makes night vision possible. To continuously measure leaf growth at night I used two infrared light-emitting diodes (LEDs) with a peak wavelength of 850 nm, which were attached to the Pi NoIR camera (Shenzhen Xingmu Technology Co., Ltd, Shenzhen, China; purchased on alibaba.com).

Pictures were taken every five minutes at resolutions of 1 and 8 megapixels (MP); JPEG compression was applied to reduce the file size. The 1 MP images were uploaded to a server which allowed for continuous monitoring of the experiment, and also served as a backup. The infrared LEDs were switched on five seconds before taking a picture, and switched off afterwards to minimise any potential effect on physiological processes. This was controlled using an Arduino Nano board (Arduino SA, Chiasso, Switzerland) connecting the Raspberry Pi with a relay in the LED's power supply. A detailed sketch of the technical components is given in Figure 4. All processes were executed in a Python script (version 3.5, Python Software Foundation, Delaware, USA) running on the Raspberry Pi.

The instrument design included a frame where the leaf was fixed, a housing parallel to that frame containing the camera and LEDs, a separate housing for the Raspberry Pi and other components, and a third external housing containing a Huawei E5330 mobile 3G router (Huawei Technologies Co. Ltd., Shenzhen, China), and a power converter. The frame and camera box were rotated upwards by an angle of 20°, which has been found to be a suitable rotation for the experiment species *A. marina*. The camera was placed 25 cm above the leaf frame. For the design I used the free software OpenSCAD (Figure 5; Kintel, 2015); individual elements were laser cut from 6 mm thick acrylic and glued together. During the experiment the
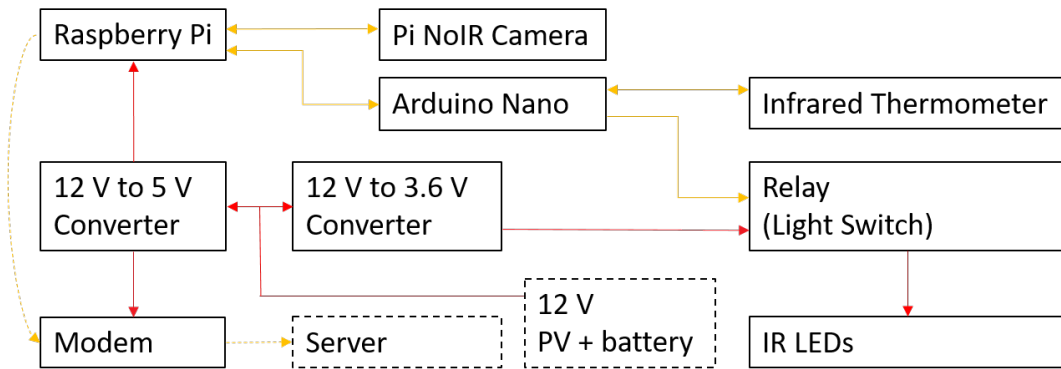
Figure 4. Different components of the instrument. Red arrows represent power flow, yellow arrows represent information flow. Dashed arrows represent wireless connections, and dashed boxes represent external elements. PV: photovoltaic; IR: infrared; LED: light-emitting diode.

instrument was covered with an aluminium hood for additional rain and radiation protection.

I also attached a Melexis MLX90614ESF-BCI-000-SP infrared thermometer (Melexis N.V., Ieper, Belgium) to the Arduino board with the intention to measure leaf surface temperature. However, the measured temperatures reached unreasonably high peaks of more than 40°C. Therefore, those measurements were not included in the analysis. The thermometer was pointing to the middle of the frame. It has a field of view of 5 degrees, which translates to a measured area of approximately 15 cm^2 at the leaf plane (circle with a radius of 2.19 cm). This means that the whole leaf but also a considerable amount of background was included in the measurement, which may have corrupted the signal.

The instrument was fixed with T-head bolts on a matching frame built with aluminium strut profiles (Bosch Rexroth AG, Lohr am Main, Germany), that was strapped to a horizontal pole. The leaf was fixed and kept flat using five small wooden pegs connected to small lead weights of 7 g each. The surfaces of the pegs were coloured black using a waterproof pen with one spot left blank to serve as the marker for the image analysis (Figure 3). The application of tensile forces to the leaf could potentially cause
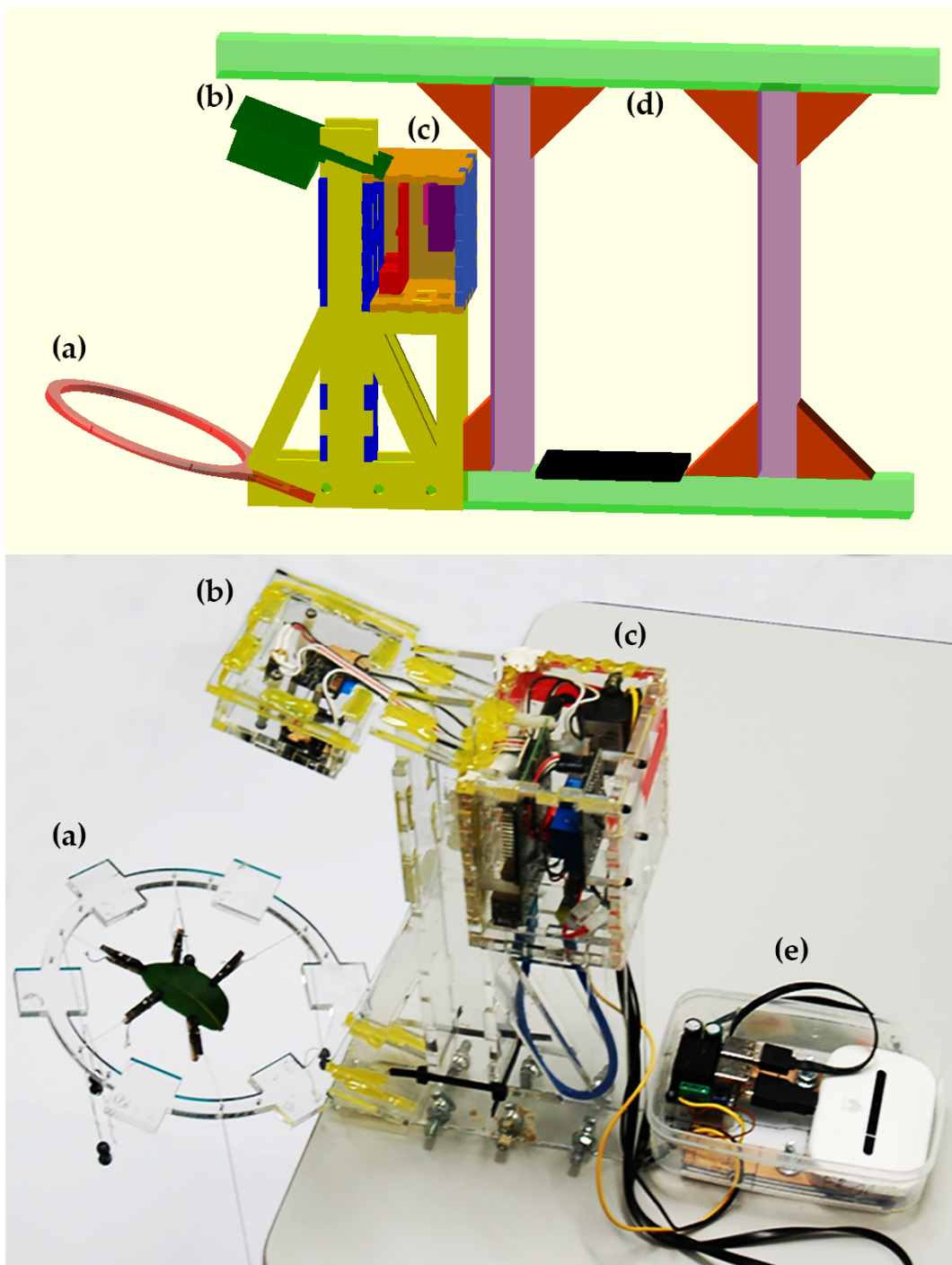
Figure 5. Design of the instrument in OpenSCAD and assembled components. (a) Frame where the leaf is placed. (b) Camera box parallel to frame. (c) Box where electronics component are located; the Raspberry Pi is represented in red. (d) Frame to mount the structure. (e) Additional box with modem and power converter.

changes in growth behaviour. In a control experiment I showed that the treatment did not affect long-term leaf growth in *A. marina* (Figure 6). In general, the forces need to be high enough to keep the leaf in place in windy conditions, but low enough to not impact growth. *Avicennia marina* has quite sclerophyllous leaves, and the leaf was not damaged by the pegs or the tensile force. However, after the experiment the fixation points were clearly visible by a lack of chlorophyll on the adaxial surface and slightly visible on the abaxial surface (Figure 7). Additionally, leaf 1 seemed to have a slight growth reduction at the fixation points at the leaf side (Figure 7a). A general limitation of this method is that it cannot be used for young leaves that are too small or too fragile for fixation. Further, the fixation of leaves can alter growth patterns in species with leaf hyponasty, even when low tensile forces are applied (Walter et al., 2002). I therefore analysed leaf angle variations from unrestricted leaves visible within the picture frames, but while they changed randomly with wind throughout the day, there was no diurnal trend (not shown).

Experiment

The measurements were conducted on a mature tree of the mangrove *Avicennia marina* (Forssk.) Vierh. subsp. *australasica*. The research site was located in the Mangawhai Heads estuary at the east coast of New Zealand's North Island (36.097°S, 174.573°E). In this environment *A. marina* grows in uniform, monospecific forests with trees reaching mean heights of 3.1 m (Tran, Gritcan, Cusens, Alfaro & Leuzinger, 2017). The forest covers an area of approximately 0.8 km^2 located around Tara Creek. Power was available from a small photovoltaic system.

The experiment was conducted on two different leaves on the same tree, first from mid December 2016 to early January 2017, and again from early February to early March 2017. Young leaves at the top of the canopy facing north were selected for the experiment to minimise shading from the instru-
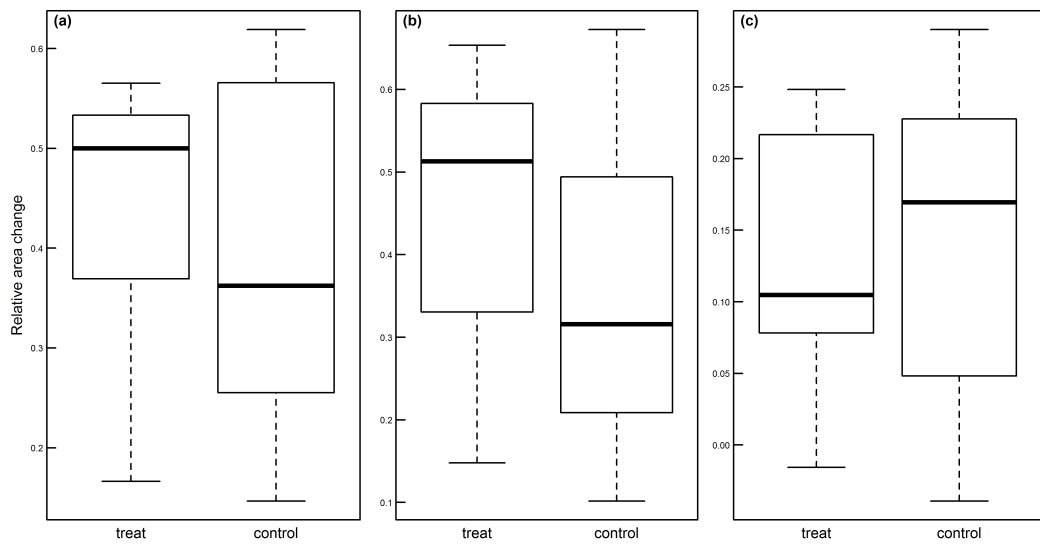
Figure 6. Control experiment testing the effect of tensile forces on the long-term growth of *A. marina* leaves. (a) From 4 to 13 December 2017, a Wilcoxon signed rank test showed that there was no difference between the two groups, $p = 0.625$, $n = 5$. (b) From 4 December 2017 to 28 February 2018, $p = 0.500$, $n = 3$. (c) From 13 December 2017 to 28 February 2018, $p = 1.000$, $n = 5$. During the first measurement period one leaf got damaged, and one got infected by a disease. Therefore, both leaves were replaced.
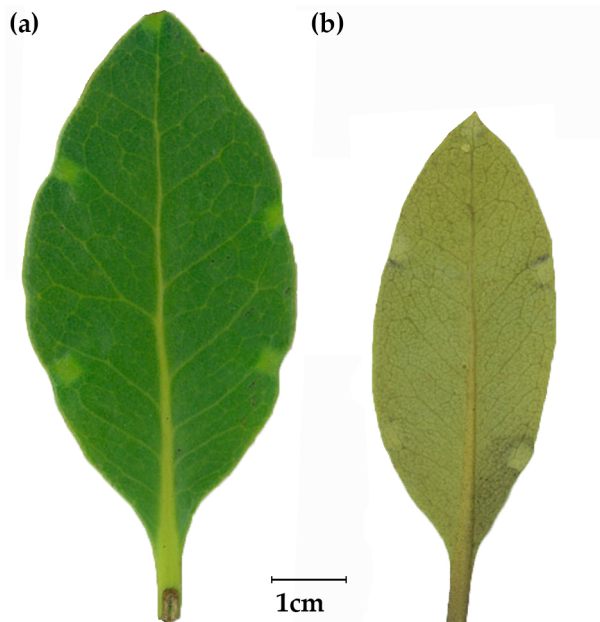
Figure 7. Leaves after the experiment. (a) Adaxial surface of leaf 1. (b) Abaxial surface of leaf 2.

ment. Additionally, for the second run a relatively large leaf was chosen in order to observe growth cessation. To restrict movements of the leaf, the branch on which it was growing was fixed to the strut frame using Velcro straps (Velcro Ltd, Middlewich, United Kingdom). The leaf opposite to the observed one was bent backwards because it would otherwise have obstructed the view of the markers (Figure 3). The final installation is shown in Figure 8. In December I also installed two leaf turgor pressure probes in the same tree (YARA ZIM Plant Technology GmbH, Hennigsdorf, Germany). Those sensors measure a magnetic force between two clamps that is inversely proportional to leaf turgor (Zimmermann et al., 2008). It can only be interpreted as a relative signal of turgor change, because the measured pressure depends on the cell elastic modulus, which can vary with temperature.

During the first run, one thread got stuck in the frame which lead to a bending of the leaf and to a corruption of the growth measurements. The first occurrence of this incident was determined by manually inspecting the pictures, and the time series was stopped at this point. After the second run, the data on the Raspberry Pi was lost completely, and only the 1 MP images on the backup server could be used for the image analysis. The most likely case for the failure was an error in my custom made controlling software, because I did not account for the possibility of no free disk space, and at the same time I forced the software to restart in case of failure causing the system to crash. Comparison of the image analysis with 1 or 8 MP resolution did not show any significant difference, therefore I used the 1 MP images for all analysis to allow for consistency between the two runs.

Environmental data were measured close to the leaf as well as above canopy on a tower approximately 5 m away from the experiment. Leaf illuminance was measured in intervals of one minute using six HOBO UA-002-64 data logger (Onset Computer Corporation, Bourne, USA; spectral range 150 nm to 1200 nm) that were placed around the leaf (Figure 3). Local air

temperature T_{air} and relative humidity, denoted by H_{rel}, were measured in intervals of five minutes using a HOBO Pro v2 U23-002 data logger (Onset Computer Corporation, Bourne, USA) located below to the leaf (Figure 8). The saturation water pressure P_{sat} and vapour-pressure deficit (VPD), denoted by P_{vpd}, were calculated from T_{air} and H_{rel}:

$$P_{\text{sat}} = a \cdot \exp\left(\frac{b \cdot T_{\text{air}}}{c + T_{\text{air}}}\right), \tag{2}$$

$$P_{\text{vpd}} = P_{\text{sat}} \cdot \left(1 - \frac{H_{\text{rel}}}{100}\right), \tag{3}$$

with the coefficients $a = 0.61121\,\text{kPa}$, $b = 17.368$, and $c = 238.88°\text{C}$ for the temperature range from 0°C to 50°C (Buck, 1981).

Above canopy solar radiation was measured using a pyranometer (Model PYR, Decagon Devices, Inc., Pullman, WA, USA; spectral range 380 nm to 1120 nm). Precipitation was measured using a Tipping Bucket Rain Gauge (Model 52203, R. M. Young Company, Traverse City, USA; resolution of 0.1 mm per tip). The precipitation sensor broke between the first and the second experimental run. For the second period, the time of precipitation was determined from inspecting the recorded images, and the intensity was estimated using measurements from the Mangawhai Heads Weather Station, located approximately 2 km from the research site. Potential evapotranspiration (PET) was measured using an ETgage (Model E, Style #54, ETgage Company, Loveland, CO, USA; signal resolution of 0.254 mm). Unfortunately, the sensor broke on 11 February 2017 during the second run, and the data was not included in the analysis. Tidal flooding was reconstructed from previous measurements and data from Land Information New Zealand (2017), see Appendix. All sensors listed in this paragraph had a measurement interval of around five minutes.

I also conducted a seasonal leaf growth experiment from May 2017 until February 2018 to test for seasonal leaf growth variations. The experiment took place at Panmure Basin, Auckland (36.907°S, 174.845°E). I started co-

Figure 8. Installation of the leaf growth meter. The branch was fixed to the strut frame using Velcro straps. The temperature and relative humidity sensor was placed in the radiation shield below the leaf.

horts in fall (May 2017), winter (July 2017), and summer (December 2017, January 2018). For each cohort I selected ten young leaves on five different trees (two leaves per tree). Leaf length and maximal width were measured every few weeks with callipers.

Data Analysis

Relative expansive leaf growth was measured using a custom made marker tracking software similar to *Martrack Leaf* (Mielewczik et al., 2013). I did not use *Martrack Leaf* because it turned out to be sensitive to movements due to wind. However, in non-windy conditions my software and *Martrack Leaf* show similar results (Figure 9). I also conducted a control run with a carbon fibre plate instead of a leaf. I did not observe any systematic diel trends, and the measurement error of the aggregated data was approximately 0.5% (not
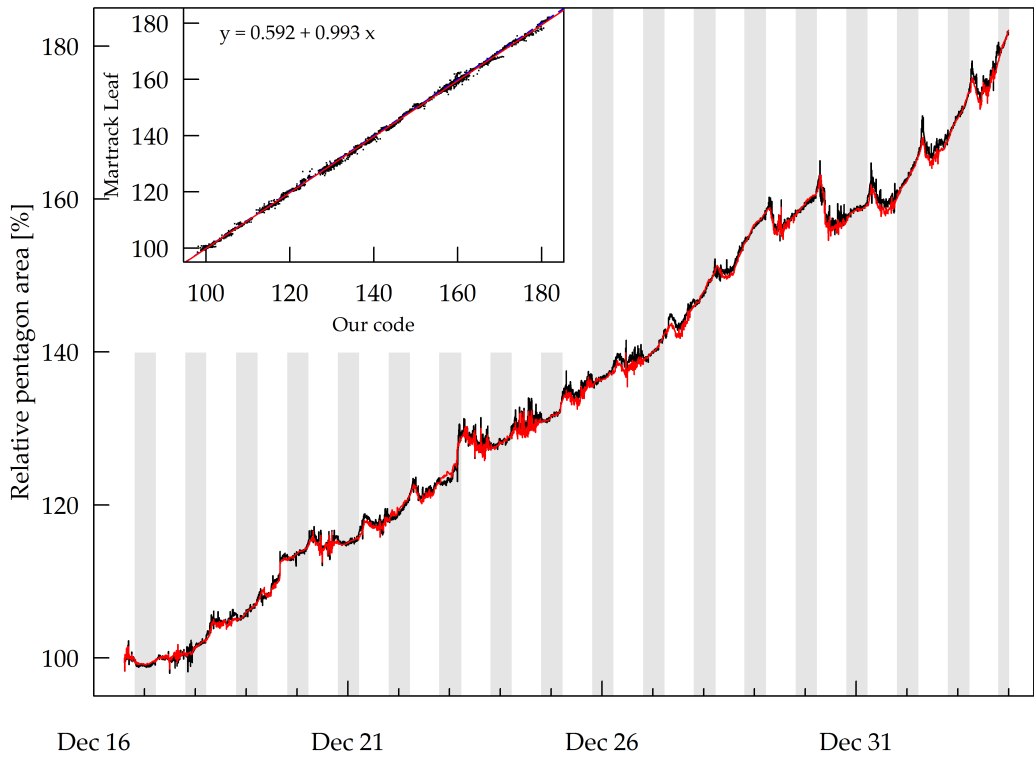
Figure 9. Comparison of my image analysis software (black) with *Martrack Leaf* (red) before outlier removal and smoothing. The inset shows a linear regression in red with the unity line in dashed blue.

shown).

My marker tracking software is semi-automated; in case of misdetections the user needs to redefine the marker location. This happened in windy conditions when the leaf was moved more than the software's maximal search range set at an upper limit of approximately 2.8 mm. The software is a console application written in C++ (Standard C++ Foundation, Redmond, USA) using the open source image analysis library OpenCV (version 3.4.1; Bradski & Kaehler, 2008). The principal functionality is similar to *Martrack Leaf*: (1) Each marker is selected individually in the first image of the time series. (2) The software searches for the markers in each following frame and displays the detected point; the search range can be changed by the user. (3) For each image the area covered by the detected points is calculated and saved in a csv-file together with the filename that contains a time

stamp.

The marker size and shape is determined by the manual selection in the first frame. The user draws a rectangle around the marker and confirms the automated detection. The image is converted to grayscale, and for each region of interest potential markers are detected by histogram equalisation and subsequent thresholding. A suitable threshold was determined before the analysis. In each following frame the marker is detected by searching for it around the previous location in the user defined range, and the best match after histogram equalisation and subsequent thresholding is selected. To account for potential miss-detections due to wind movements or in case of speckles with similar shapes to the marker, the software also tests whether the points are plausible, by comparing them to the previous frame. This approach has a tendency to fail during rain, when glare from raindrops can obscure the markers, or be miss-classified as marker (Figure 10).

The detected marker locations can be noisy due to slight movements of the leaf caused by wind, or due to changes in illumination. Therefore, the measured relative leaf area was adjusted by outlier removal and subsequent smoothing. I applied the *loess* smoothing (Cleveland, 1979; Cleveland & Devlin, 1988) with second degree polynomial regression, weighted least squares fitting, and a neighbourhood of 49 data points, which translates to a smoothing window of approximately four hours. The leaf turgor data was smoothed using the same parameters.

Statistical analysis was conducted using R version 3.4.2 (R Core Team, 2017); environmental data were matched to the nearest leaf area measurement sing the rolling join function of the R package data.table (Dowle et al., 2017). The data from the six light sensors around the leaf was aggregated over the five minutes before a picture was taken. Instantaneous relative area change (c_{rac}) was calculated for every measurement from the smoothed values:

$$c_{rac} = \frac{A_i - A_{i-1}}{A_{i-1}} \cdot 100 \,, \tag{4}$$
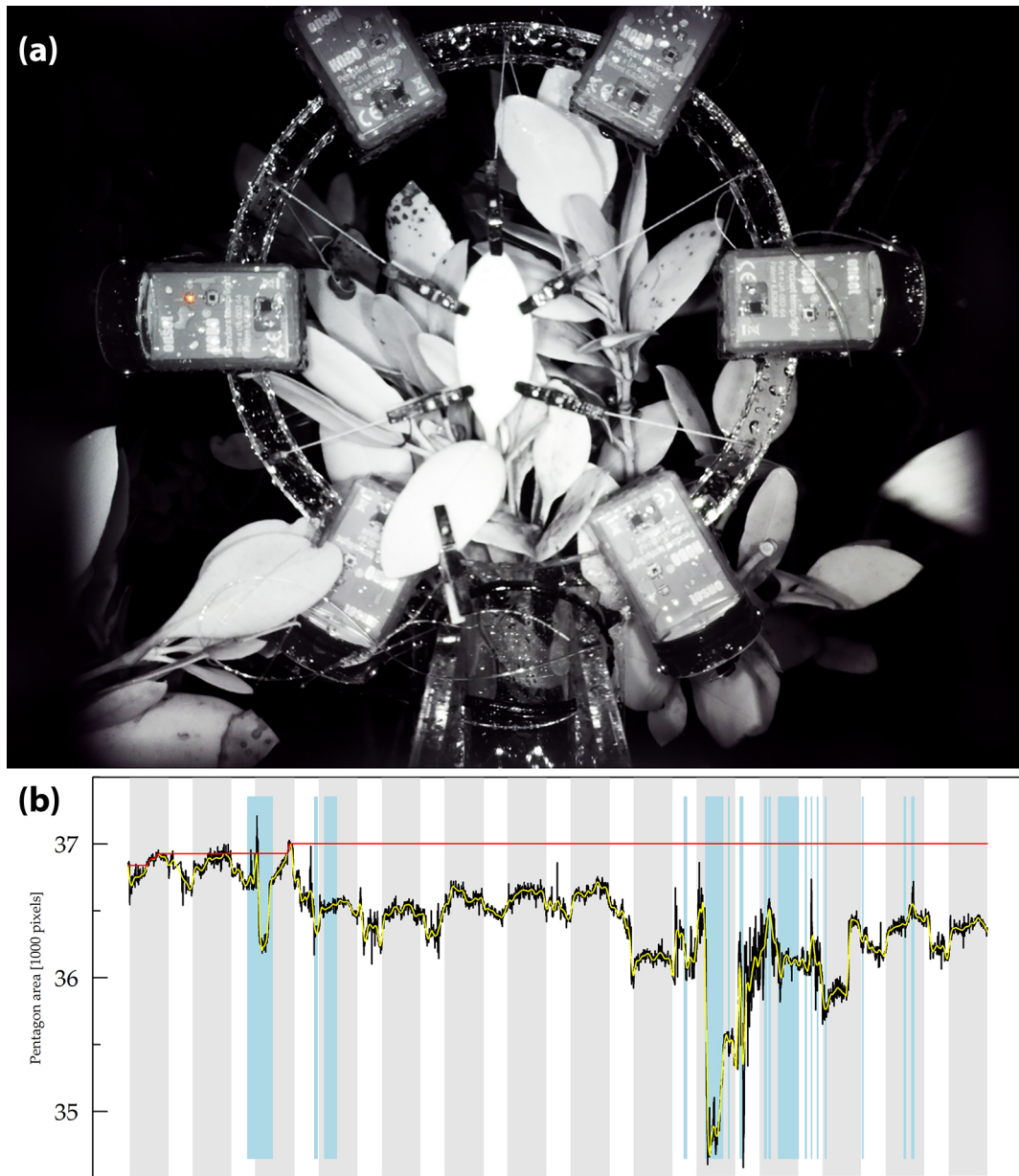
Figure 10. Marker tracking during rain. (a) Example of a picture taken at night during rain. Glare from rain drops may lead to miss-detections. (b) Rain events can lead to temporal tracking errors. Data from the control run with a carbon fibre plate. Blue bars represent rain events, output from image analysis in black, smoothened curve in yellow, and cumulative maximum in red.

where A_i represents the pentagon area for measurement i. The relative growth rate (RGR, denoted as g_{rgr}) was calculated based on the exponential growth formula (Blackman, 1919):

$$g_{\mathrm{rgr}} = \frac{\ln\left(\frac{A_i}{A_{i-1}}\right)}{\boldsymbol{t}_i - \boldsymbol{t}_{i-1}} \cdot 100 \ , \tag{5}$$

where $\boldsymbol{t}_i$ represents a point in time, and the time difference between two measurements is expressed in hours. For periods of leaf shrinkage I calculated the relative *leaf water deficit* (LWD, denoted as d_{lwd}) compared to the previous maximum area:

$$d_{\mathrm{lwd}} = \frac{max\left(A_{j \leq i}\right) - A_i}{max\left(A_{j \leq i}\right)} \cdot 100 \ . \tag{6}$$

Leaf water deficit is similar to the concept of *tree water deficit* used to describe stem shrinkage (Zweifel et al., 2016). A distinction between a water deficit and a growth phase rather than between a shrinkage and an expansion phase assumes that structural growth is largely absent in water deficit periods. During deficit periods, RGR does not actually measure growth, but rather elastic leaf area changes. Normalised leaf turgor change (c_{tgr}) was calculated like:

$$d_i = \frac{1}{P_i} - \frac{1}{P_{i-1}} \ , \tag{7}$$

$$c_{\mathrm{tgr}_i} = d_i \cdot \frac{1}{max\left(\left|min\left(\boldsymbol{d}\right)\right|, \left|max\left(\boldsymbol{d}\right)\right|\right)} \ , \tag{8}$$

where P_i represents the clamp pressure at time i, and $\boldsymbol{d}$ represents a vector of all observed turgor changes d_i. Leaf growth and environmental data are shown in Figure 11. The absolute leaf area was estimated from a regression model based on pixel counting (Figure 12), with the pixel size known from the camera geometry and object distance.
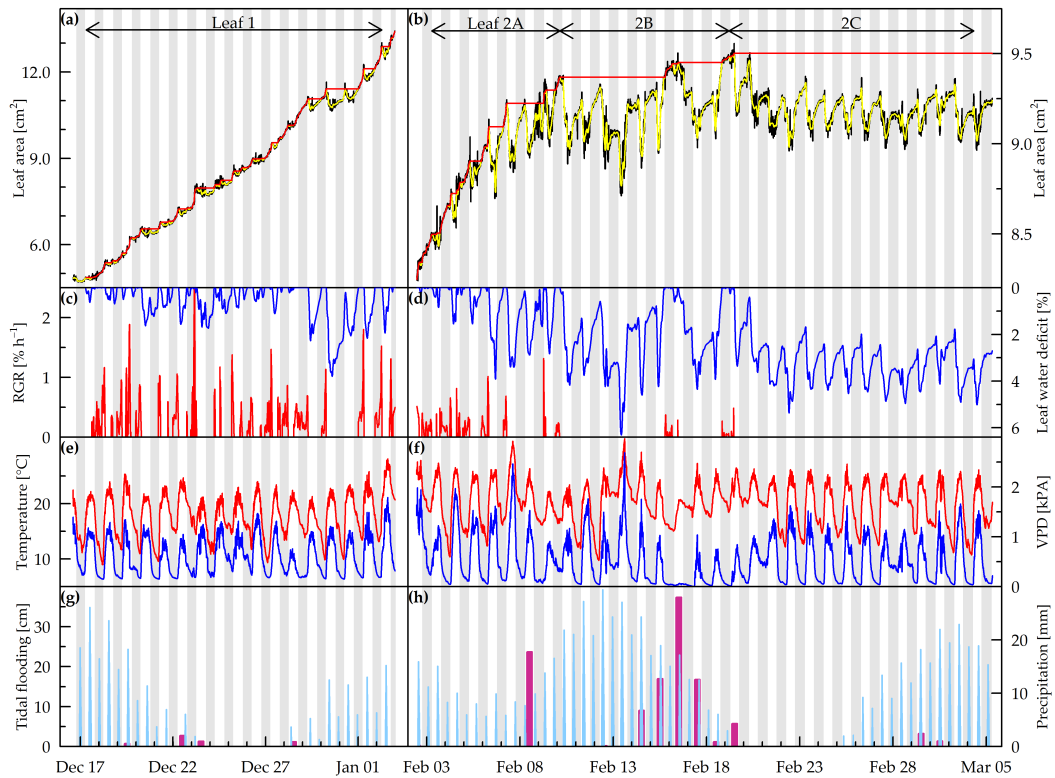
Figure 11. Leaf area change and environmental variables. (a, b) Absolute leaf area development: raw data in black, smoothed curve in yellow, cumulative maximum based on smoothed curve in red. The arrows indicate different growth phases (see text). (c, d) Relative growth rate (RGR) from frame to frame in red (only shown for growth periods), leaf water deficit in blue. (e, f) Local air temperature in red, vapour-pressure deficit (VPD) in blue. (g, h) Water depth during tidal flooding in light blue, precipitation sum per diel cycle in purple. Shaded areas represent night as measured by the illuminance sensors next to the leaf.
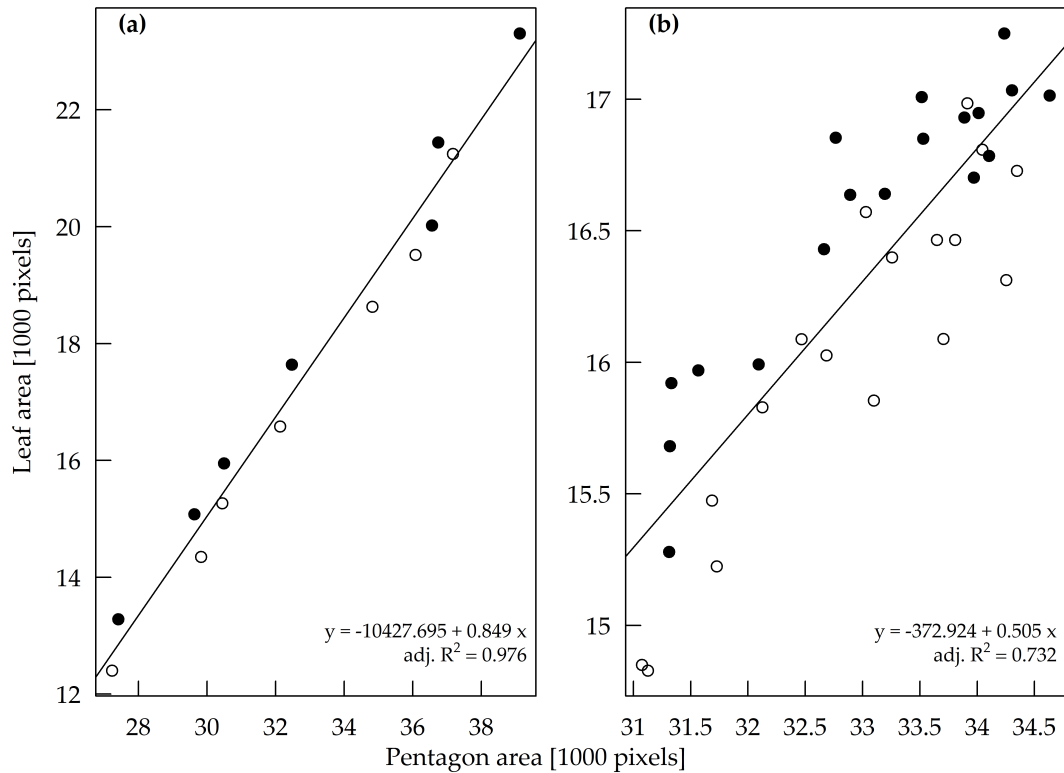
Figure 12. Linear regression between smoothed pentagon area and manu-ally measured leaf pixels to calculate absolute leaf area. (a) Leaf 1. (b) Leaf 2. Filled dots represent measurements during nighttime.

3.3. Results

I measured instantaneous leaf area change on a mature tree in its natural environment over several weeks. My measurements show a distinct diel leaf growth cycle that starts in the morning after dawn when the leaf area reaches a local maximum. Subsequently, the leaf is shrinking until a local minimum is reached around noon, after which it is expanding again in the afternoon and during the night (Figures 11a,b, 13). The mean daily net growth was 2.9% (standard deviation $\sigma = 2.1\%$), and the mean maximum shrinkage was 1.1% ($\sigma = 1.0\%$) when aggregated by time since the last peak (Figure 13). On average, leaf shrinkage was 37% of the daily net growth. The re-expansion to the previous maximum took place until late afternoon, which means that most of the net growth occurred at night. In general, a
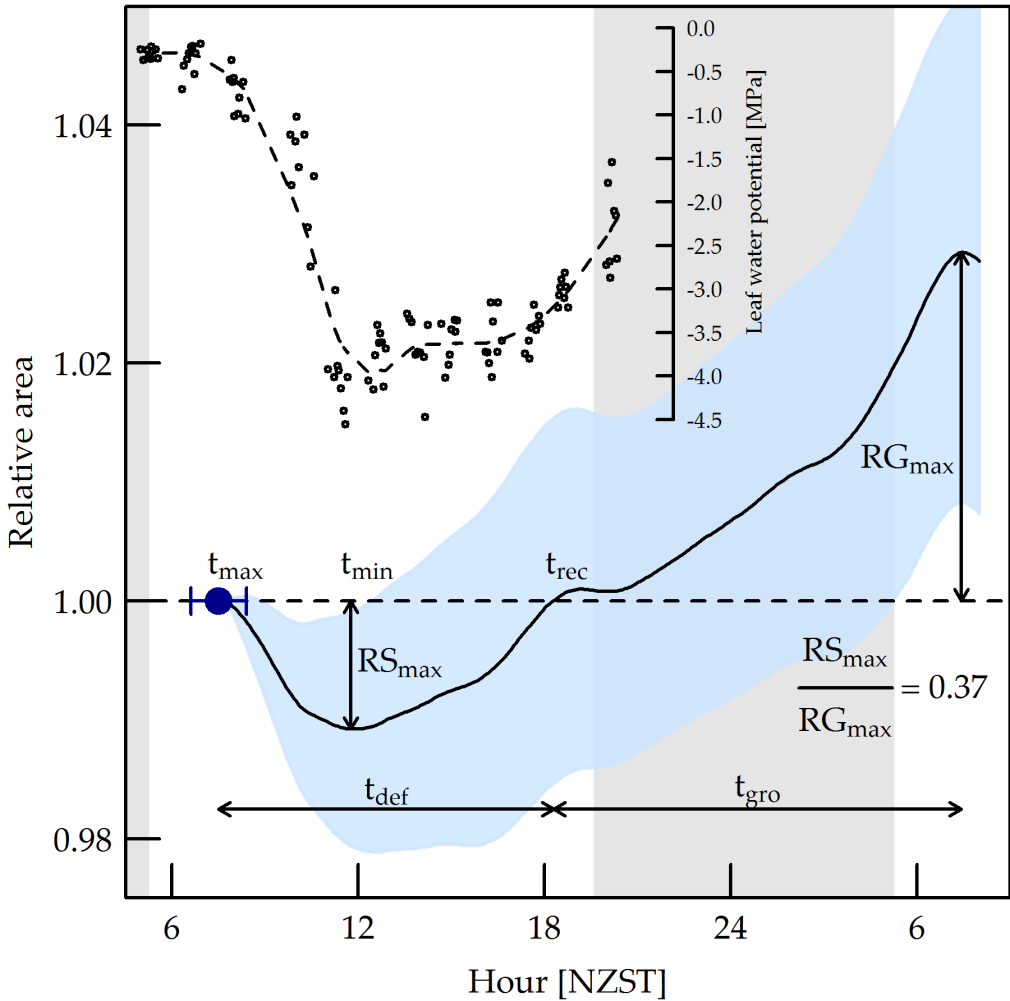
Figure 13. Mean relative diel growth cycle from one local maximum to the next for leaves 1 and 2A ($n = 23$). One standard deviation of the area is shaded in blue. The standard deviation of t_{max} is given by the dark blue error bar. The x-axis shows time since t_{max}, but converted to 24 h clock time for better readability. The inset shows leaf water potential measurements from 13 February 2015 (Donnellan Barraclough, Zweifel, Cusens & Leuzinger, 2018).

small shrinkage was followed by a larger net growth (Figure 14c). Relative leaf area change was strongly correlated with changes in leaf turgor (Figure 14a,b).

Leaf 1 was observed over a period of 16 diel cycles from 17 December 2016 to 2 January 2017 (Figure 11a). During the experiment it expanded from a minimum of approximately 472 mm^2 in the night after the installa-
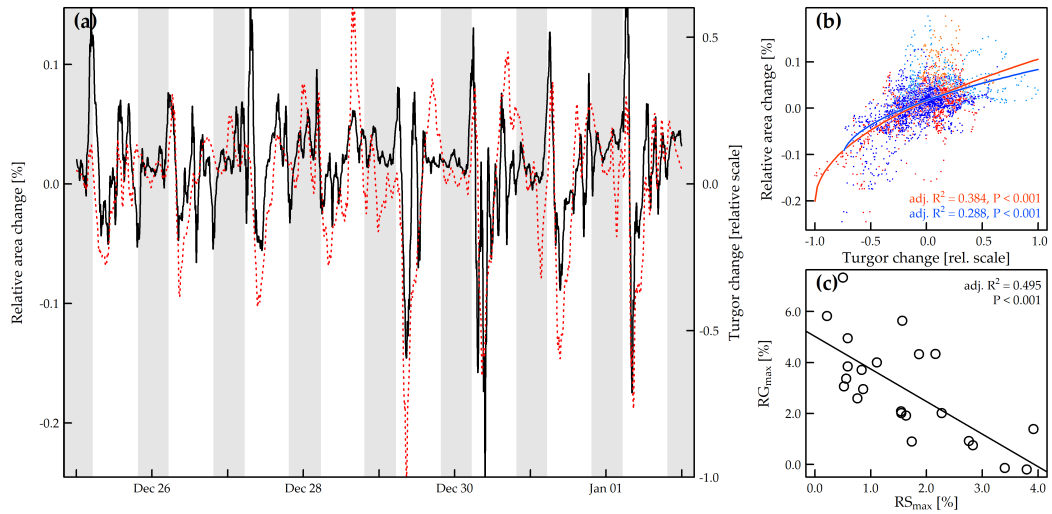
Figure 14. Correlation of leaf water status with leaf area changes. (a) Time series of relative area change (black) and turgor change of a different leaf on the same tree (dotted red) from 25 December 2016 to 1 January 2017. (b) Regression curve for the same sensor in light red; red points represent observations during leaf water deficit, orange points during growth phases, and the same for a second turgor sensor that preceded leaf growth by ca. 55 min in blue; dark blue points represent observations during leaf water deficit, light blue points during growth phases. Linear models were fit after shifting the data to non-negative values, and square root transformation. (c) Linear regression between maximum diel growth (RG_{max}) and shrinkage (RS_{max}) for leaves 1 and 2A combined.

tion to 1340 mm^2 at the end of the measurement, which is an increase by 183.8%. The second leaf was observed over 29 diel cycles and only showed a small area increase of 15.2% from approximately 824 mm^2 to 950 mm^2 (Figure 11b). The growth mainly occurred in the first seven days after the start of the measurement from 3 February to 10 February 2017, referred to as leaf 2A. This was followed by phase 2B, a nine day period of strong leaf shrinkages and gradual recovery, ending on 19 February 2017 after two days of little net growth. During the last 13 days of the measurement until 4 March 2017, phase 2C, the leaf did not grow any further but continued a diel cycle of area shrinkage and expansion. I hypothesize that the early growth cessation of leaf 2 might reflect a seasonal effect. The seasonal leaf growth experiment confirmed leaf growth variations throughout the year.
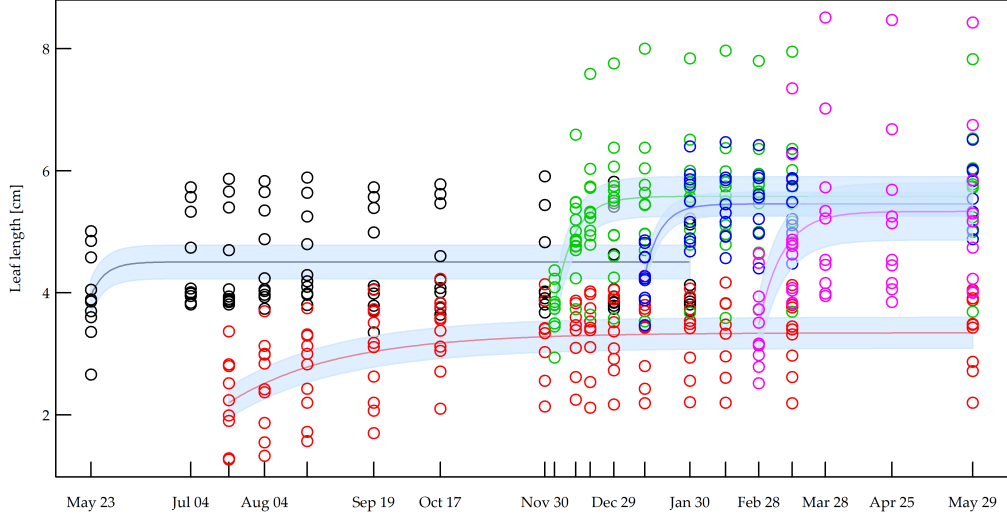
Figure 15. Seasonal leaf growth patterns from May 2017 to February 2018. In summer leaves grow faster and to a longer length than in autumn, while in winter growth is slower, and the final length is shorter. At the start of each cohort ten young, light green leaves were selected. Monomolecular models of the form Length $L = L_{\max} - e^{-rt} \cdot (L_{\max} - L_0)$ were fit. The shaded areas show the maximal standard error of individual measurements for each cohort.

Leaves which emerged in December 2017 or January 2018 were growing at higher rates and to larger sizes than leaves which emerged in May 2017, while leaves which emerged in July 2017 were growing at lower rates and remained smaller (Figure 15).

Figure 13 shows the mean diel growth cycle from leaf 1 and leaf 2A ($n = 23$) aggregated by time after the local area maximum, and defines key metrics for our analysis. I divided the diel growth cycle into two phases: a water deficit phase during which the leaf area is below the previously measured maximum in the early morning, and a growth phase, exceeding the previous maximum. The deficit phase can be further divided into a shrinkage and a recovery phase. The shrinkage phase starts at the time of the local area maximum in the morning ($t_{\max}$) and ends when the area reaches a minimum ($t_{\min}$). During the recovery phase, the leaf expands again to the previous area maximum which is reached at t_{rec}. The relative net growth
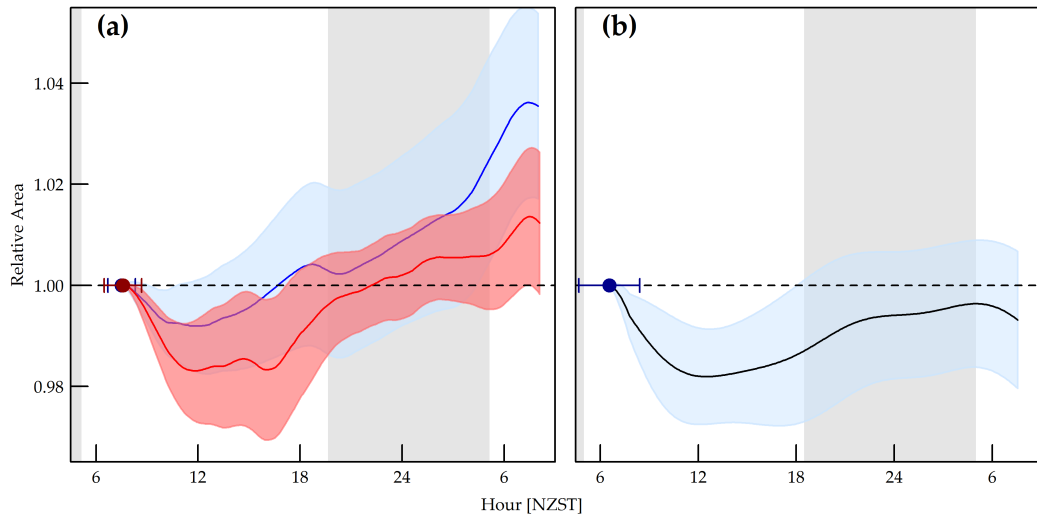
Figure 16. Diel growth cycles. (a) Leaves 1 in blue and 2A in red. (b) Leaves 2B and 2C combined.

RG_{max} in one diel cycle is the leaf area at the end relative to the start. It cannot be quantified which part of RG_{max} is the result of growth processes, and which part results from elastic swelling. The relative maximal shrinkage RS_{max} is the minimal leaf area during a diel cycle relative to the initial leaf area. The analysis also includes two diel cycles with slightly negative RG_{max} (effectively a net shrinkage): from December 30 to 31 2016 with a net area decrease of 0.18%, and from February 7 to 8 2017 with a decrease of 0.13%.

The leaf shrinkage started at 7:21 a.m. New Zealand Standard Time (NZST, $\sigma = 53$ min), or 119 min after dawn ($\sigma = 59$ min). Dawn was defined as a leaf illuminance of more than 425 lux. The diel growth cycles for each leaf individually are shown in Figure 16a. The two observed leaves started shrinking at the same hour of the day. However, leaf 1 had a lower RS_{max}, and a higher RG_{max} than leaf 2A. The aggregated t_{min} for leaves 1 and 2A combined was at 11:45 a.m. NZST; there was no significant difference between the two leaves. In phases 2B and 2C the timing of the diel cycle was not as distinct as in leaf 1 and 2A. The shrinkage started usually around dawn as well, but sometimes earlier. Additionally, t_{min} was only reached in the early afternoon (Figure 16b).

Table 4 shows linear correlations between environmental variables aggregated over the night and day time, respectively, and the extent of RS_{max}, RG_{max}, as well as t_{max}, and the duration of the deficit phase, t_{def}. The mean night temperature preceding the observed diel cycle marginally correlated with RS_{max}, RG_{max}, and t_{def}. The warmer the previous night, the higher was the relative shrinkage, the longer was the LWD period, and the smaller was the relative growth. However, none of these measures correlated with the mean VPD of the previous night. For the mean day temperature I observed a marginally significant correlation with RS_{max}, but no correlation with any of the other variables. For the mean daytime VPD, on the other hand, I observed a marginally significant positive correlation with RS_{max}, and a significant negative correlation with RG_{max}. The mean radiation was also significantly negatively correlated with RG_{max}. Tidal flooding and precipitation are not included in Table 4, because I could not find any correlation between the time or height of the tide and leaf growth parameters, and there were too few rain events in my dataset for a quantitative analysis. For the daily cycle, I observed a strong negative correlation between RS_{max} and RG_{max} (Figure 14c).

The in in situ relative leaf area change and change of leaf turgor followed a similar diel pattern, and were strongly correlated in a non-linear way (Figure 14a,b). Both turgor sensors showed a similar trend (not shown), but with a time lag of 55 min between the two observed leaves, which was corrected before the correlation analysis. Linear models were fit after shifting the turgor change data to non-negative values, and square root transformation:

$$c_{rac_i} = a \cdot \sqrt{|min\left(\mathbf{c}_{tgr}\right)| + c_{tgr_i}} + b + \epsilon \ . \tag{9}$$

During leaf water deficit periods turgor had a stronger impact on relative area changes (shrinkage and re-expansion) than during growth periods (Figure 14b). I also tested for correlations between in situ RGR and environ-

Table 4. Correlations between key metrics defined in Figure 13 and average environmental conditions (temperature (T), vapour-pressure deficit (VPD), and radiation (E)) in the night previous to the cycle (np), and during the day (d).

	$\overline{T_{\mathrm{np}}}$	$\overline{\mathrm{VPD}_{\mathrm{np}}}$	$\overline{T_{\mathrm{d}}}$	$\overline{\mathrm{VPD}_{\mathrm{d}}}$	$\overline{E_{\mathrm{d}}}$
$\mathrm{RS}_{\mathrm{max}}$	↗ • 0.087	ns	↗ • 0.098	↗ • 0.085	ns
$\mathrm{RG}_{\mathrm{max}}$	↘ • 0.117	ns	ns	↘ ** 0.245	↘ * 0.177
t_{def}	↗ • 0.089	ns	ns	ns	↗ • 0.123
$\boldsymbol{t}_{\mathrm{max}}$	ns	ns	n/a	n/a	n/a

The arrows indicate the direction of the correlation; significance of p values are indicated as follows: • $0.10 < p$; * $0.05 < p$; ** $0.01 < p$; adjusted R^2 values are given below; $\boldsymbol{t}_{\mathrm{max}}$ was expressed in decimal hour of day; ns: not significant.

mental variables. I did not find any pattern other than small but highly significant negative correlations with temperature, VPD, and irradiance, which reflects the opposite diel cycles of leaf area and temperature, VPD, and irradiance, respectively. Scatterplots of environmental variables and RGR for different growth phases are shown in Figure 17.

3.4. Discussion

This chapter reports the development of a bespoke, inexpensive, and open-source instrument for long-term measurements of instantaneous leaf area changes in the field. I observed a clear diel growth pattern with considerable leaf area shrinkage in the morning, and leaf expansion in the afternoon and at night. On average the shrinkage was 37% of the diel net growth, which, to my knowledge, is the highest value ever observed over a prolonged growth period. Diel leaf growth was limited by the amount of leaf shrinkage immediately preceding growth, and relative leaf area changes were strongly correlated with leaf turgor changes. Together these correlations strongly
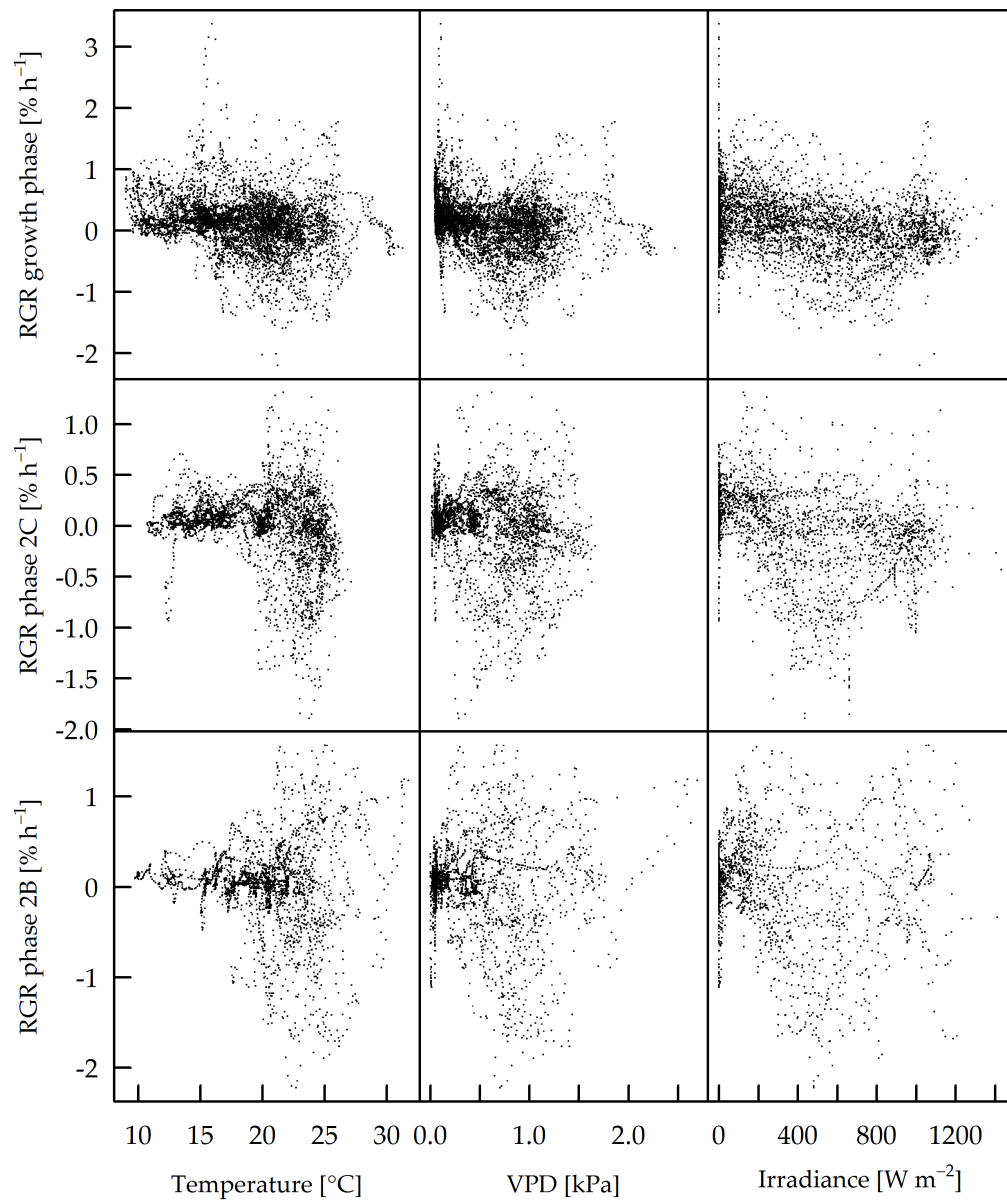
Figure 17. Scatterplots of relative growth rate (RGR) and environmental variables temperature, vapour-pressure deficit (VPD), and irradiance for different leaf growth phases.

suggest that in *A. marina* instantaneous leaf growth patterns are driven by leaf water relations, and not by carbon assimilation. This supports the view that leaf growth is generally limited by hydraulics (Pantin et al., 2012).

Leaf expansion can directly be limited by water stress, e.g. leaf elongation in *Zea mays* shows an immediate response to changes in soil water potential (Hsiao et al., 1970), or evaporative demand (Bouchabké, Tardieu & Simonneau, 2006). In *Helianthus annuus* a soil water deficit leads to a decrease in long-term relative leaf growth rates, resulting from a reduction in cell number, or cell size, depending on leaf ontogeny (Granier & Tardieu, 1999b). In general, soil water deficits have a much stronger negative effect on shoot growth than on photosynthesis (Muller et al., 2011). My results strongly support these findings.

Avicennia marina has a high salinity tolerance, and long-term leaf area expansion rates decrease with increasing salinity (Ball, 1988). Here I showed that water stress did not only lead to an *in situ* growth reduction, but to a pronounced period of leaf area shrinkage. Leaf shrinkage in growing leaves has been described before in *Tripolium pannonicum* (*Aster tripolium*) and *Beta vulgaris* exposed to salt water (Rozema, Arp, Diggelen, Kok & Letschert, 1987; Waldron, Terry & Nemson, 1985). Short periods of leaf area decrease of up to two hours have also been observed in *Glycine max* (Mielewczik et al., 2013), or *Arabidopsis thaliana* (Apelt et al., 2017).

My observations suggest that the extent of the diurnal leaf shrinkage limits diel growth (Figure 14c). The decrease in leaf area seems to be driven by water loss through transpiration, concurrent with a strong drop in leaf water potential (Figure 13), and a decrease in leaf turgor (Figure 14a,b). Despite a lower leaf water potential in the late afternoon compared to mid-morning, I observed shrinkage in the morning and leaf expansion in the late afternoon (Figure 13). This is a classic hysteresis response and can only be due to changes in osmolyte concentrations, or plant-intrinsic hydraulic properties (elastic modulus, xylem conductivity, cell wall extensibility). The correl-

ation between leaf turgor and area change was nonlinear, suggesting that turgor had a stronger impact on elastic deformation during water deficit periods, than on growth.

It has recently been reported that extracellular water storage, and water uptake from the air by trichomes contribute to the maintenance of leaf water status of *A. marina* (H. T. Nguyen, Meir, Wolfe, Mencuccini & Ball, 2017). I often observed an RGR peak in the early morning (Figure 11c,d) and it could be speculated that this reflects direct leaf water uptake from dew or air of high relative humidity surrounding the leaf, and not expansive growth. Earlier measurements of water relations of the same species and at the same site support this: highest stomatal conductance values were observed in the morning, after which they declined (Donnellan Barraclough, Zweifel, Cusens & Leuzinger, 2018). Leaf water potential measurements on February 13 2015 ranged from a predawn maximum of -0.6 MPa to a minimum of -4.1 MPa in the early afternoon (Donnellan Barraclough et al., 2018). Pressure–volume curves of the same species growing in Australia showed that a decrease in water potential below -0.9 MPa is driven by a decline in turgor (H. T. Nguyen, Meir, Sack et al., 2017). My observed midday leaf water potentials are close to the turgor loss point which depends on salinity and occurs between -4.5 MPa and -5.1 MPa in *A. marina* subsp. *australasica* (H. T. Nguyen, Meir, Sack et al., 2017). In this domain the relative leaf water content decreases from approximately 87% to 76%, which translates to a decrease in leaf volume of about 13%. This potential volume loss results from a modulus of elasticity of about 26 MPa (H. T. Nguyen, Meir, Sack et al., 2017). The highest leaf area shrinkage observed in our experiment was 6.4% on 13 February 2017. If we assume that leaf thickness decreased by a similar amount, the total volume loss would be close to the total water storage before turgor loss. Therefore, I conclude that the observed leaf area shrinkage was driven by water loss similar to the observed decline in turgor (Figure 14a,b) and leaf water potential (Figure 13).

I did not investigate whether the observed growth was driven by cell proliferation, or expansion, or both. Based on the approximately linear long-term growth (Figure 11a,b) I assume that turgor driven cell expansion was the dominant process, but this may well be different for emerging leaves, where ontogenetic growth regulation is important (Pantin et al., 2011). Some limited growth activities may still be present during water deficit periods, as it has been observed for stem shrinkage (Zweifel et al., 2016). Such "stored growth" leads to higher initial growth rates after the deficit period. However, I was unable to detect this effect in the present study.

My marker tracking software performed well in all but the windiest or rainiest conditions. I obtained a slightly noisy relative leaf area signal that required smoothing for further analysis (Figure 11a,b). The choice of smoothing parameters does affect the observed in situ RGR, as well as the exact t_{max}, t_{min}, and t_{rec}. However, the general observation of a diel growth cycle is unaffected, and the extent of the relative shrinkage RS_{max} and relative growth RG_{max} are largely independent of the smoothing parameters. Applying the same analysis to the control data obtained with a carbon fibre plate showed that there was no artifactual diel trend (Figure 18). The method could be further improved by a better marker design that would allow for a less noisy tracking, for example by using the ArUco library (Garrido-Jurado, Muñoz-Salinas, Madrid-Cuevas & Marín-Jiménez, 2014). Although, the problem of glare (Figure 10) might still be present.

I found marginally significant correlations between the mean temperature of the previous night and RS_{max}, and RG_{max}, respectively (Table 4). I cannot think of any hydraulic process that could explain this correlation, especially because night VPD did not correlate with any of the measured parameters. However, it could be speculated that higher night temperatures lead to a depletion of carbohydrate reserves, which reduces the ability to maintain turgor in the morning. A mechanistic explanation would need a set of dedicated additional measurements such as high-resolution
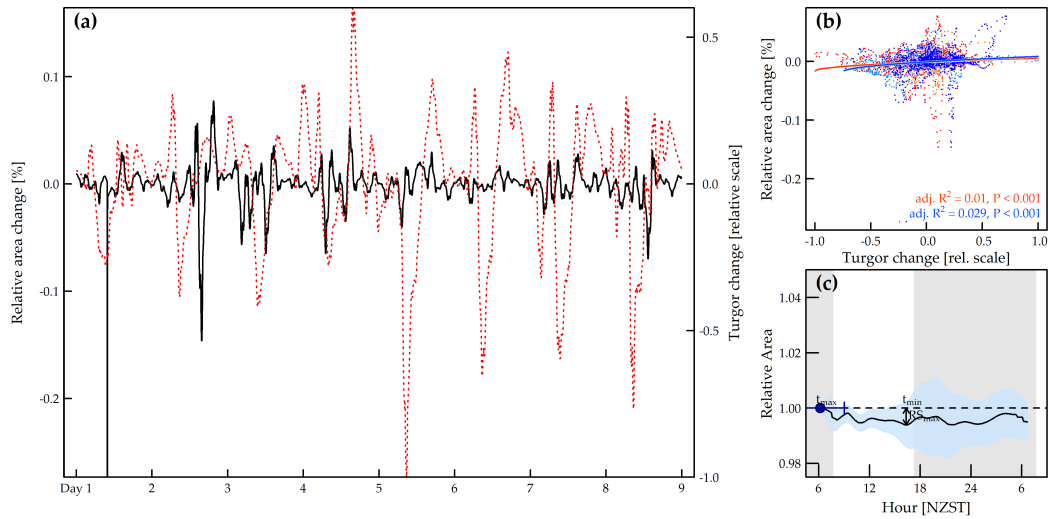
Figure 18. Results from the control run with a carbon fibre plate instead of a leaf. (a, b) Equivalent to Figure 14a,b. (c) Equivalent to Figure 13 (n = 13). Data analysis and figure formatting are similar to the originals.

leaf osmotic potential, and leaf starch and sugar content. On the other hand, mean daytime VPD correlated marginally positively with RS_{max}, and negatively with RG_{max}. It can be expected that a higher VPD increases leaf water stress and thus leaf water deficit, and so indirectly decreases the potential for growth (Figure 14c). The observed negative correlation between mean radiation and RG_{max} might reflect an indirect effect, since radiation and VPD were highly correlated (not shown).

This study demonstrates the importance of high-resolution leaf growth measurements to detect and characterise minute changes in leaf area. In an experiment with only one or two measurements per day, for example by using a smartphone app such as Petiole (petioleapp.com), the diurnal shrinkage could have remained undetected, and the dependence of leaf growth on water relations in *A. marina* would have been much harder to establish. By measuring instantaneous leaf area changes I showed a strong correlation with leaf turgor (Figure 14a,b). Leaf turgor seems to have a stronger influence on shrinkage and re-expansion than on structural growth (Figure 14b), and the extent of diel shrinkage limits diel growth (Figure 14c). The limitation of leaf growth by water relations has been shown before for

agricultural crops, or the model species *A. thaliana*, and the importance of turgor for cell expansion is reflected in the Lockhart model (Lockhart, 1965; Ortega, 1985; Equation 1) . Here I show that water limitations also directly limit instantaneous leaf growth of a mature tree, namely the mangrove *A. marina*. Measurements of non-structural carbohydrates at the same site indicate that while carbon is important as an osmolyte (sugar), it is hardly limiting under natural conditions. I therefore argue that there is no carbon trade-off involved, and instantaneous growth patterns are largely driven by plant hydraulic relations in this species. This may simply be a consequence of life in saline conditions, but, if confirmed for other species, may point at a subordinate role of carbon in comparison to water when plant growth, at least at the scale reported here, is concerned. This adds to the paradigm that plant growth processes are generally decoupled from carbon assimilation, as has been shown for larger spatiotemporal scales (Körner, 2003b). High-resolution leaf growth data under realistic in situ conditions are understudied but urgently needed to inform plant hydraulic and growth models (e.g. Steppe, De Pauw, Lemeur & Vanrolleghem, 2006), whose improvement in turn is pivotal for a better understanding of vegetation modelling in a future climate (Fatichi, Pappas & Ivanov, 2016).

Chapter 4
Measurements using Stereo Vision

In this chapter I explore the suitability of a stereo vision system for outdoor measurements of leaf area, which is the prerequisite for growth estimates. I built a prototype using machine vision cameras, lenses, and filters to optimise image acquisition in direct sunlight, while relying on open source software for the image analysis part. The results show a good correlation of leaf area measurements with ground truth data from scanning.

4.1. Introduction

In Chapter 3, I successfully adopted the leaf fixation and marker tracking method to study instantaneous leaf growth in the field. While this approach is very simple, the application of tensile forces is not suitable for all types of leaves, and it requires laborious control measurements. It is therefore desirable to have a method that allows us to directly measure leaf area and growth without any direct interaction with the plant. As reviewed in Chapter 2 this can be achieved from statistical correlations, or from three-dimensional (3D) reconstruction (Fiorani & Schurr, 2013; Gibbs et al., 2016). The statistical approach works well for entire shoots but not for individual organs. Therefore, I only considered 3D methods to measure the leaf area. Additionally, the method should be suitable for continuous outdoor measurements. Following the overview in Chapter 1, below I briefly discuss the advantages and disadvantages of some 3D methods.

Each method has its tradeoffs in terms of costs, accuracy, and potential to

be used in the field, see Table 5. Particular challenges for outdoor measurements are sensor overexposure, or interference due to sunlight, movements due to wind, and raindrops on the leaf, or sensor lens. Sunlight and rain pose similar problems for all 3D methods, while sensitivity to movements depends on the method. I decided to use a stereo vision set up for measuring the leaf area because of its (potentially) high image resolution and rather low cost.

By comparison, structure from motion (SfM) is also a low cost method if free software is used, but it is less flexible because it requires a lot of input images and extensive post-processing. On the other hand, SfM can provide a more detailed geometrical model than a stereo vision system, which only gives the depth projection of a scene. Time of flight systems give similar data to stereo vision, but at a lower image resolution. There are low cost consumer grade systems available, for example the Microsoft Kinect v2. Structured light systems can generate high-resolution data, but they might be hard to set up outdoors, and sunlight interference may be particularly challenging. I did not consider laser scanning or light-field systems, because of their high cost. Medium cost light-field systems are available, but their suitability for plant phenotyping is limited (Schima et al., 2016). Surprisingly, stereo vision has not yet been fully implemented for automated leaf area growth measurements, despite good results for indoor leaf area measurements (Xiong et al., 2017).

4.2. Materials and methods

Ground truth from scanned leaves

The lamina area was measured from scanned leaves and used as a ground truth for the 3D analysis. This requires three steps: leaf segmentation, petiole removal, and area calculation. Leaf segmentation can be achieved by

Table 5. Qualitative comparison of selected 3D methods.

	Method	Sensitive to object movement	x-y resolution	Depth accuracy	Cost
Active	Laser scanning	Yes	High	High	High
	Time of flight	No	Low	Low	Low
	Structured light	No	Low to high	Low to high	Low to medium
Passive	Stereo vision	Sometimes	Low to high	Low to high	Low to medium
	Structure from motion	Yes	n/a	n/a	Low to medium
	Light-field	No	Low to high	Low to high	Medium to high

Note: Laser scanning refers to laser triangulation. Stereo vision's sensitivity to movement depends on camera shutter type and exposure time. Structure from motion requires reference points for real world dimensions.

hue thresholding. Most plant species have green leaves, but leaf colours can range from red, purple, and blue for some species, to yellow in case of autumn colouring, disease, or decay. It is therefore not possible to define a general hue range to identify leaves, but most leaves can easily be segmented when scanned against a blue background, see Figure 19a. In my analysis I did not determine whether parts of the leaf were damaged or decaying, and all non-blue pixels were included.

Petiole removal requires some knowledge about leaf geometry. A straightforward approach is to restrict the analysis to leaves that are scanned upright (Borianne & Brunel, 2012; Maloof, Nozue, Mumbach & Palmer, 2013). I took a more general approach, by allowing leaves with an unknown orientation, which is closer to real world scenarios. I tried to detect the petiole based on the leaf shape only. The general idea was that the leaf contour direction changes sharply at the petiole. To detect such "turning points" I fitted thick digital straight segments (DSS) along the leaf contour (Debled-Rennesson, Rémy & Rouyer-Degli, 2005). I used the OpenCV (Bradski &
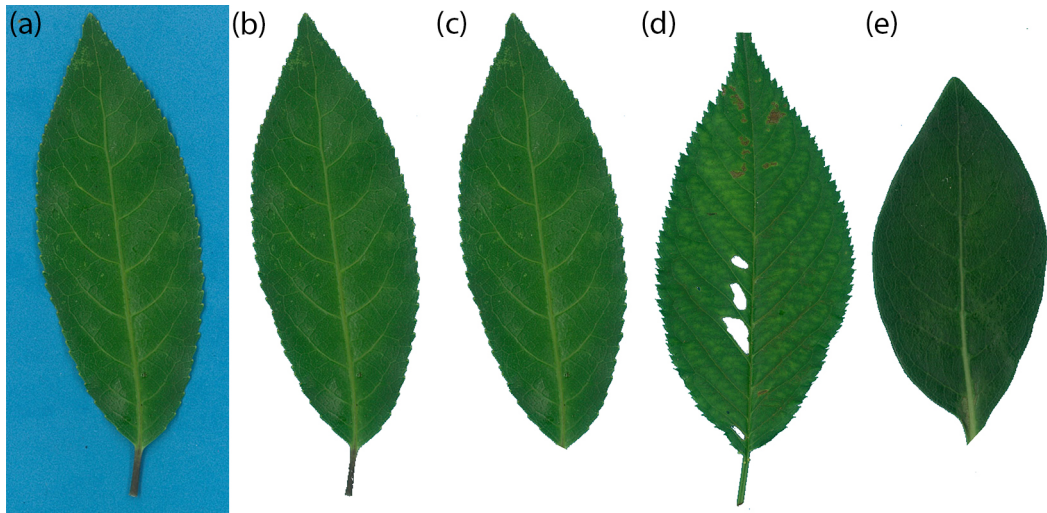
Figure 19. Petiole removal from scanned leaves. (a) Scanned leaf on blue background. (b) Segmented leaf. (c) Leaf lamina. (d) False positive. Tip instead of petiole was removed. (e) Petiole detected correctly, but not cut at the right points.

Kaehler, 2008) rotating callipers algorithm which is implemented using the convex hull algorithm by Sklansky (1982). Turning points were classified as points where subsequent DSS orientations lay in different quarters of the unit cycle. This approach avoids to set a fixed angle threshold, but turning points vary with different leaf directions. Therefore, it is not suitable for a general shape description.

Many of the detected turning points were not part of the petiole. To identify potential petiole points, I analysed the mean width and the width fluctuation along the DSS normal. The width fluctuation was quantified as the slope of a linear regression, with the element width along the DSS normal at each contour point as the dependent variable, and the contour index as the independent variable. In most cases during my tests, the DSS with the lowest width fluctuation was part of the petiole. If no DSS was within a pre-defined threshold range for mean width and width fluctuation, I assumed that no petiole was present.

As a petiole has a linear structure, the algorithm is searching for DSS which are oriented parallel to the potential petiole DSS at the opposite side

of the object. I considered two DSS close enough to parallel when their angle was 180°± 45°. If there was no parallel DSS, it was assumed that the analysed element was not a petiole. When there were multiple matches, I proceeded with the DSS closest to 180°. From both detected DSS I fitted further DSS along the leaf until an object width-threshold was exceeded. The orientation of the DSS extension was set depending on its direction towards the object's mass centre. Depending on the leaf shape, the petiole cutting point was determined at the beginning or end of the last DSS.

In my test dataset I had 28 leaves, and I achieved a correct petiole classification rate of 75% , see Figure 19a-c for an example. Cases of false positive detections included leaf tips being mistaken for the petiole (Figure 19d). This happened when the parallelness at some part of the tip was higher than anywhere in the petiole. The algorithm did not test the extrema, because the end of the petiole may be irregular. Because the petiole cut off point was set at the end of a DSS, it also happened that the petiole was correctly detected, but the removal did not take place at the right point (Figure 19e). Because of these inaccuracies, I decided to manually segment the petiole for the ground truth. Another simple approach would be to physically cut off the petiole before scanning, but this may be avoided because a trait like the specific leaf area includes the petiole area.

Once the lamina region R is segmented, its metric area A can be calculated from the pixel area $\mathcal{A}(R)$, and the scanner resolution r given in dots per inch:

$$A = \mathcal{A}(R) \cdot \left(\frac{25.4 \, \frac{\text{mm}}{\text{in}}}{r} \right)^2 . \tag{10}$$

This method measures the projected two-dimensional (2D) lamina area. It is not suitable for non-flat leaves, such as needles, or leaves with very curly surfaces.

Leaf features

Leaves have a huge variety of shapes and sizes between species, but also within species, and in some cases even during the development of a single leaf. Therefore, I tried to come up with a set of general features that are suitable to describe a leaf, and could be used for segmentation. All leaves are attached to the stem, so the presence of a petiole is a potential feature. However, leaves can also be sessile, or the petiole can be occluded in an image. Instead of the petiole the presence of veins seems to be a better feature, even though not all species have visible veins at the leaf surface.

Leaf venation patterns can be extracted using a series of simple morphological operations (Zheng & Wang, 2010, see Figure 20). First, the input image was converted to grayscale, and blurred with a Gaussian kernel. Then, the vein structure was extracted by subtracting the black top hat transform from the white top hat transform. These are morphological operations based on erosion and dilation. In both operations a filter kernel W is moved over the image I so that each pixel is changed.

In this example, the kernel W is a square with an odd side length. Erosion changes each pixel value to the minimum value in the neighbourhood defined by W; it is denoted by $I \ominus W$. Dilation is the opposite operation, and every pixel value is replaced by the maximum value in the neighbourhood; it is denoted by $I \oplus W$. Performing these operations subsequently is called opening and closing, respectively. The opening operation is the dilation of the erosion, denoted by $I \circ W = (I \ominus W) \oplus W$. Similarly, the closing operation is the erosion of the dilation, denoted by $I \bullet W = (I \oplus W) \ominus W$.

In binary images, the opening operation is used to remove small foreground objects (white dots), and the closing operation fills small holes (black dots). Such small objects can be extracted by subtracting the result of the opening respectively closing operation from the input image, which is called top hat transform. The white top hat transform is denoted by $I - I \circ W$,
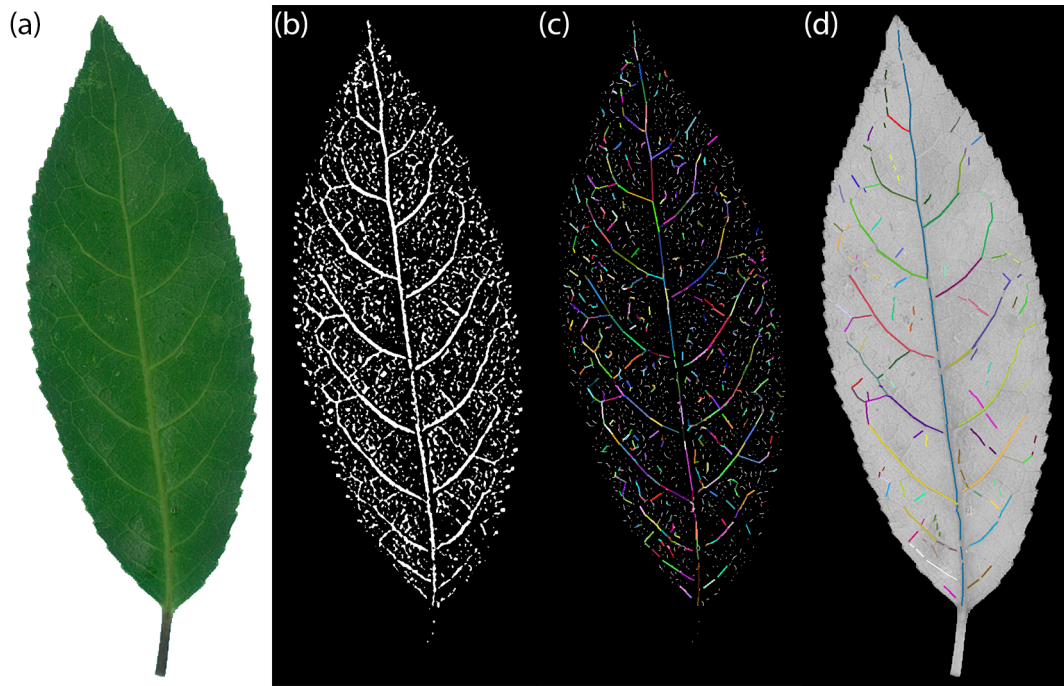
Figure 20. Leaf venation pattern. (a) Input. (b) Result of the morphological operations after normalisation and thresholding. (c) Detected vein segments after skeletonisation and straight segment fitting. (d) Connected vein segments. The grayscale image has been inverted for display.

and the black top hat transform is denoted by $I - I \bullet W$. On a grayscale leaf image with veins brighter than the lamina, the white top hat transform enhances vein pixels, while the black top hat transform enhances non-vein pixels.

The extracted differences are actually very small. Therefore, it is necessary to threshold the image before further processing. I usually achieved good results by first normalising the image, and then thresholding it using Otsu's method (Otsu, 1979), but in some cases another thresholding method is preferred. In the next step, the extracted veins were thinned using the skeletonization algorithm by T. Zhang and Suen (1984). Along the vein skeleton I fit DSSs, as described above. Finally, the vein DSSs, were clustered based on their location in the leaf, and their directions (Figure 20d).

For some species the veins are not visible at the leaf surface. In this case symmetry is another general feature that applies to most species. However,
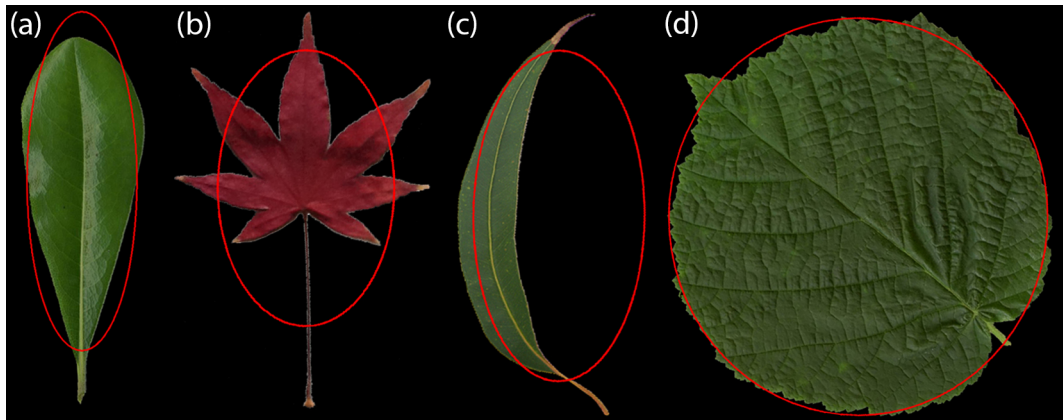
Figure 21. Leaf symmetry and direction determination. (a, b) Symmetry and direction correctly determined. (c) Non-symmetry and direction correctly determined. The eucalyptus leaf is more symmetric along the semi minor axis but this was not tested, because the shape is not circular. (d) The most symmetric orientation that was tested was not the correct direction. Leaves have been rotated upright for display.

many other objects are also symmetric, therefore this feature is not generally applicable. It has to be implicitly assumed that leaves are expected in the analysed scene.

The symmetry was determined as follows. First an ellipse was fit to the object contour using the algorithm by Fitzgibbon, Pilu and Fisher (1999). Many species have ellipse-like leaf shapes, but this approach also works well for different shapes such as maple leaves, see Figure 21b. The object was then split in half along the direction of the semi-major ellipse axis.

Symmetry was simply approximated by the ratio of the areas of both sides not exceeding $\pm$ 20%. In cases of nearly circular objects I also tested the symmetry along the semi-minor axis, as well as the same ratios after rotating the axes by 45°. The direction with the highest symmetry was assumed to be the direction of leaf. This logic worked well for scanned leaves, but failed in some cases, see Figure 21.

In real world scenarios with different viewing angles this approach is very limited, because it relies on the perceived 2D shape. Therefore, I did not use this symmetry classification, but the even simpler ellipseness. That
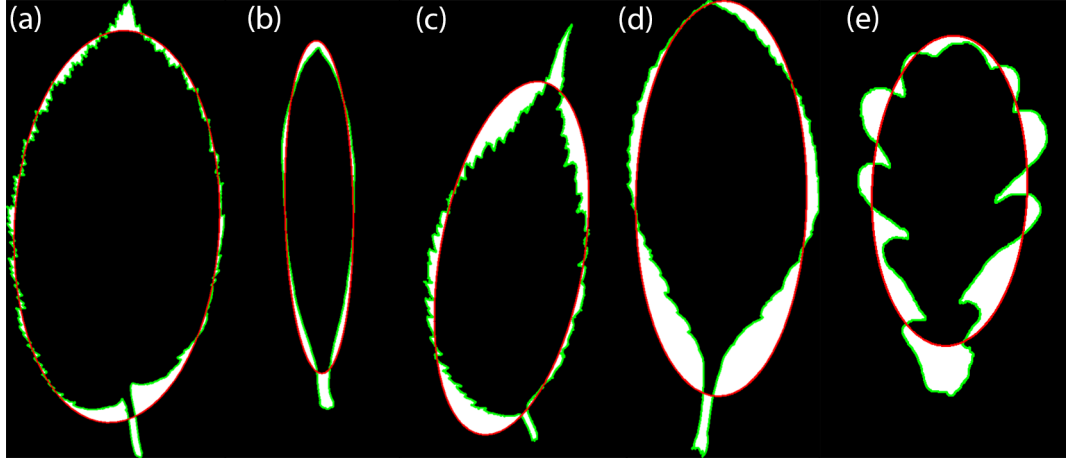
Figure 22. Ellipseness of scanned leaves (a) 92.4% (b) 86.4% (c) 80.6% (d) 77.5% (e) 69.7%. The leaf outline is marked in green, the ellipse outline is marked in red. White represent non-overlapping areas used for the ellipseness calculation.

is, how well the fitted ellipse corresponds with the object, calculated by

$$1 - \frac{\mathcal{A}\left(R_{ob} \triangle E(R_{ob})\right)}{\mathcal{A}\left(E(R_{ob})\right)} \, , \tag{11}$$

where R_{ob} is the region of the object, E denotes the ellipse fitting, $\mathcal{A}$ is the area of a region, and $\triangle$ denotes the symmetric difference of two regions. In a graphical representation, the white regions in Figure 22 are compared to the ellipse region. Ellipseness is quite a crude feature as seemingly elliptic leaves can have a relatively low value, while non-elliptic leaves can still have a relatively high value; see Figure 22d,e.

Stereo vision setup

In a stereo vision system, two cameras are used to calculate the distance of an object to the cameras. Each camera needs to be calibrated individually to determine its camera matrix and distortion coefficients (Bradski & Kaehler, 2008). The cameras are set up in a stereo rig with a fixed distance to each other. The exact geometrical relation of the cameras is determined by stereo calibration. The depth Z of one real world point can then be calculated from

the baseline distance b between the two cameras, the disparity d of the point in the two images, the focal length f of the cameras (part of the camera matrix), and the pixel size s by the formula

$$Z = b \cdot \frac{f}{d \cdot s} \, . \tag{12}$$

To find the disparity, corresponding points need to be detected in both images. The search for corresponding points is simplified by first rectifying the images so that the points are on the same image rows. The rectification relies on the previously obtained calibration information.

Once the disparity is found by a stereo matching algorithm, the depth Z can be calculated using the equation above. Based on the depth and the camera matrix, the coordinates X and Y can then also be determined resulting in a 3D representation for either of the two input images. Some points cannot be matched in both images because they are either only visible in one of the two images due to different perspectives, or because there is no clear correspondence because of a uniform texture. Consequently, no coordinates can be calculated for such points. For camera calibration and image rectification I was using the open source computer vision library OpenCV (Bradski & Kaehler, 2008). For the calibration I used a printed checkerboard pattern, which was glued to a flat piece of wood.

To be able to continuously observe a growing leaf, it is necessary to illuminate it during nighttime. The illumination needs to be at a wavelength that does not interfere with growth or photosynthetic processes which is the case in the near infrared spectrum at around 900 nm (Gates, Keegan, Schleter & Weidner, 1965; Walter et al., 2009). Image sensors that are used in consumer grade cameras are able to detect light at wavelengths of up to 1100 nm, although the sensor efficiency is decreasing with increasing wavelengths. Cameras are typically equipped with an infrared cut-off filter to only represent visible light in the image. In contrast, when infrared

illumination is used for continuous plant monitoring, a bandpass filter can be used to block visible light leading to a more uniform image exposure throughout the day.

For outdoor measurements, the influence of direct sunlight can be minimised with a bandpass filter at 940 nm because of the water vapour absorbance band at this wavelength (Hill & Jones, 2000). This feature has been utilised for leaf imaging before (W. Zhang, Hansen, Smith, Smith & Grieve, 2018). Another approach to minimise the influence of sunlight is the use of a linear polarising filter to block glare (Bao, Tang, Breitzman, Fernandez & Schnable, 2018). Colour image sensors largely record the same information at wavelengths higher than approximately 800 nm. Therefore, no additional information can be gained from a colour image and the use of a monochrome sensor is preferred.

The goal of this project was to explore the potential of stereo vision for outdoor leaf growth measurements using components that would allow the design of a small device that is easy to install. Therefore, I restricted the camera selection to small industrial grade cameras that offer a higher image quality and more customisation options than consumer grade webcams. To minimise the effects of object movements, a camera with a global shutter is required. This means that all sensor pixels are exposed at the same time, as opposed to rolling shutter cameras. I selected the Basler daA1600-60um camera (Basler AG, Ahrensburg, Germany) which is a small module with a size of 29 mm × 29 mm, and a weight of 15 g. The sensor has a pixel resolution of 1,600 × 1,200 with a pixel size of 4.5 µm. The pixel depth is 10 bit, which means that the maximum number of different pixel intensities is $2^{10} = 1024$. (Although the camera software inflates this to 12 bit per pixel.)

For the lens I selected the NMV-8M23 (Navitar, Inc., Rochester, NY, USA) with a focal length of 8 mm. The appropriate focal length depends on the distance to the object, and the object size. A shorter distance or a larger object requires a shorter focal length (larger viewing angle). It also needs to

be considered that the object has to be fully visible in both cameras. Furthermore, the distance to the leaf needs to be sufficiently large to ensure that the cameras do not interfere with plant growth, for example by intercepting light. The lens also needs to be infrared transparent, which was relatively hard to find. For the illumination I used LISIPAROI LEDs with a wavelength of 940 nm (Cyntech Components Ltd, Milton Keynes, United Kingdom), and a corresponding bandpass filter was selected to minimise the influence of sunlight (BN940, Midwest Optical Systems, Inc., Palatine, IL, USA).

The cameras were mounted with a baseline distance of 40 mm, which is the smallest possible distance with the lenses I used. Cooling for the cameras was provided by a fan. The LEDs were mounted above and below the lenses. A computer power supply was used for the fan and LEDs. The whole installation was fixed to a tripod to support height and viewing angle adjustments; see Figure 23. The focal plane was about 20 cm from the lenses and 25 cm from the cameras. The cameras were connected to a computer over USB 3 cables, and image acquisition was controlled using Basler's pylon software.

The camera exposure was triggered using software which could result in slightly different image acquisition time points for the two cameras. In a series of test pictures with a stopwatch I determined that both cameras usually triggered within the same millisecond. Initial tests of plant images showed that the two images had very different histograms when the exposure time was automatically determined by the camera software. As this poses a potential problem for the stereo matching algorithm, I decided to set the exposure time manually. To achieve a good illumination, exposure times between about 1 ms in full sunlight and 40 ms in indoor settings were required. This rather long exposure time is presumably a consequence of the low sensor efficiency at 940 nm. Such a long exposure time renders the discussion about shutter and trigger time obsolete, as any object move-

Figure 23. Stereo camera. (a) Image acquisition outdoors. (b) Camera on tripod with power supply below. (c) Rear view showing camera boards and USB cables.

ment will result in motion blur. The exposure time could potentially be reduced by stronger illumination, or by camera gain (amplifying the sensor signal). Despite the manually set exposure time, corresponding points in the two images sometimes still had very different pixel values, possibly resulting from different reflection angles. Tests with illumination from different angles could not remove this effect.

Data acquisition

It was necessary to have a portable software that can run on any modern computer with the Windows operating system, to facilitate outdoor data acquisition (Figure 23). I wrote a console application using Basler's pylon C++ application programming interface, and OpenCV to acquire pictures. It was also required to install Basler's camera driver. The application is extremely simple; it allows to set the exposure time, displays a preview image, and takes images based on keyboard commands.

I acquired two test datasets: one indoors, and one outdoors. For the

indoor setting, I recorded eight different scenes of freshly harvested plants (seven different species), and measured a total of 15 leaves. The species distribution in this dataset was not even, with two species constituting nine specimens. For the outdoor setting, I recorded 11 different scenes (all different species), and measured a total of 13 leaves. I intentionally selected challenging scenes with varying lighting conditions from no direct sunlight, to partial sun exposure, and full sunlight. The image exposure time was set between 0.8 ms and 8 ms. In some scenes there was a mild wind, but no motion blur was apparent.

Setting up the tripod, and manually setting the exposure time was time consuming. In the outdoor tests it took up to 20 min until a good perspective and exposure was found. I only selected leaves which were fully visible, and I did not acquire outdoor images at night. I also did not test the effect of water drops on the leaf surface. During the indoor measurements, the leaves were scanned for ground truthing immediately after image acquisition. During the outdoor measurements, leaves were harvested and stored in a zipper bag in a fridge until scanning.

Stereo matching

The 10 bit per pixel sensor data is inflated by the camera to 12 bit, and then stored as a 16 bit image. This means that the maximum pixel value equals 4,095, and the rest of the 16 bit container is unused. A higher pixel depth potentially leads to a more accurate stereo matching. However, the matching algorithms I tested only accept 8 bit images, which requires to normalise the image to values between 0 and 255.

For indoor settings only the plant in the foreground was visible, while the background was mostly black, presumably because of the bandpass filter and low infrared reflectance. The algorithms I tested cannot cope well with large uniform areas. Therefore, I inserted an artificial background pattern before stereo matching; see Figure 24. The pattern was shifted by the

Figure 24. Artificial background pattern for better stereo matching. (a) Normalised input image. (b) The background and some ill lit leaves are replaced by an irregular pattern.

minimum expected disparity between the left and right image.

I tested four different algorithms for stereo matching: Efficient large-scale stereo matching (ELAS; Geiger, Roser & Urtasun, 2010), semi global matching (SGM; Hirschmüller, 2005), constant-space belief propagation (Q. Yang, Wang & Ahuja, 2010), and efficient belief propagation for early vision (Felzenszwalb & Huttenlocher, 2006). The C++ code for ELAS has been downloaded from the author's website, and the OpenCV implementation was used for the other algorithms. For SGM I additionally tested the OpenCV post-filtering algorithm based on Min et al. (2014). The best results were obtained with ELAS; see Figure 25b. All algorithms implemented in OpenCV produced large miss-matched foreground areas (Figure 25c-f).

The ELAS algorithm first detects "support points" that have a strong stereo correspondence, and then uses triangulation between these points. This approach can lead to good results in low texture areas such as some leaf
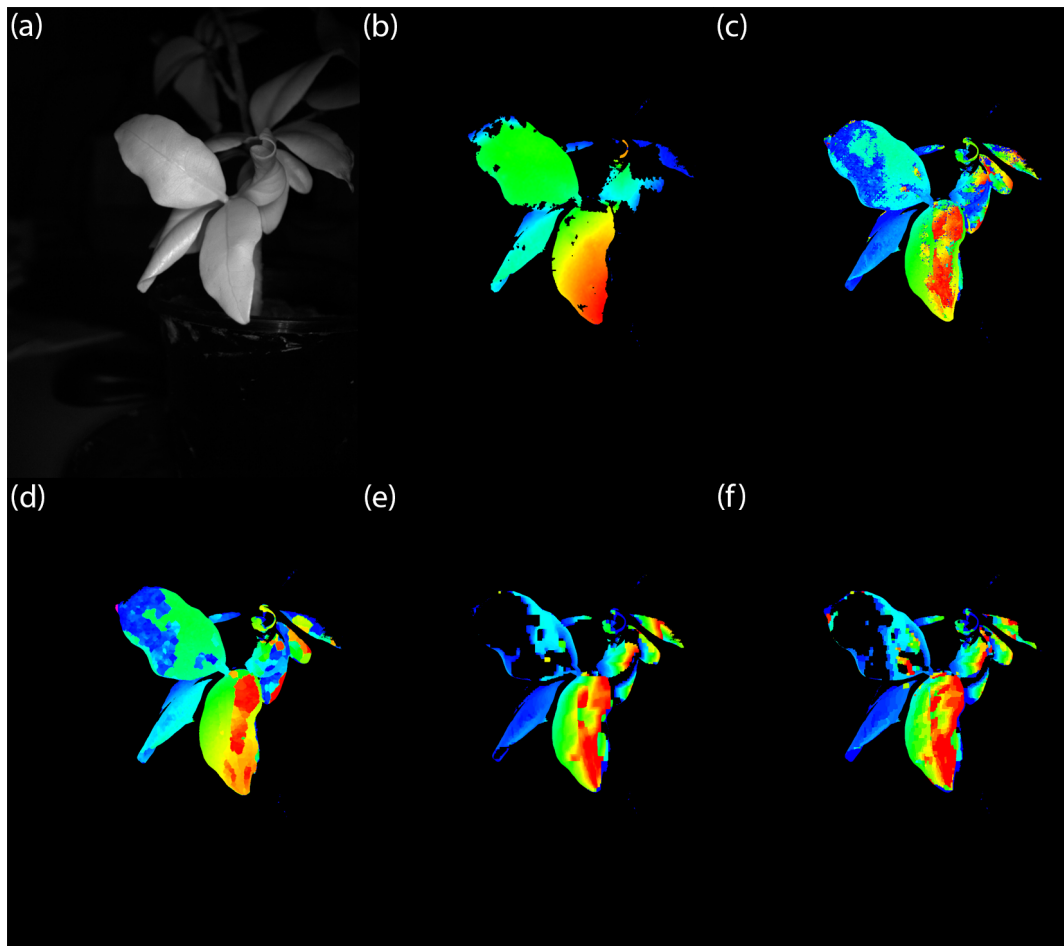
Figure 25. Comparison of stereo matching algorithms. (a) Input image (without background pattern) (b) Efficient large-scale stereo matching. (c) Semi global matching without, and (d) with post-filtering. (e) Constant-space belief propagation. (f) Efficient belief propagation. The background has been removed after stereo matching.

surfaces. There is a tradeoff between incorrect support points and a dense disparity map. I obtained good results by using a threshold of $\tau = 0.9$, as suggested by the authors (Geiger et al., 2010).

Leaf segmentation

Given a colour or grayscale image, and corresponding depth information, leaves can be segmented based on distance transform (Apelt et al., 2015), edge blending and region growing (Song et al., 2014), or multi object active contour models (Xia, Wang, Chung & Lee, 2015) for sparse canopies. For more complex cases, leaves can be over-segmented based on the intensity image, and then be clustered based on 2D shape models (Aksoy et al., 2015), or 3D surface models (Alenya, Dellen, Foix & Torras, 2013). Recently, a deep-learning-based leaf segmentation method has been presented that shows good results for dense canopies using only 2D colour images as input (Morris, 2018).

Here, I follow Alenya et al. (2013) in applying the graph-based segmentation algorithm by Felzenszwalb and Huttenlocher (2004). This algorithm aims to segment an image into similar regions by considering edges within and between regions. In particular, a threshold function is applied to determine whether two components R are similar or not using the function

$$\tau(R) = \frac{k}{\mathcal{A}(R)} \, , \tag{13}$$

where k is a constant. For the image resolution and leaf sizes in my test images, a value of $k = 800$ usually resulted in desired over-segmentation; see Figure 26c,f,j. Then, leaf components were merged based on three criteria: depth, venation, and shape.

I assumed that foreground clusters were likely part of a leaf. Additionally, I defined a range of combinations of foreground share, veins share, and ellipseness to classify clusters as potential leaf segments. The foreground

share was calculated as the ratio of foreground pixels to the cluster area. This excludes background objects, but also foreground objects with a sparse disparity map. In my test I set the highest foreground distance to 28 cm. Veins were extracted as described above, except the white top hat transform was subtracted from the black top hat transform, because the veins were darker than the leaf blade in my test images. The veins share was calculated as the ratio of vein pixels to the cluster area. Finally, I also included clusters with an ellipseness higher than 0.7 or 0.8, depending on foreground, or veins share. Even though I tested the ellipseness of a cluster rather than of a leaf, this criterion helped to exclude weirdly shaped clusters which were usually not part of a leaf.

From the clusters classified as potential leaf parts, I proceeded with the one that had the highest foreground share. Around that cluster, I identified all other clusters lying on an overlapping depth region. I then extracted all potential veins in the main cluster. To exclude noise, I only selected those which had an angle of less than 20° to the semi-major or minor axis of the best fit cluster ellipse.

Some of the identified potential veins were actually leaf edges, which was detected by their proximity to a depth edge. Along the remaining vein candidates I identified new clusters to be merged with. Clusters were merged if the tested vein was the longest vein (i.e. likely the midrib), or if the ellipseness of the merged clusters was larger than the previous ellipseness. This logic was iteratively applied to all vein segments starting with the longest, or until the ellipseness of the merged clusters exceeded 0.8. This strong reliance on ellipseness also worked for non-elliptic leaves (not shown).

It cannot be assumed that all clusters contain veins. Therefore, I added a second merging iteration testing for concavity defects, that is the distance between the object contour and its convex hull. Small defects were ignored to account for serrated leaf contours, while large defects were always filled,

if the components were lying on the same depth level. This is an opportunistic approach which may not work if concave leaves are strongly overlapping, or if the stereo matching is inaccurate. Medium convexity defects were merged if it improved the ellipseness.

This relatively simple approach worked quite well for scenes with uniform illumination (see Figure 26a,d), while it failed for clusters of sunlight and shadow; see Figure 26h. It entirely relies on graph-based segmentation, and currently does not correct inaccuracies in its clustering. I generally achieved good clustering results with this algorithm running on a 16 bit image; see Figure 26c,f,j. Furthermore, the leaf segmentation strongly depends on the accuracy of the stereo matching. In the outdoor test images the disparity map was rather sparse; see Figure 26e,i. Also, the depth edge was not exactly on the object edge of the intensity image. Because of such inaccuracies I also segmented the leaves manually to obtain the best possible area measurement with my hardware setup.

Leaf surface reconstruction

After stereo matching, the 3D coordinates were calculated using OpenCV, and then processed using Point Cloud Library (Rusu & Cousins, 2011). Particularly for the outdoor data the disparity maps were sparse, and for the matched areas the 3D data was noisy; see Figure 27. This required some heavy preprocessing before the surface reconstruction. First, outliers were removed from the point cloud by applying geometrical and statistical thresholds. Points were removed if they had fewer than 100 neighbours in a sphere with a radius of 1 cm, or when they were more than one standard deviation away from the mean in a neighbourhood of 100 points. From the remaining points, I only continued with points on the concave hull (negative aplpha-hull; Edelsbrunner, Kirkpatrick & Seidel, 1983). Second, sliding least square smoothing was applied to the hull points. The smoothing neighbourhood was set to a sphere with a relatively high radius of 3 cm
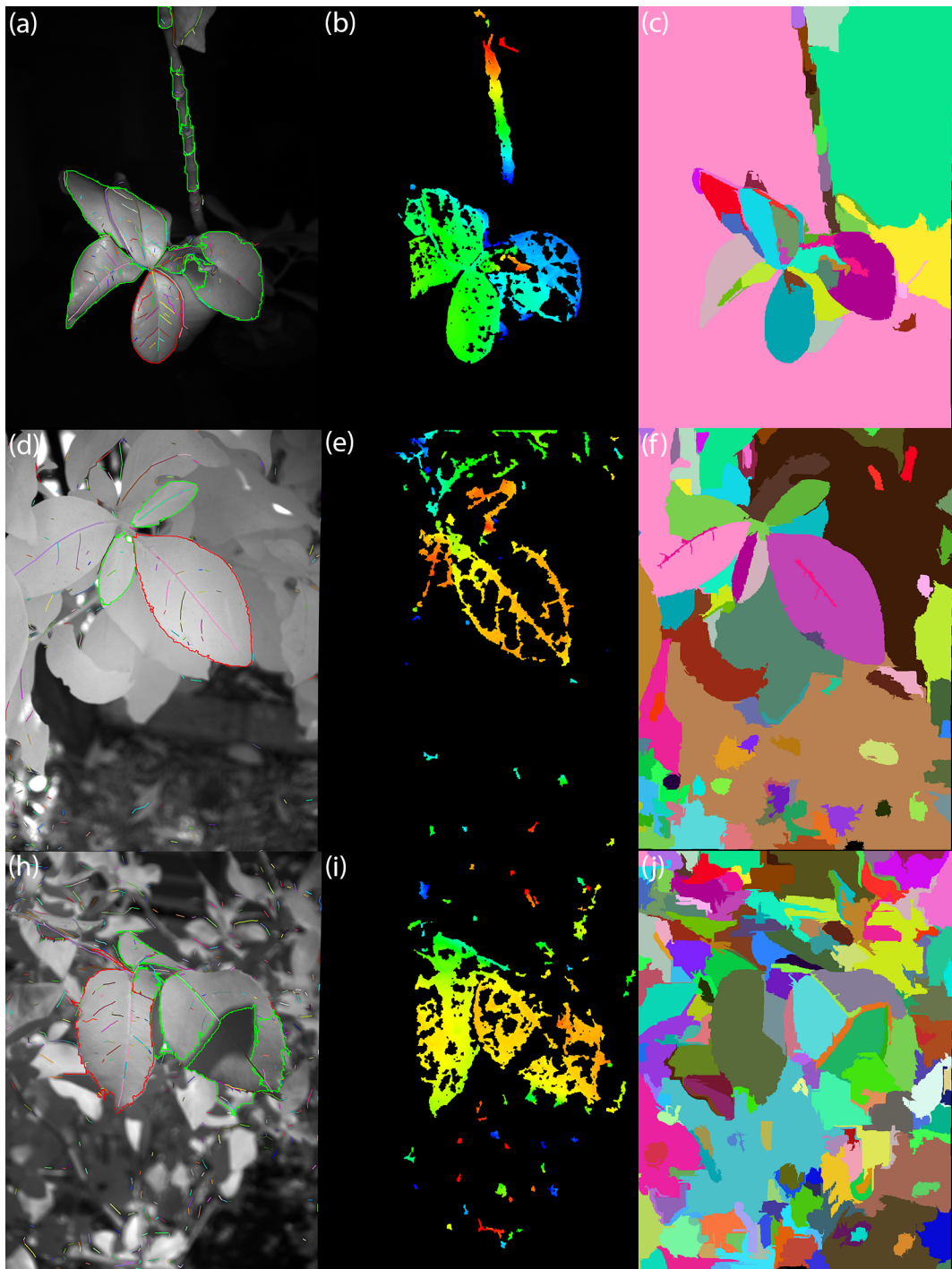
Figure 26. Leaf segmentation examples. (a-c) Indoors. (d-j) Outdoors. (a, d, h) Intensity images with the detected leaf outlined in red, further potential leaves outlined in green, and potential veins in random colours. (b, e, i) Depth map after background removal. Red indicates close values, blue indicates distant values. (c, f, j) Output of the graph-based image segmentation in random colours. (a) Most fully visible leaves correctly detected, but stem segments also identified as potential leaves. (d) Most leaves detected. (h) One leaf mostly detected, one leaf not detected due to a shadow patch.
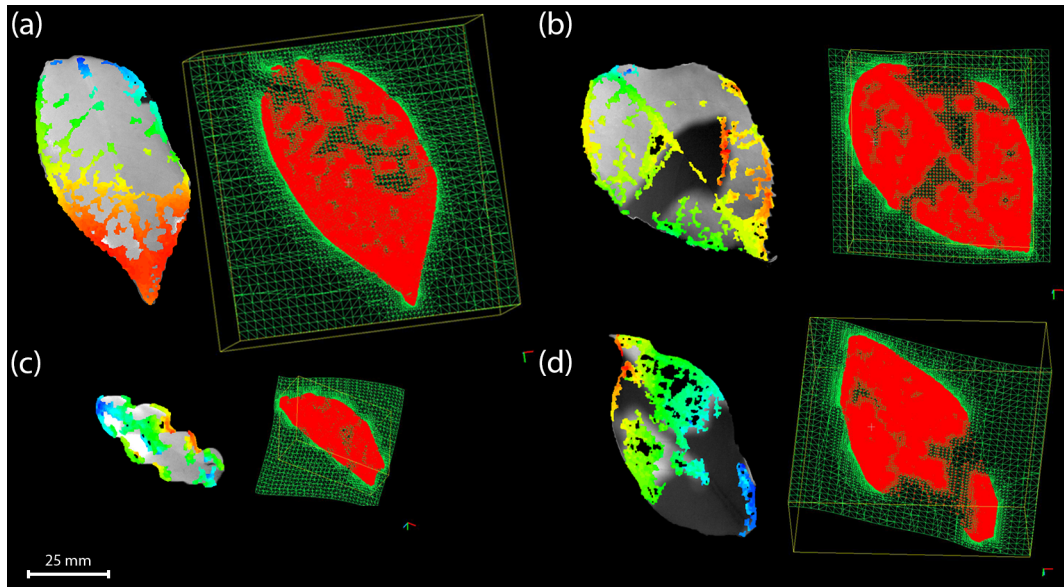
Figure 27. Leaf surface reconstruction examples from the outdoor test. The reconstructed Poisson surface mesh is shown in green, and the leaf inlier points in red. (a) Decent disparity map, and good reconstruction, relative error of -4,9% compared to ground truth. (b) Mediocre disparity map, but good reconstruction, error of -4.4%. (c) Mediocre disparity map, but bad reconstruction because of smoothing, error of -16.7%. (d) Sparse disparity map due to shadow, and incomplete reconstruction, error of -10.3%. Leaves have been segmented manually to generate the input point cloud. All leaf point clouds are approximately at scale to each other, indicated by the bar at the bottom left.

compared to the analysed leaf sizes.

Finally, Poisson surface reconstruction was applied to the smoothed point cloud (Kazhdan, Bolitho & Hoppe, 2006). This algorithm produces a watertight triangulated surface that exceeds the leaf boundaries; see Figure 27. Leaf points were determined if they were inside the convex hull of the filtered or smoothed point cloud. For the inliers, the leaf area has been calculated as the sum of all individual surface triangles using the "shoelace algorithm":

$$A = \sum_{k=1}^{n} \frac{1}{2} \left(\left| \sum_{i=1}^{2} v_{i,k} \times v_{i+1,k} \right| + \left| v_{3,k} \times v_{1,k} \right| \right) , \qquad (14)$$

where n is the number of triangles and $v_{i,k}$ is a vertex of a triangle.

4.3. Results

Linear regressions of the ground truth with reconstructed leaf areas showed high correlations for indoor and outdoor measurements. Both tests coincidentally had the same coefficient of determination of 0.994; see Figure 28. I segmented the leaves manually before stereo matching to test the best possible 3D reconstruction with my hardware and software setup. Outliers with incomplete stereo matching due to the images being out of focus, or due to unfavourable image exposure were excluded from the analysis. This test was across species, and with an unbalanced species mix in the indoor dataset. It shows the general performance across different leaf sizes, shapes, and textures. For compound leaves, only individual leaflets were considered.

While the general regression correlation was good, the relative measurement errors were still quite high. The mean absolute errors were 5.8% (σ = 6.7%) for the indoor test, and 6.7% (σ = 4.8%) for the outdoor test. Because of the low sample sizes of 14 in the indoor dataset and 11 in the outdoor dataset, the results have to be interpreted cautiously. Furthermore, the two tests did not have the same regression slope. The indoor analysis suggests that the reconstructed area is higher than the ground truth area, while the outdoor analysis shows the opposite. For the indoor data there is no apparent reason for the positive deviation from the unity line, while for the outdoor data insufficient surface reconstruction could explain the negative deviation.

4.4. Discussion

The results presented here confirm the general viability of stereo vision for leaf area measurements, which has been reported before for indoor measurements (Xiong et al., 2017). I further showed that this method also works
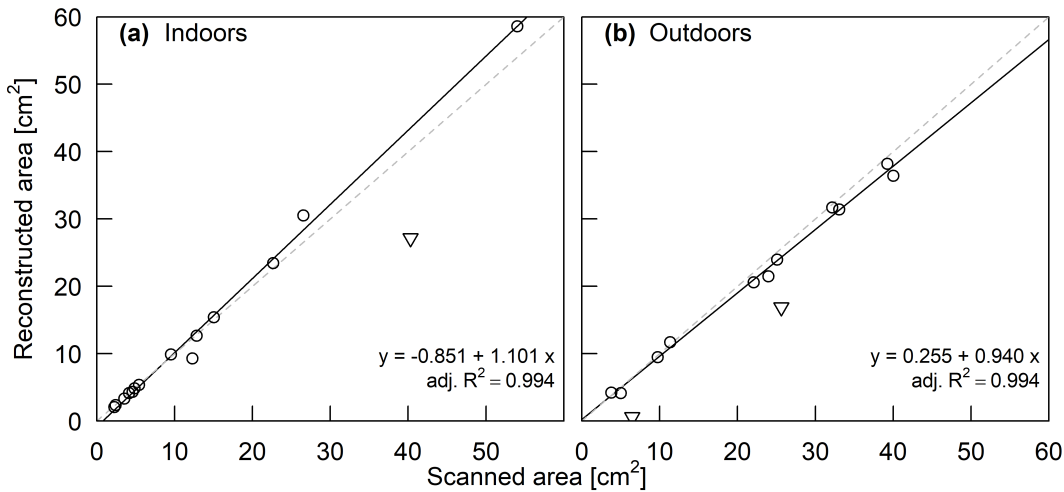
Figure 28. Linear regression of ground truth area measurements from leaf scans, and leaf area reconstruction from stereo-vision-based on manual leaf segmentation. (a) Indoor measurements. (b) Outdoor measurements. Outliers are marked with triangles; they have been excluded from the analysis because of incomplete stereo matching, because the image was out of focus, or underexposed. The unity line is indicated in dashed gray.

for outdoor measurements in direct sunlight, provided that the camera setup is suitable. Nevertheless, the measurement accuracy was insufficient to capture minute leaf area changes required for high-resolution growth measurements. My results are similar or slightly better than those reported using other methods. Structure from motion showed R^2 values of up to 0.99 for indoor leaf area reconstruction (Rose, Paulus & Kuhlmann, 2015), while values for outdoor measurements were lower at 0.94 (Jay et al., 2015). Indoor measurements with the Microsoft Kinect v2 time of flight device showed an R^2 value of 0.95 (Hu et al., 2018), and I am not aware of a similar analysis under outdoor conditions. Different studies may not be directly comparable due to different point cloud processing approaches.

There are a couple of hardware and software improvements, which could reduce the measurement errors and bring the regression slope closer to one. Stronger infrared LEDs might reduce the contrast between sunlit and shadow areas, and lead to better stereo matching in daylight conditions. I also did not test different camera baseline distances, or focal lengths

of lenses, which could be altered to match the leaf size of the target species. Better results would also be expected with single-lens reflex cameras (Muller-Linow et al., 2015), but I have not considered such a solution under the premise that the components should be as small as possible. The ultimate goal would be a system in one box with a single board computer controlling data acquisition, and potentially processing.

It may be worth testing the Intel Realsense D435 sensor as an alternative to the custom made system presented here. It combines stereo vision and structured light, which may overcome the problem of sparse disparity maps encountered in this study. It showed good performance over a range of light conditions from twilight to direct sunlight (Vit & Shani, 2018), but I am not aware of a study evaluating its performance in complete darkness. The structured light laser projection is at 850 nm which is at the lower end of suitable wavelengths. A commercial product would also have the advantage that preparatory steps for image acquisition, camera calibration, and stereo matching would be simpler or redundant.

In terms of stereo matching algorithms, I limited myself to open source software available in C++ and with a simple OpenCV interface. I found that the OpenCV implementation of semi global matching (SGM; Hirschmüller, 2005) did not perform well, while ELAS (Geiger et al., 2010) showed good results (Figure 25). A possible explanation for the comparatively bad results of SGM is that the algorithm is not designed for curved surfaces. It only distinguishes between changes of neighbouring disparities of one pixel, or more than one pixel. Furthermore, OpenCV uses a cost function which prefers flat surfaces with constant disparities (Birchfield & Tomasi, 1999).

The disparity maps were sparse and noisy which required strong outlier filtering and smoothing of the point cloud. A first improvement would be to make these steps size-dependent, instead of using fixed thresholds. The general 3D leaf shape was preserved by smoothing, but small surface features such as wrinkles were flattened out. From a theoretical point of view,

surface area triangulation can never give the true value (Schwartz, 1890). Better results could be achieved with normal integration (Coeurjolly, Flin, Teytaud & Tougne, 2003), provided that the normals are evenly distributed, or from planar surface patches (Klette & Sun, 2001). However, with the noisy 3D data in my tests, this is hardly a concern.

I simplified the analysis by manually segmenting the leaves. This is not suitable for growth measurements, particularly in outdoor settings where movements due to wind are expected. The rule-based segmentation approach shown in Figure 26 was a decent first step, but it relies on a couple of different algorithms and assumptions. It may be hard to improve the reliability for a vast range of scenes with different leaf sizes and densities. Artificial-intelligence-based methods seem more promising for this task. An initial study showed good results (Morris, 2018), and the combination with depth data should make it simple to remove background noise. Leaf segmentation and stereo matching during rain may be challenging due to glare and raindrops obscuring the view. Such a situation has not been tested here.

The intended next step would be actual growth measurements, which follows a simple logic: repeatedly measure leaf area over time. Besides the measurement accuracy, there are two practical challenges: leaf segmentation, as discussed above, and image exposure time. Because I initially got inconsistent histograms for the two stereo cameras when using automatic exposure, I decided to set the exposure manually for this test. This is no issue for experiments in growth chambers where the exposure time can be adjusted to the ambient illumination, but for greenhouse or outdoor measurements with varying illumination this is not possible. Potentially, there is a camera setting that would support automated image acquisition without artefacts. Alternatively, I could imagine an iterative image grabbing process until leaf pixel intensities are in a desired range.

Once these issues are resolved, there are a couple of other features that would be interesting to analyse in addition to leaf area growth. First, the

3D leaf shape could be extracted, as the knowledge on shape development is limited (Runions, Tsiantis & Prusinkiewicz, 2017). Building on this, leaf shape reconstruction could also be used to predict the area of partly occluded leaves. Second, the tracking of points on the leaf surface would allow us to calculate growth rates of different leaf regions. Third, the extracted venation patterns could be analysed quantitatively, for example by measuring vein angles. In conclusion, the results presented here are a promising step towards the study of leaf development in situ.

Chapter 5

Conclusions

In this thesis, I first explored the different aspects of plant growth, how they can be measured, and why growth measurements matter. Growth can be described in terms of structural growth, expansive growth, or meristem growth (Figure 1), and the focus of interest can shift depending on the spatiotemporal scale of the analysis (Figure 2). Similar to the distinction between structural and expansive growth, most growth measurement methods quantify either plant mass, or plant size (Table 2). There is an obvious difference between destructive and non-destructive measurements: analyses at the sub-organ level, or biomass measurements generally require the harvesting of plants or organs, while most size metrics, and indices such as the LAI, or NDVI allow non-destructive observations.

In addition to the system variable (main metric; see Table 2), one or more reference metrics need to be defined. For growth analyses, time is always one of the reference metrics, and usually ranges between hours and years. Instead of chronological time, thermal time can be a more meaningful reference metric, as it facilitates the comparison between experiments with different growth conditions (Table 3; Gallagher, 1979; Granier & Tardieu, 1998a). Growth analysis fundamentally changes when the focus shifts from

the organ, or plant level to the community, or landscape level, where the reference metric shifts from *per organ, or plant* to *per unit surface area* (Section 2.2).

Some methods directly measure the system variable, while others measure the change (absolute growth) between two points in time. For example, stereo vision can measure the absolute leaf area (Figure 28), while a method like the linear variable differential transformer (Hsiao et al., 1970) only measures absolute leaf elongation. The formulaic description of growth has briefly been discussed in Table 3. Linear models are widely used, particularly the exponential growth formula, but for long-term analyses non-linear models are more appropriate (Paine et al., 2012).

While this thesis focuses on short-term leaf growth, I tried to see the tree for the leaf and the forest for the tree. Therefore, the review in Chapter 2 covers the spatial scales from cells to ecosystems, and the temporal scales from hours to centuries. The importance of one particular leaf for the whole plant depends on the total leaf area, and on the leaf position in the canopy, among other factors. This one leaf has hardly an impact at the ecosystem scale, but the net change of all leaf emergence and loss processes can be observed using remote sensing methods.

The knowledge about short-term individual leaf growth drivers is relatively sparse, compared to whole shoot, but also root growth of herbaceous plants. This is partly due to methodological challenges to accurately measure or approximate two-dimensional leaf area expansion, while one-dimensional leaf elongation is simpler to measure. Shoot growth is easier to approximate than individual leaves, because it integrates all above-ground parts, and one-dimensional root growth can be tracked using dedicated experimental systems such as rhizotrons (Section 2.3).

Ultimately, the aim of plant growth measurements is to understand and model the influence of ontogenetic and environmental factors on growth (Section 2.4). Temperature is a relatively well understood factor, and

species-specific response curves can be established (Parent et al., 2010; Parent & Tardieu, 2012). As long as the temperature is in the optimal range, thermal time can be linearly approximated (Table 3; Gallagher, 1979; Granier & Tardieu, 1998a). Observations on *Arabidopsis thaliana* show an interesting temperature response: while long-term leaf growth follows thermal time (Granier et al., 2002), short-term leaf growth is not affected by different sub-daily temperature patterns (Poire et al., 2010). This suggests that under the experimental settings endogenous growth controls were stronger than temperature effects.

Besides the direct "enzymatic" effect of temperature on growth, there are also indirect effects such as the dependence of vapour-pressure deficit (VPD) on temperature (Equations 2-3), which also impacts growth. Generally, the importance of environmental factors on growth can be classified as either growth drivers, or the provision of material. Aside from temperature, soil water potential and VPD are important factors for expansive growth, with turgor pressure being a major driver (Equation 1). The acquisition of building material occurs through carbon assimilation, and nutrient uptake, with their respective dependences on temperature, radiation, VPD, soil water potential, soil pH values, etc. In this simple framework it is straightforward to postulate that any environmental factor can be limiting and causing a growth reduction away from the ontogenetic potential (Körner, 2015), and with sufficient plant growth measurements it becomes possible to model such effects (Tardieu et al., 2017).

Nevertheless, the view that growth is driven or limited by photosynthesis and carbon availability is widespread and almost all dynamic vegetation models are based on this logic (Fatichi et al., 2014; Section 2.4). It has been argued that our understanding of growth regulation is skewed towards photosynthetic *source* activities, and away from metabolic *sink* activities because of the ease of gas exchange measurements in comparison to integral growth measurements (Körner, 2015). Source driven vegetation mod-

els are relatively simple to formulate in comparison to sink driven mechanistic models (Fatichi et al., 2019). An accurate representation of sink activities has to take into account plant ontogeny as well as dynamic responses to fluctuating environmental conditions, such as changing biomass allocation (Section 2.2). Ideally, different organs are considered individually, as well as in relation to the whole plant. Turgor-driven plant growth models exist (Coussement, De Swaef, Lootens, Roldán-Ruiz & Steppe, 2018), but they currently don't include other growth factors.

For many species, growth experiments under controlled conditions are not feasible, which only leaves outdoor observations, which are extremely challenging. Adverse weather conditions can cause erroneous measurements, or damage the equipment, which leads to noisy, or incomplete data. Therefore, a high number of observations is required, which can be achieved with long time series, or many repetitions. There are elaborate systems which allow growth measurements in agricultural fields (e.g. Kirchgessner et al., 2016), but particularly for tall trees direct growth measurements methods are sparse (Section 2.3). I specifically focused on in situ leaf area and growth measurements in such challenging conditions.

In Chapter 3, I adopted the established leaf fixation method for outdoor use. This required the design of a weather-proof instrument for image acquisition (Figure 5), as well as the programming of a marker tracking software that was performing well under the experimental conditions. While this method is extremely simple in principle, it was tedious to install the instrument in the canopy so that it was placed in the right position to fix a leaf (Figure 8). Furthermore, a tedious control experiment was required to verify that the tensile forces did not affect long-term leaf growth (Figure 6).

I observed a clear diel trend with leaf area shrinkage in the morning, followed by re-expansion and growth (Figure 13). This suggests that in *Avicennia marina* leaf expansion is limited by hydraulics, which was also supported by leaf turgor measurements (Figure 14), and aggregated environmental

variables (Table 4). Other direct influences of environmental conditions on leaf area change could not be established. Despite several weeks of observations, I only had a small dataset of 23 growth days, and the unaggregated data did not show a direct effect of environmental variables (Figure 17).

Because of the effort required for testing and installing the leaf growth meter based on the fixation method, I also tested the suitability of a stereo vision system for outdoor leaf area measurements (Chapter 4). Previous publications gave a mixed picture with reports of a commercial stereo camera being insufficient for outdoor leaf measurements (Kazmi et al., 2014), but good results for outdoor leaf angle measurements (Muller-Linow et al., 2015), and indoor leaf area measurements (Xiong et al., 2017). I decided to build a small custom-made device with optical filters to mitigate the adverse effects of direct sunlight. The cost was relatively high at about NZD 3,000.00 for cameras, lenses, and filters.

First results were promising (Figure 28), and there are a couple of potential hardware improvements that could increase the measurement accuracy; see Section 4.4. However, the results are based on perfect manual leaf segmentation. Accurate automated segmentation may be achieved using deep learning (Morris, 2018). I did not test the performance in (simulated) rain conditions, and I assume that rain drops could impair the stereo matching, as well as the leaf surface reconstruction. Furthermore, the results suggest that there is an effect of illumination on the measurement, which needs to be removed or accounted for to enable reliable growth observations. There may be a "halo effect" due to illumination, which also seemed to be apparent in the field study at night (Figure 12).

In summary, the leaf fixation method had a high accuracy with relative errors of about 0.5% in all weather conditions, while stereo vision had a lower accuracy with relative errors of more than 5.0% in good conditions. The leaf fixation method did have a low measurement precision, which required smoothing and data aggregation, but it was reliable and accurate

enough to detect the leaf shrinkage in *A. marina*. With a mean relative shrinkage of 1.1% it is uncertain whether my stereo vision system could have detected the same effect. I therefore conclude that the fixation method is well suited for outdoor measurements of high-resolution leaf growth, while for stereo vision some practical issues first need to be resolved.

The fixation method sets a benchmark of high accuracy and reliability at low cost, which makes up for the high installation effort and limited applicability. As discussed in Section 4.4, new consumer grade devices are being developed which possibly could give similar or better results than my stereo vision system, and at a much lower cost. Cost is an important factor in method selection, and the acquisition of high accuracy laser scanning or light-field systems is not feasible for many researchers.

The in situ installation of a contactless measurement device may not be much simpler than the leaf fixation method. It would still require careful placement in the canopy, and potentially some twig fixation to restrict movements due to wind. The smaller and lighter the device, the simpler the installation tends to be. The ideal system would be low cost and easy to install. If the cost is low enough, a high number of measurements could potentially also compensate for a medium measurement accuracy.

Much of my time was spent writing software. Plant image analysis is a relatively young research field. Therefore, few established methods exist, and many research groups develop their own custom-made solutions. I intend to make my code publicly available to follow best practice (Lobet, 2017), and to encourage other researchers to conduct similar work.

References

Acevedo, E., Hsiao, T. C. & Henderson, D. W. (1971). Immediate and subsequent growth responses of maize leaves to changes in water status. *Plant Physiology*, *48*(5), 631–636. doi:10.1104/pp.48.5.631

Aksoy, E. E., Abramov, A., Worgotter, F., Scharr, H., Fischbach, A. & Dellen, B. (2015). Modeling leaf growth of rosette plants using infrared stereo image sequences. *Computers and Electronics in Agriculture*, *110*, 78–90. doi:10.1016/j.compag.2014.10.020

Alenya, G., Dellen, B., Foix, S. & Torras, C. (2013). Robotized plant probing: Leaf segmentation utilizing time-of-flight data. *IEEE Robotics & Automation Magazine*, *20*(3), 50–59. doi:10.1109/MRA.2012.2230118

Alenya, G., Dellen, B. & Torras, C. (2011). 3D modelling of leaves from color and ToF data for robotized plant measuring. In *2011 IEEE International Conference on Robotics and Automation* (pp. 3408–3414). Institute of Electrical and Electronics Engineers (IEEE). doi:10.1109/ICRA.2011. 5980092

Alvarez, J. P., Furumizu, C., Efroni, I., Eshed, Y. & Bowman, J. L. (2016). Active suppression of a leaf meristem orchestrates determinate leaf growth. *eLife*, *5*, e15023. doi:10.7554/eLife.15023

Andujar, D., Dorado, J., Fernandez-Quintanilla, C. & Ribeiro, A. (2016). An approach to the use of depth cameras for weed volume estimation. *Sensors*, *16*(7), 972. doi:10.3390/s16070972

Andujar, D., Fernandez-Quintanilla, C. & Dorado, J. (2015). Matching the best viewing angle in depth cameras for biomass estimation based on poplar seedling geometry. *Sensors*, *15*(6), 12999–13011. doi:10.3390/s150612999

Apelt, F., Breuer, D., Nikoloski, Z., Stitt, M. & Kragler, F. (2015). Phyto-typing4D: A light-field imaging system for non-invasive and accurate monitoring of spatio-temporal plant growth. *Plant Journal*, *82*(4), 693–706. doi:10.1111/tpj.12833

Apelt, F., Breuer, D., Olas, J. J., Annunziata, M. G., Flis, A., Nikoloski, Z., ... Stitt, M. (2017). Circadian, carbon, and light control of expansion growth and leaf movement. *Plant Physiology*, *174*(3), 1949–1968. doi:10.1104/pp.17.00503

Arvidsson, S., Perez-Rodriguez, P. & Mueller-Roeber, B. (2011). A growth phenotyping pipeline for *Arabidopsis thaliana* integrating image analysis and rosette area modeling for robust quantification of genotype effects. *New Phytologist*, *191*(3), 895–907. doi:10.1111/j.1469-8137.2011.03756.x

Asner, G. P., Scurlock, J. M. O. & Hicke, J. A. (2003). Global synthesis of leaf area index observations: Implications for ecological and remote sensing studies. *Global Ecology and Biogeography*, *12*(3), 191–205. doi:10.1046/j.1466-822X.2003.00026.x

Bailey, V. L., Bond-Lamberty, B., DeAngelis, K., Grandy, A. S., Hawkes, C. V., Heckman, K., ... Todd-Brown, K. E. (2018). Soil carbon cycling proxies: Understanding their critical role in predicting climate change feedbacks. *Global Change Biology*, *24*(3), 895–905. doi:10.1111/gcb.13926

Baldocchi, D., Falge, E., Gu, L. H., Olson, R., Hollinger, D., Running, S., ... Wofsy, S. (2001). FLUXNET: A new tool to study the temporal and spa-

tial variability of ecosystem-scale carbon dioxide, water vapor, and energy flux densities. *Bulletin of the American Meteorological Society*, *82*(11), 2415–2434. doi:10.1175/1520-0477(2001)082⟨2415:FANTTS⟩ 2.3.CO;2

Ball, M. C. (1988). Salinity tolerance in the mangroves *Aegiceras corniculatum* and *Avicennia marina*. I. Water use in relation to growth, carbon partitioning, and salt balance. *Functional Plant Biology*, *15*(3), 447–464. doi:10.1071/PP9880447

Bao, Y., Tang, L., Breitzman, M. W., Fernandez, M. G. S. & Schnable, P. S. (2018). Field-based robotic phenotyping of sorghum plant architecture using stereo vision. *Journal of Field Robotics*, *36*(2), 397–415. doi:10.1002/rob.21830

Bar-Sinai, Y., Julien, J.-D., Sharon, E., Armon, S., Nakayama, N., Adda-Bedia, M. & Boudaoud, A. (2016). Mechanical stress induces remodeling of vascular networks in growing leaves. *PLoS Comput Biol*, *12*(4), e1004819. doi:10.1371/journal.pcbi.1004819

Barbier de Reuille, P., Routier-Kierzkowska, A.-L., Kierzkowski, D., Bassel, G. W., Schüpbach, T., Tauriello, G., ... Smith, R. S. (2015). MorphoGraphX: A platform for quantifying morphogenesis in 4D. *eLife*, *4*, e05864. doi:10.7554/eLife.05864

Barron, J. L. & Liptay, A. (1994). Optical flow to measure minute increments in plant growth. *Bioimaging*, *2*(1), 57–61. doi:10.1002/1361-6374(199403)2:1⟨57::AID-BIO5⟩3.0.CO;2-D

Barron, J. L. & Liptay, A. (1997). Measuring 3-D plant growth using optical flow. *Bioimaging*, *5*(2), 82–86. doi:10.1002/1361-6374(199706)5:2⟨82::AID-BIO5⟩3.0.CO;2-F

Bassel, G. W. & Smith, R. S. (2016). Quantifying morphogenesis in plants in 4D. *Current Opinion in Plant Biology*, *29*, 87–94. doi:10.1016/j.pbi.2015.11.005

Batz, J., Méndez-Dorado, M. A. & Thomasson, J. A. (2016). Imaging for high-throughput phenotyping in energy sorghum. *Journal of Imaging*, *2*(1), 4. doi:10.3390/jimaging2010004

Beemster, G. T. S. & Baskin, T. I. (1998). Analysis of cell division and elongation underlying the developmental acceleration of root growth in *Arabidopsis thaliana*. *Plant Physiology*, *116*(4), 1515–1526. doi:10.1104/pp. 116.4.1515

Bellasio, C., Olejnickova, J., Tesar, R., Sebela, D. & Nedbal, L. (2012). Computer reconstruction of plant growth and chlorophyll fluorescence emission in three spatial dimensions. *Sensors*, *12*(1), 1052–1071. doi:10. 3390/s120101052

Birchfield, S. & Tomasi, C. (1999). Depth discontinuities by pixel-to-pixel stereo. *International Journal of Computer Vision*, *35*(3), 269–293. doi:10. 1023/A:1008160311296

Biskup, B., Scharr, H., Schurr, U. & Rascher, U. (2007). A stereo imaging system for measuring structural parameters of plant canopies. *Plant, Cell & Environment*, *30*(10), 1299–1308. doi:10.1111/j.1365-3040.2007. 01702.x

Blackman, V. H. (1919). The compound interest law and plant growth. *Annals of Botany*, *33*(131), 353–360.

Bogeat-Triboulot, M. B., Brosche, M., Renaut, J., Jouve, L., Le Thiec, D., Fayyaz, P., ... Dreyer, E. (2007). Gradual soil water depletion results in reversible changes of gene expression, protein profiles, ecophysiology, and growth performance in *Populus euphratica*, a poplar growing in arid regions. *Plant Physiology*, *143*(2), 876–892. doi:10.1104/pp.106. 088708

Borianne, P. & Brunel, G. (2012). Automated valuation of leaves area for large-scale analysis needing data coupling or petioles deletion. In *2012 IEEE 4th International Symposium on Plant Growth Modeling, Simulation,*

Visualization and Applications (pp. 50–57). Institute of Electrical and Electronics Engineers (IEEE). doi:10.1109/PMA.2012.6524812

Bouchabké, O., Tardieu, F. & Simonneau, T. (2006). Leaf growth and turgor in growing cells of maize (*Zea mays* L.) respond to evaporative demand under moderate irrigation but not in water-saturated soil. *Plant, Cell & Environment*, *29*(6), 1138–1148. doi:10.1111/j.1365-3040.2005.01494.x

Bours, R., Muthuraman, M., Bouwmeester, H. & van der Krol, A. (2012). OSCILLATOR: A system for analysis of diurnal leaf growth using infrared photography combined with wavelet transformation. *Plant Methods*, *8*, 12. doi:10.1186/1746-4811-8-29

Boyer, J. S. & Silk, W. K. (2004). Hydraulics of plant growth. *Functional Plant Biology*, *31*(8), 761–773. doi:10.1071/FP04062

Bradski, G. & Kaehler, A. (2008). *Learning OpenCV*. Sebastopol, CA: O'Reilly Media, Inc.

Brichet, N., Fournier, C., Turc, O., Strauss, O., Artzet, S., Pradal, C., … Cabrera-Bosquet, L. (2017). A robot-assisted imaging pipeline for tracking the growths of maize ear and silks in a high-throughput phenotyping platform. *Plant Methods*, *13*(1), 96. doi:10.1186/s13007-017-0246-7

Briggs, G. E., Kidd, F. & West, C. (1920). A quantitative analysis of plant growth: Part II. *Annals of Applied Biology*, *7*(2-3), 202–223. doi:10.1111/j.1744-7348.1920.tb05308.x

Brown, H. T. & Escombe, F. (1905). Researches on some of the physiological processes of green leaves, with special reference to the interchange of energy between the leaf and its surroundings. *Proceedings of the Royal Society of London Series B-Containing Papers of a Biological Character*, *76*(507), 29–111. doi:10.1098/rspb.1905.0002

Brown, S., Schroeder, P. & Birdsey, R. (1997). Aboveground biomass distribution of US eastern hardwood forests and the use of large trees as an

indicator of forest development. *Forest Ecology and Management*, *96*(1), 37–47. doi:10.1016/S0378-1127(97)00044-3

Buck, A. L. (1981). New equations for computing vapor pressure and enhancement factor. *Journal of Applied Meteorology*, *20*(12), 1527–1532. doi:10.1175/1520-0450(1981)020⟨1527:nefcvp⟩2.0.co;2

Cabrera-Bosquet, L., Fournier, C., Brichet, N., Welcker, C., Suard, B. & Tardieu, F. (2016). High-throughput estimation of incident light, light interception and radiation-use efficiency of thousands of plants in a phenotyping platform. *New Phytologist*, *212*(1), 269–281. doi:10.1111/nph.14027

Calders, K., Newnham, G., Burt, A., Murphy, S., Raumonen, P., Herold, M., . . . Kaasalainen, M. (2015). Nondestructive estimates of above-ground biomass using terrestrial laser scanning. *Methods in Ecology and Evolution*, *6*(2), 198–208. doi:10.1111/2041-210X.12301

Cardinale, B. J., Wright, J. P., Cadotte, M. W., Carroll, I. T., Hector, A., Srivastava, D. S., . . . Weis, J. J. (2007). Impacts of plant diversity on biomass production increase through time because of species complementarity. *Proceedings of the National Academy of Sciences*, *104*(46), 18123–18128. doi:10.1073/pnas.0709069104

Chaudhury, A. & Barron, J. L. (2018). Machine vision system for 3D plant phenotyping. *IEEE/ACM Transactions on Computational Biology and Bioinformatics*, 1. doi:10.1109/TCBB.2018.2824814

Chene, Y., Rousseau, D., Lucidarme, P., Bertheloot, J., Caffier, V., Morel, P., . . . Chapeau-Blondeau, F. (2012). On the use of depth camera for 3D phenotyping of entire plants. *Computers and Electronics in Agriculture*, *82*, 122–127. doi:10.1016/j.compag.2011.12.007

Chenu, K., Rey, H., Dauzat, J., Guilioni, L. & Lecoeur, J. (2008). Estimation of light interception in research environments: A joint approach using directional light sensors and 3D virtual plants applied to sunflower (*Helianthus annuus*) and *Arabidopsis thaliana* in natural and artificial

conditions. *Functional Plant Biology*, *35*(9-10), 850–866. doi:10.1071/fp08057

Chhin, S., Hogg, E. H., Lieffers, V. J. & Huang, S. (2010). Growth–climate relationships vary with height along the stem in lodgepole pine. *Tree Physiology*, *30*(3), 335–345. doi:10.1093/treephys/tpp120

Cleveland, W. S. (1979). Robust locally weighted regression and smoothing scatterplots. *Journal of the American Statistical Association*, *74*(368), 829–836. doi:10.2307/2286407

Cleveland, W. S. & Devlin, S. J. (1988). Locally weighted regression: An approach to regression analysis by local fitting. *Journal of the American Statistical Association*, *83*(403), 596–610. doi:10.1080/01621459.1988.10478639

Coen, E., Rolland-Lagan, A.-G., Matthews, M., Bangham, J. A. & Prusinkiewicz, P. (2004). The genetics of geometry. *Proceedings of the National Academy of Sciences of the United States of America*, *101*(14), 4728–4735. doi:10.1073/pnas.0306308101

Coeurjolly, D., Flin, F., Teytaud, O. & Tougne, L. (2003). Multigrid convergence and surface area estimation. In T. Asano, R. Klette & C. Ronse (Eds.), *Geometry, morphology, and computational imaging* (pp. 101–119). Berlin, Germany: Springer.

Cookson, S. J., Van Lijsebettens, M. & Granier, C. (2005). Correlation between leaf growth variables suggest intrinsic and early controls of leaf size in *Arabidopsis thaliana*. *Plant, Cell & Environment*, *28*(11), 1355–1366. doi:10.1111/j.1365-3040.2005.01368.x

Cornelissen, J., Lavorel, S., Garnier, E., Diaz, S., Buchmann, N., Gurvich, D., … Van Der Heijden, M. (2003). A handbook of protocols for standardised and easy measurement of plant functional traits worldwide. *Australian Journal of Botany*, *51*(4), 335–380.

Cosgrove, D. J. (1993). Wall extensibility: Its nature, measurement and relationship to plant cell growth. *New Phytologist*, *124*(1), 1–23. doi:10.1111/j.1469-8137.1993.tb03795.x

Cosgrove, D. J. (2016). Plant cell wall extensibility: Connecting plant cell growth with cell wall structure, mechanics, and the action of wall-modifying enzymes. *Journal of Experimental Botany*, *67*(2), 463–476. doi:10.1093/jxb/erv511

Coussement, J. R., De Swaef, T., Lootens, P., Roldán-Ruiz, I. & Steppe, K. (2018). Introducing turgor-driven growth dynamics into functional–structural plant models. *Annals of Botany*, *121*(5), 849–861. doi:10.1093/aob/mcx144

Cuny, H. E., Rathgeber, C. B. K., Frank, D., Fonti, P. & Fournier, M. (2014). Kinetics of tracheid development explain conifer tree-ring structure. *New Phytologist*, *203*(4), 1231–1241. doi:10.1111/nph.12871

Das Gupta, M. & Nath, U. (2015). Divergence in patterns of leaf growth polarity is associated with the expression divergence of miR396. *The Plant Cell*, *27*(10), 2785–2799. doi:10.1105/tpc.15.00196

De Vylder, J., Vandenbussche, F., Hu, Y., Philips, W. & Van der Straeten, D. (2012). Rosette Tracker: An open source image analysis tool for automatic quantification of genotype effects. *Plant Physiology*, *160*(3), 1149–1159. doi:10.1104/pp.112.202762

de Saussure, N. T. (1804). *Recherches chimiques sur la vegetation*. Nyon.

Debled-Rennesson, I., Rémy, J.-L. & Rouyer-Degli, J. (2005). Linear segmentation of discrete curves into blurred segments. *Discrete Applied Mathematics*, *151*(1), 122–137. doi:10.1016/j.dam.2005.03.007

Dobrescu, A., Scorza, L. C. T., Tsaftaris, S. A. & McCormick, A. J. (2017). A "Do-It-Yourself" phenotyping system: Measuring growth and morphology throughout the diel cycle in rosette shaped plants. *Plant Methods*, *13*(1), 95. doi:10.1186/s13007-017-0247-6

Donnellan Barraclough, A., Zweifel, R., Cusens, J. & Leuzinger, S. (2018). Daytime stem swelling and seasonal reversal in the peristaltic depletion of stored water along the stem of *Avicennia marina* (Forssk.) Vierh. *Tree Physiology*, *38*(7), 965–978. doi:10.1093/treephys/tpy021

Dornbusch, T., Lorrain, S., Kuznetsov, D., Fortier, A., Liechti, R., Xenarios, I. & Fankhauser, C. (2012). Measuring the diurnal pattern of leaf hyponasty and growth in *Arabidopsis* - a novel phenotyping approach using laser scanning. *Functional Plant Biology*, *39*(10-11), 860–869. doi:10.1071/fp12018

Dornbusch, T., Michaud, O., Xenarios, I. & Fankhauser, C. (2014). Differentially phased leaf growth and movements in *Arabidopsis* depend on coordinated circadian and light regulation. *Plant Cell*, *26*(10), 3911–3921. doi:10.1105/tpc.114.129031

Dosio, G. A. A., Rey, H., Lecoeur, J., Izquierdo, N. G., Aguirrezabal, L. A. N., Tardieu, F. & Turc, O. (2003). A whole-plant analysis of the dynamics of expansion of individual leaves of two sunflower hybrids. *Journal of Experimental Botany*, *54*(392), 2541–2552. doi:10.1093/jxb/erg279

Dowle, M., Srinivasan, A., Gorecki, J., Short, T., Lianoglou, S. & Antonyan, E. (2017). Package 'data.table' [Computer software]. Retrieved from https://cran.r-project.org/web/packages/data.table/index.html

Duan, T., Chapman, S., Holland, E., Rebetzke, G., Guo, Y. & Zheng, B. (2016). Dynamic quantification of canopy structure to characterize early plant vigour in wheat genotypes. *Journal of Experimental Botany*. doi:10.1093/jxb/erw227

Dupuis, J., Holst, C. & Kuhlmann, H. (2017). Measuring leaf thickness with 3D close-up laser scanners: Possible or not? *Journal of Imaging*, *3*(2), 22.

Edelsbrunner, H., Kirkpatrick, D. & Seidel, R. (1983). On the shape of a set of points in the plane. *IEEE Transactions on Information Theory*, *29*(4), 551–559.

Eguchi, H. & Matsui, T. (1977). Computer control of plant growth by image processing II. Pattern recognition of growth in on-line system. *Environment Control in Biology*, *15*(2), 37–45. doi:10.2525/ecb1963.15.37

Elser, J. J., Fagan, W. F., Denno, R. F., Dobberfuhl, D. R., Folarin, A., Huberty, A., . . . Sterner, R. W. (2000). Nutritional constraints in terrestrial and freshwater food webs. *Nature, 408*, 578–580. doi:10.1038/35046058

Erickson, R. O. & Sax, K. B. (1956). Rates of cell division and cell elongation in the growth of the primary root of *Zea mays*. *Proceedings of the American Philosophical Society*, *100*(5), 499–514.

Fahlgren, N., Feldman, M., Gehan, M. A., Wilson, M. S., Shyu, C., Bryant, D. W., . . . Baxter, I. (2015). A versatile phenotyping system and analytics platform reveals diverse temporal responses to water availability in *Setaria. Molecular Plant*, *8*(10), 1520–1535. doi:10.1016/j.molp.2015.06.005

Faragó, D., Sass, L., Valkai, I., Andrási, N. & Szabados, L. (2018). PlantSize offers an affordable, non-destructive method to measure plant size and color in vitro. *Frontiers in Plant Science*, *9*(219). doi:10.3389/fpls.2018.00219

Fatichi, S., Leuzinger, S. & Körner, C. (2014). Moving beyond photosynthesis: From carbon source to sink-driven vegetation modeling. *New Phytologist*, *201*(4), 1086–1095. doi:10.1111/nph.12614

Fatichi, S., Pappas, C. & Ivanov, V. Y. (2016). Modeling plant–water interactions: An ecohydrological overview from the cell to the global scale. *Wiley Interdisciplinary Reviews: Water*, *3*, 327–368. doi:10.1002/wat2.1125

Fatichi, S., Pappas, C., Zscheischler, J. & Leuzinger, S. (2019). Modelling carbon sources and sinks in terrestrial vegetation. *New Phytologist*, *221*(2), 652–668.

Felzenszwalb, P. F. & Huttenlocher, D. P. (2004). Efficient graph-based image segmentation. *International Journal of Computer Vision*, *59*(2), 167–181. doi:10.1023/B:VISI.0000022288.19776.77

Felzenszwalb, P. F. & Huttenlocher, D. P. (2006). Efficient belief propagation for early vision. *International Journal of Computer Vision*, *70*(1), 41–54. doi:10.1007/s11263-006-7899-4

Fiorani, F. & Beemster, G. T. S. (2006). Quantitative analyses of cell division in plants. *Plant Molecular Biology*, *60*(6), 963–979. doi:10.1007/s11103-005-4065-2

Fiorani, F. & Schurr, U. (2013). Future scenarios for plant phenotyping. *Annual Review of Plant Biology*, *64*, 267–291. doi:10.1146/annurev-arplant-050312-120137

Fitzgibbon, A., Pilu, M. & Fisher, R. B. (1999). Direct least square fitting of ellipses. *IEEE Transactions on Pattern Analysis and Machine Intelligence*, *21*(5), 476–480. doi:10.1109/34.765658

Fox, S., Southam, P., Pantin, F., Kennaway, R., Robinson, S., Castorina, G., ... Coen, E. (2018). Spatiotemporal coordination of cell division and growth during organ morphogenesis. *PLOS Biology*, *16*(11), e2005952. doi:10.1371/journal.pbio.2005952

Gai, J., Tang, L. & Steward, B. (2015). Plant recognition through the fusion of 2D and 3D images for robotic weeding. In *2015 ASABE Annual International Meeting* (p. 1). 152181371. American Society of Agricultural and Biological Engineers. doi:10.13031/aim.20152181371

Gallagher, J. N. (1979). Field studies of cereal leaf growth. I. Initiation and expansion in relation to temperature and ontogeny. *Journal of Experimental Botany*, *30*(4), 625–636. doi:10.1093/jxb/30.4.625

Garrido-Jurado, S., Muñoz-Salinas, R., Madrid-Cuevas, F. J. & Marín-Jiménez, M. J. (2014). Automatic generation and detection of highly reliable fiducial markers under occlusion. *Pattern Recognition*, *47*(6), 2280–2292. doi:10.1016/j.patcog.2014.01.005

Gates, D. M., Keegan, H. J., Schleter, J. C. & Weidner, V. R. (1965). Spectral properties of plants. *Applied Optics*, *4*(1), 11–20. doi:10.1364/ao.4.000011

Gazquez, A. & Beemster, G. T. S. (2017). What determines organ size differences between species? A meta-analysis of the cellular basis. *New Phytologist*, *215*(1), 299–308. doi:10.1111/nph.14573

Geiger, A., Roser, M. & Urtasun, R. (2010). Efficient large-scale stereo matching. In *Asian conference on computer vision* (pp. 25–38). Berlin, Germany: Springer. doi:10.1007/978-3-642-19315-6_3

Gibbs, J. A., Pound, M., French, A. P., Wells, D. M., Murchie, E. & Pridmore, T. (2016). Approaches to three-dimensional reconstruction of plant shoot topology and geometry. *Functional Plant Biology*, *44*(1), 62–75. doi:10.1071/fp16167

Giuffrida, M. V., Doerner, P. & Tsaftaris, S. A. (2018). Pheno-Deep Counter: A unified and versatile deep learning architecture for leaf counting. *The Plant Journal*, *96*(4), 880–890.

Golbach, F., Kootstra, G., Damjanovic, S., Otten, G. & van de Zedde, R. (2015). Validation of plant part measurements using a 3D reconstruction method suitable for high-throughput seedling phenotyping. *Machine Vision and Applications*, 1–18. doi:10.1007/s00138-015-0727-5

Gonzalez, N., Vanhaeren, H. & Inzé, D. (2012). Leaf size control: Complex coordination of cell division and expansion. *Trends in Plant Science*, *17*(6), 332–340. doi:10.1016/j.tplants.2012.02.003

Goodall, C. R. & Green, P. B. (1986). Quantitative analysis of surface growth. *Botanical Gazette*, *147*(1), 1–15. doi:10.1086/337562

Grace, J. C. (1987). Theoretical ratio between "one-sided" and total surface area for pine needles. *New Zealand Journal of Forestry Science*, *17*(2/3), 292–296.

Granier, C., Massonnet, C., Turc, O., Muller, B., Chenu, K. & Tardieu, F. (2002). Individual leaf development in *Arabidopsis thaliana*: A stable

thermal-time-based programme. *Annals of Botany*, *89*(5), 595–604. doi:10.1093/aob/mcf085

Granier, C. & Tardieu, F. (1998a). Is thermal time adequate for expressing the effects of temperature on sunflower leaf development? *Plant, Cell & Environment*, *21*(7), 695–703. doi:10.1046/j.1365-3040.1998.00319.x

Granier, C. & Tardieu, F. (1998b). Spatial and temporal analyses of expansion and cell cycle in sunflower leaves: A common pattern of development for all zones of a leaf and different leaves of a plant. *Plant Physiology*, *116*(3), 991–1001. doi:10.1104/pp.116.3.991

Granier, C. & Tardieu, F. (1999a). Leaf expansion and cell division are affected by reducing absorbed light before but not after the decline in cell division rate in the sunflower leaf. *Plant, Cell & Environment*, *22*(11), 1365–1376. doi:10.1046/j.1365-3040.1999.00497.x

Granier, C. & Tardieu, F. (1999b). Water deficit and spatial pattern of leaf development. Variability in responses can be simulated using a simple model of leaf development. *Plant Physiology*, *119*(2), 609–619. doi:10.1104/pp.119.2.609

Granier, C. & Tardieu, F. (2009). Multi-scale phenotyping of leaf expansion in response to environmental changes: The whole is more than the sum of parts. *Plant, Cell & Environment*, *32*(9), 1175–1184. doi:10.1111/j.1365-3040.2009.01955.x

Green, P. B. (1976). Growth and cell pattern formation on an axis: Critique of concepts, terminology, and modes of study. *Botanical Gazette*, *137*(3), 187–202. doi:10.1086/336858

Gregory, F. G. (1921). Studies in the energy relations of plants. I. The increase in area of leaves and leaf surface of *Cucumis sativus*. *Annals of Botany*, *35*(137), 93–123.

Guillemot, J., Francois, C., Hmimina, G., Dufrêne, E., Martin-StPaul, N. K., Soudani, K., . . . Delpierre, N. (2017). Environmental control of carbon

allocation matters for modelling forest growth. *New Phytologist, 214*(1), 180–193. doi:10.1111/nph.14320

Hales, S. (1727). *Vegetable staticks: Or, an account of some statical experiments on the sap in vegetables: Being an essay towards a natural history of vegetation. Also, a specimen of an attempt to analyse the air, by a great variety of chymio-statical experiments; which were read at several meetings before the royal society.* London: W., J. Innys and T. Woodward.

Halperin, O., Gebremedhin, A., Wallach, R. & Moshelion, M. (2017). High-throughput physiological phenotyping and screening system for the characterization of plant–environment interactions. *The Plant Journal, 89*(4), 839–850.

Hargreaves, C. E., Gregory, P. J. & Bengough, A. G. (2009). Measuring root traits in barley (*Hordeum vulgare* ssp. *vulgare* and ssp. *spontaneum*) seedlings using gel chambers, soil sacs and X-ray microtomography. *Plant and Soil, 316*(1), 285–297. doi:10.1007/s11104-008-9780-4

Hartmann, A., Czauderna, T., Hoffmann, R., Stein, N. & Schreiber, F. (2011). HTPheno: An image analysis pipeline for high-throughput plant phenotyping. *BMC Bioinformatics, 12*, 9. doi:10.1186/1471-2105-12-148

Hejnowicz, Z. & Romberger, J. A. (1984). Growth tensor of plant organs. *Journal of Theoretical Biology, 110*(1), 93–114. doi:10.1016/S0022-5193(84)80017-X

Hervieux, N., Dumond, M., Sapala, A., Routier-Kierzkowska, A.-L., Kierzkowski, D., Roeder, A. H. K., ... Hamant, O. (2016). A mechanical feedback restricts sepal growth and shape in *Arabidopsis*. *Current Biology, 26*(8), 1019–1028. doi:10.1016/j.cub.2016.03.004

Higgs, K. H. & Jones, H. G. (1984). A microcomputer-based system for continuous measurement and recording fruit diameter in relation to environmental factors. *Journal of Experimental Botany, 35*(11), 1646–1655. doi:10.1093/jxb/35.11.1646

Hill, C. & Jones, R. L. (2000). Absorption of solar radiation by water vapor in clear and cloudy skies: Implications for anomalous absorption. *Journal of Geophysical Research: Atmospheres*, *105*(D7), 9421–9428. doi:10.1029/1999JD901153

Hirschmüller, H. (2005). Accurate and efficient stereo processing by semi-global matching and mutual information. In *2005 IEEE Computer Society Conference on Computer Vision and Pattern Recognition* (Vol. 2, pp. 807–814). doi:10.1109/CVPR.2005.56

Hisanaga, T., Kawade, K. & Tsukaya, H. (2015). Compensation: A key to clarifying the organ-level regulation of lateral organ size in plants. *Journal of Experimental Botany*, *66*(4), 1055–1063. doi:10.1093/jxb/erv028

Hong, L., Dumond, M., Tsugawa, S., Sapala, A., Routier-Kierzkowska, A.-L., Zhou, Y., … Roeder, A. H. K. (2016). Variable cell growth yields reproducible organ development through spatiotemporal averaging. *Developmental Cell*, *38*(1), 15–32. doi:10.1016/j.devcel.2016.06.016

Hsiao, T. C., Acevedo, E. & Henderson, D. W. (1970). Maize leaf elongation: Continuous measurements and close dependence on plant water status. *Science*, *168*(3931), 590–591. doi:10.1126/science.168.3931.590

Hu, Y., Wang, L., Xiang, L., Wu, Q. & Jiang, H. (2018). Automatic non-destructive growth measurement of leafy vegetables based on Kinect. *Sensors*, *18*(3), 806. doi:10.3390/s18030806

Huete, A., Didan, K., Miura, T., Rodriguez, E. P., Gao, X. & Ferreira, L. G. (2002). Overview of the radiometric and biophysical performance of the MODIS vegetation indices. *Remote Sensing of Environment*, *83*(1-2), 195–213. doi:10.1016/s0034-4257(02)00096-2

Hummel, I., Pantin, F., Sulpice, R., Piques, M., Rolland, G., Dauzat, M., … Muller, B. (2010). *Arabidopsis* plants acclimate to water deficit at low cost through changes of carbon usage: An integrated perspective using growth, metabolite, enzyme, and gene expression analysis. *Plant Physiology*, *154*(1), 357–372. doi:10.1104/pp.110.157008

Ivakov, A., Flis, A., Apelt, F., Fünfgeld, M., Scherer, U., Stitt, M., ... Suslov, D. (2017). Cellulose synthesis and cell expansion are regulated by different mechanisms in growing *Arabidopsis* hypocotyls. *The Plant Cell*, *29*(6), 1305–1315. doi:10.1105/tpc.16.00782

Jaffe, M. J., Wakefield, A. H., Telewski, F., Gulley, E. & Biro, R. (1985). Computer-assisted image analysis of plant growth, thigmomorphogenesis, and gravitropism. *Plant Physiology*, *77*(3), 722–730. doi:10 . 1104/pp.77.3.722

Jamieson, P. D., Semenov, M. A., Brooking, I. R. & Francis, G. S. (1998). Sirius: A mechanistic model of wheat response to environmental variation. *European Journal of Agronomy*, *8*(3), 161–179. doi:10.1016/S1161-0301(98)00020-3

Jansen, M., Gilmer, F., Biskup, B., Nagel, K. A., Rascher, U., Fischbach, A., ... Walter, A. (2009). Simultaneous phenotyping of leaf growth and chlorophyll fluorescence via GROWSCREEN FLUORO allows detection of stress tolerance in *Arabidopsis thaliana* and other rosette plants. *Functional Plant Biology*, *36*(10-11), 902–914. doi:10.1071/fp09095

Jay, S., Rabatel, G., Hadoux, X., Moura, D. & Gorretta, N. (2015). In-field crop row phenotyping from 3D modeling performed using structure from motion. *Computers and Electronics in Agriculture*, *110*, 70–77. doi:10 . 1016/j.compag.2014.09.021

Johnson, M. G., Tingey, D. T., Phillips, D. L. & Storm, M. J. (2001). Advancing fine root research with minirhizotrons. *Environmental and Experimental Botany*, *45*(3), 263–289. doi:10.1016/S0098-8472(01)00077-6

Jones, A. R., Forero-Vargas, M., Withers, S. P., Smith, R. S., Traas, J., Dewitte, W. & Murray, J. A. H. (2017). Cell-size dependent progression of the cell cycle creates homeostasis and flexibility of plant cell size. *Nature Communications*, *8*, 15060. doi:10.1038/ncomms15060

Kazhdan, M., Bolitho, M. & Hoppe, H. (2006). Poisson surface reconstruction. In A. Sheffer & K. Polthier (Eds.), *Proceedings of the fourth Euro-*

graphics Symposium on Geometry processing (Vol. 7, pp. 61–70). The Eurographics Association. doi:10.2312/SGP/SGP06/061-070

Kazmi, W., Foix, S., Alenya, G. & Andersen, H. J. (2014). Indoor and outdoor depth imaging of leaves with time-of-flight and stereo vision sensors: Analysis and comparison. *ISPRS Journal of Photogrammetry and Remote Sensing*, *88*, 128–146. doi:10.1016/j.isprsjprs.2013.11.012

Kintel, M. (2015). OpenSCAD [Computer software] (Version 2015.03). Retrieved from https://www.openscad.org

Kirchgessner, N., Liebisch, F., Yu, K., Pfeifer, J., Friedli, M., Hund, A. & Walter, A. (2016). The ETH field phenotyping platform FIP: A cable-suspended multi-sensor system. *Functional Plant Biology*, *44*(1), 154–168. doi:10.1071/FP16165

Kjaer, K. H. & Ottosen, C. O. (2015). 3D laser triangulation for plant phenotyping in challenging environments. *Sensors*, *15*(6), 13533–13547. doi:10.3390/s150613533

Klein, T., Vitasse, Y. & Hoch, G. (2016). Coordination between growth, phenology and carbon storage in three coexisting deciduous tree species in a temperate forest. *Tree Physiology*, *36*(7), 847–855. doi:10.1093/treephys/tpw030

Klette, R. & Sun, H. J. (2001). Digital planar segment based polyhedrization for surface area estimation. In C. Arcelli, L. P. Cordella & G. S. di Baja (Eds.), *Visual Form 2001* (pp. 356–366). Berlin, Germany: Springer.

Klukas, C., Chen, D. J. & Pape, J. M. (2014). Integrated analysis platform: An open-source information system for high-throughput plant phenotyping. *Plant Physiology*, *165*(2), 506–518. doi:10.1104/pp.113.233932

Knecht, A. C., Campbell, M. T., Caprez, A., Swanson, D. R. & Walia, H. (2016). Image Harvest: An open-source platform for high-throughput plant image processing and analysis. *Journal of Experimental Botany*, *67*(11), 3587–3599. doi:10.1093/jxb/erw176

Körner, C. (2003a). *Alpine plant life. Functional plant ecology of high mountain ecosystems* (2nd ed.). Berlin, Germany: Springer. doi:10.1007/978-3-642-18970-8

Körner, C. (2003b). Carbon limitation in trees. *Journal of Ecology*, *91*(1), 4–17. doi:10.1046/j.1365-2745.2003.00742.x

Körner, C. (2003c). Slow in, rapid out-Carbon flux studies and Kyoto targets. *Science*, *300*(5623), 1242–1243. doi:10.1126/science.1084460

Körner, C. (2015). Paradigm shift in plant growth control. *Current Opinion in Plant Biology*, *25*, 107–114. doi:10.1016/j.pbi.2015.05.003

Körner, C., Pelaez, M.-R. S. & John, P. (1989). Why are bonsai plants small? A consideration of cell size. *Functional Plant Biology*, *16*(5), 443–448. doi:10.1071/PP9890443

Kreusler, U. (1878). Beobachtungen über das Wachsthum der Maispflanze. *Landwirtschaftliche Jahrbücher*, *7*, 536–564.

Kuchen, E. E., Fox, S., Barbier de Reuille, P., Kennaway, R., Bensmihen, S., Avondo, J., . . . Coen, E. (2012). Generation of leaf shape through early patterns of growth and tissue polarity. *Science*, *335*(6072), 1092–1096. doi:10.1126/science.1214678

Land Information New Zealand. (2017). Sea level data downloads. Web Page. Retrieved June 15, 2017, from http://www.linz.govt.nz/sea/tides/sea-level-data/sea-level-data-downloads

Lati, R. N., Filin, S. & Eizenberg, H. (2013). Estimating plant growth parameters using an energy minimization-based stereovision model. *Computers and Electronics in Agriculture*, *98*, 260–271. doi:10.1016/j.compag.2013.07.012

Lee, K., Avondo, J., Morrison, H., Blot, L., Stark, M., Sharpe, J., . . . Coen, E. (2006). Visualizing plant development and gene expression in three dimensions using optical projection tomography. *Plant Cell*, *18*(9), 2145–2156. doi:10.1105/tpc.106.043042

Lee, K., Calder, G. M., Hindle, C. R., Newman, J. L., Robinson, S. N., Avondo, J. & Coen, E. (2016). Macro optical projection tomography for large scale 3D imaging of plant structures and gene activity. *Journal of Experimental Botany*, *68*(3), 527–538. doi:10.1093/jxb/erw452

Leemans, V., Dumont, B. & Destain, M. F. (2013). Assessment of plant leaf area measurement by using stereo-vision. In *2013 International Conference on 3D Imaging* (p. 5). Institute of Electrical and Electronics Engineers (IEEE). doi:10.1109/IC3D.2013.6732085

Leister, D., Varotto, C., Pesaresi, P., Niwergall, A. & Salamini, F. (1999). Large-scale evaluation of plant growth in *Arabidopsis thaliana* by non-invasive image analysis. *Plant Physiology and Biochemistry*, *37*(9), 671–678. doi:10.1016/s0981-9428(00)80097-2

Leuzinger, S. & Hättenschwiler, S. (2013). Beyond global change: Lessons from 25 years of CO_2 research. *Oecologia*, *171*(3), 639–651. doi:10.1007/s00442-012-2584-5

Leuzinger, S., Manusch, C., Bugmann, H. & Wolf, A. (2013). A sink-limited growth model improves biomass estimation along boreal and alpine tree lines. *Global Ecology and Biogeography*, *22*(8), 924–932. doi:10.1111/geb.12047

Li, Y., Fan, X., Mitra, N. J., Chamovitz, D., Cohen-Or, D. & Chen, B. (2013). Analyzing growing plants from 4D point cloud data. *ACM Transactions on Graphics (TOG)*, *32*(6), 157. doi:10.1145/2508363.2508368

Lieth, H. & Whittaker, R. (1975). *Primary productivity of the biosphere*. New York, NY: Springer. doi:10.1007/978-3-642-80913-2

Lim, K., Treitz, P., Wulder, M., St-Onge, B. & Flood, M. (2003). LiDAR remote sensing of forest structure. *Progress in Physical Geography: Earth and Environment*, *27*(1), 88–106. doi:10.1191/0309133303pp360ra

Lipowczan, M., Piekarska-Stachowiak, A., Elsner, J. & Pietrakowski, J. (2013). The tensor-based model of plant growth applied to leaves of

Arabidopsis thaliana: A two-dimensional computer model. *Comptes Rendus Biologies, 336*(9), 425–432. doi:10.1016/j.crvi.2013.09.001

Lizaso, J. I., Batchelor, W. D. & Westgate, M. E. (2003). A leaf area model to simulate cultivar-specific expansion and senescence of maize leaves. *Field Crops Research, 80*(1), 1–17. doi:10.1016/S0378-4290(02)00151-X

Lobet, G. (2017). Image analysis in plant sciences: Publish then perish. *Trends in Plant Science, 22*(7), 559–566. doi:10.1016/j.tplants.2017.05.002

Lockhart, J. A. (1965). An analysis of irreversible plant cell elongation. *Journal of Theoretical Biology, 8*(2), 264–275. doi:10.1016/0022-5193(65)90077-9

Maddonni, G. A., Otegui, M. E. & Cirilo, A. G. (2001). Plant population density, row spacing and hybrid effects on maize canopy architecture and light attenuation. *Field Crops Research, 71*(3), 183–193. doi:10.1016/S0378-4290(01)00158-7

Maksymowych, R. (1973). *Analysis of leaf development*. Cambridge: Cambridge University Press.

Maloof, J. N., Nozue, K., Mumbach, M. R. & Palmer, C. M. (2013). LeafJ: An ImageJ plugin for semi-automated leaf shape measurement. *Jove-Journal of Visualized Experiments*, (71). doi:10.3791/50028

Massonnet, C., Tisné, S., Radziejwoski, A., Vile, D., De Veylder, L., Dauzat, M. & Granier, C. (2011). New insights into the control of endoreduplication: Endoreduplication could be driven by organ growth in *Arabidopsis* leaves. *Plant Physiology, 157*(4), 2044. doi:10.1104/pp.111.179382

Matsubara, S., Hurry, V., Druart, N., Benedict, C., Janzik, I., Chavarria-Krauser, A., … Schurr, U. (2006). Nocturnal changes in leaf growth of *Populus deltoides* are controlled by cytoplasmic growth. *Planta, 223*(6), 1315–1328. doi:10.1007/s00425-005-0181-0

McCormick, R. F., Truong, S. K. & Mullet, J. E. (2016). 3D sorghum reconstructions from depth images identify QTL regulating shoot architecture. *Plant Physiology*, *172*(2), 823–834. doi:10.1104/pp.16.00948

Mercado, L. M., Medlyn, B. E., Huntingford, C., Oliver, R. J., Clark, D. B., Sitch, S., . . . Cox, P. M. (2018). Large sensitivity in land carbon storage due to geographical and temporal variation in the thermal response of photosynthetic capacity. *New Phytologist*, *218*(4), 1462–1477. doi:10. 1111/nph.15100

Merret, R., Moulia, B., Hummel, I., Cohen, D., Dreyer, E. & Bogeat-Triboulot, M.-B. (2010). Monitoring the regulation of gene expression in a growing organ using a fluid mechanics formalism. *BMC Biology*, *8*(1), 18. doi:10.1186/1741-7007-8-18

Mielewczik, M., Friedli, M., Kirchgessner, N. & Walter, A. (2013). Diel leaf growth of soybean: A novel method to analyze two-dimensional leaf expansion in high temporal resolution based on a marker tracking approach (Martrack Leaf). *Plant Methods*, *9*, 13. doi:10.1186/1746-4811-9-30

Min, D., Choi, S., Lu, J., Ham, B., Sohn, K. & Do, M. N. (2014). Fast global image smoothing based on weighted least squares. *IEEE Transactions on Image Processing*, *23*(12), 5638–5653. doi:10.1109/TIP.2014.2366600

Minervini, M., Abdelsamea, M. M. & Tsaftaris, S. A. (2014). Image-based plant phenotyping with incremental learning and active contours. *Ecological Informatics*, *23*, 35–48. doi:10.1016/j.ecoinf.2013.07.004

Minervini, M., Giuffrida, M. V., Perata, P. & Tsaftaris, S. A. (2017). Phenotiki: An open software and hardware platform for affordable and easy image-based phenotyping of rosette-shaped plants. *The Plant Journal*, *90*(1), 204–216. doi:10.1111/tpj.13472

Minervini, M., Scharr, H. & Tsaftaris, S. A. (2015). Image analysis: The new bottleneck in plant phenotyping. *IEEE Signal Processing Magazine*, *32*(4), 126–131. doi:10.1109/msp.2015.2405111

Monsi, M. & Saeki, T. (2005). On the factor light in plant communities and its importance for matter production. *Annals of Botany*, *95*(3), 549–567. doi:10.1093/aob/mci052

Monteith, J. L. (1977). Climate and the efficiency of crop production in Britain. *Philosophical Transactions of the Royal Society of London. B, Biological Sciences*, *281*(980), 277–294. doi:10.1098/rstb.1977.0140

Moreno-Ortega, B., Fort, G., Muller, B. & Guédon, Y. (2017). Identifying developmental zones in maize lateral root cell length profiles using multiple change-point models. *Frontiers in Plant Science*, *8*(1750). doi:10.3389/fpls.2017.01750

Morris, D. (2018). A pyramid CNN for dense-leaves segmentation. In *2018 15th Conference on Computer and Robot Vision* (pp. 238–245). Institute of Electrical and Electronics Engineers (IEEE). doi:10.1109/CRV.2018.00041

Muller-Linow, M., Pinto-Espinosa, F., Scharr, H. & Rascher, U. (2015). The leaf angle distribution of natural plant populations: Assessing the canopy with a novel software tool. *Plant Methods*, *11*, 16. doi:10.1186/s13007-015-0052-z

Muller, B., Pantin, F., Genard, M., Turc, O., Freixes, S., Piques, M. & Gibon, Y. (2011). Water deficits uncouple growth from photosynthesis, increase C content, and modify the relationships between C and growth in sink organs. *Journal of Experimental Botany*, *62*(6), 1715–1729. doi:10.1093/jxb/erq438

Muller, B., Reymond, M. & Tardieu, F. (2001). The elongation rate at the base of a maize leaf shows an invariant pattern during both the steady-state elongation and the establishment of the elongation zone. *Journal of Experimental Botany*, *52*(359), 1259–1268. doi:10.1093/jexbot/52.359.1259

Nagel, K. A., Putz, A., Gilmer, F., Heinz, K., Fischbach, A., Pfeifer, J., … Schurr, U. (2012). GROWSCREEN-Rhizo is a novel phenotyping ro-

bot enabling simultaneous measurements of root and shoot growth for plants grown in soil-filled rhizotrons. *Functional Plant Biology*, *39*(11), 891–904. doi:10.1071/fp12023

Nagelmüller, S., Kirchgessner, N., Yates, S., Hiltpold, M. & Walter, A. (2016). Leaf Length Tracker: A novel approach to analyse leaf elongation close to the thermal limit of growth in the field. *Journal of Experimental Botany*, *67*(6), 1897–1906. doi:10.1093/jxb/erw003

Nath, U., Crawford, B. C. W., Carpenter, R. & Coen, E. (2003). Genetic control of surface curvature. *Science*, *299*(5611), 1404–1407. doi:10.1126/science.1079354

Neufeld, H. S., Durall, D. M., Rich, P. M. & Tingey, D. T. (1989). A rootbox for quantitative observations on intact entire root systems. *Plant and Soil*, *117*(2), 295–298. doi:10.1007/bf02220725

Nguyen, H. T., Meir, P., Sack, L., Evans, J., Oliveira, R. S. & Ball, M. C. (2017). Leaf water storage increases with salinity and aridity in the mangrove *Avicennia marina*: Integration of leaf structure, osmotic adjustment and access to multiple water sources. *Plant, Cell & Environment*, *40*(8), 1576–1591. doi:10.1111/pce.12962

Nguyen, H. T., Meir, P., Wolfe, J., Mencuccini, M. & Ball, M. C. (2017). Plumbing the depths: Extracellular water storage in specialized leaf structures and its functional expression in a three-domain pressure-volume relationship. *Plant, Cell & Environment*, *40*(7), 1021–1038. doi:10.1111/pce.12788

Nguyen, T. T., Slaughter, D. C., Maloof, J. N. & Sinha, N. (2016). Plant phenotyping using multi-view stereo vision with structured lights. In *Autonomous Air and Ground Sensing Systems for Agricultural Optimization and Phenotyping* (Vol. 9866, pp. 986608-986608-9). International Society for Optics and Photonics. doi:10.1117/12.2229513

Nonogaki, H., Bassel, G. W. & Bewley, J. D. (2010). Germination—still a mystery. *Plant Science*, *179*(6), 574–581. doi:10.1016/j.plantsci.2010.02.010

O'Neal, M. E., Landis, D. A. & Isaacs, R. (2002). An inexpensive, accurate method for measuring leaf area and defoliation through digital image analysis. *Journal of Economic Entomology*, *95*(6), 1190–1194. doi:10.1603/0022-0493-95.6.1190

Ortega, J. K. E. (1985). Augmented growth equation for cell wall expansion. *Plant Physiology*, *79*(1), 318–320. doi:10.1104/pp.79.1.318

Otsu, N. (1979). A threshold selection method from gray-level histograms. *IEEE Transactions on Systems, Man, and Cybernetics*, *9*(1), 62–66. doi:10.1109/TSMC.1979.4310076

Paine, C. E. T., Marthews, T. R., Vogt, D. R., Purves, D., Rees, M., Hector, A. & Turnbull, L. A. (2012). How to fit nonlinear plant growth models and calculate growth rates: An update for ecologists. *Methods in Ecology and Evolution*, *3*(2), 245–256. doi:10.1111/j.2041-210X.2011.00155.x

Pantin, F., Simonneau, T. & Muller, B. (2012). Coming of leaf age: Control of growth by hydraulics and metabolics during leaf ontogeny. *New Phytologist*, *196*(2), 349–366. doi:10.1111/j.1469-8137.2012.04273.x

Pantin, F., Simonneau, T., Rolland, G., Dauzat, M. & Muller, B. (2011). Control of leaf expansion: A developmental switch from metabolics to hydraulics. *Plant Physiology*, *156*(2), 803–815. doi:10.1104/pp.111.176289

Paproki, A., Sirault, X., Berry, S., Furbank, R. & Fripp, J. (2012). A novel mesh processing based technique for 3D plant analysis. *BMC Plant Biology*, *12*, 63. doi:10.1186/1471-2229-12-63

Parent, B. & Tardieu, F. (2012). Temperature responses of developmental processes have not been affected by breeding in different ecological areas for 17 crop species. *New Phytologist*, *194*(3), 760–774. doi:10.1111/j.1469-8137.2012.04086.x

Parent, B. & Tardieu, F. (2014). Can current crop models be used in the phenotyping era for predicting the genetic variability of yield of plants subjected to drought or high temperature? *Journal of Experimental Botany*, *65*(21), 6179–6189. doi:10.1093/jxb/eru223

Parent, B., Turc, O., Gibon, Y., Stitt, M. & Tardieu, F. (2010). Modelling temperature-compensated physiological rates, based on the coordination of responses to temperature of developmental processes. *Journal of Experimental Botany*, *61*(8), 2057–2069. doi:10 . 1093 / jxb / erq003

Paulus, S., Behmann, J., Mahlein, A. K., Plumer, L. & Kuhlmann, H. (2014). Low-cost 3D systems: Suitable tools for plant phenotyping. *Sensors*, *14*(2), 3001–3018. doi:10.3390/s140203001

Paulus, S., Schumann, H., Kuhlmann, H. & Leon, J. (2014). High-precision laser scanning system for capturing 3D plant architecture and analysing growth of cereal plants. *Biosystems Engineering*, *121*, 1–11. doi:10. 1016/j.biosystemseng.2014.01.010

Pfeffer, W. (1881). *Pflanzenphysiologie. Ein Handbuch des Stoffwechsels und Kraftwechsels in der Pflanze. Zweiter Band. Kraftwechsel.* Leipzig: Wilhelm Engelmann.

Pfeffer, W. (1900). Die Anwendung des Projectionsapparates zur Demonstration von Lebensvorgängen. *Jahrbücher für wissenschaftliche Botanik*, *35*, 711–745.

Pfeffer, W. (1903). *The physiology of plants. A treatise upon the metabolism and sources of energy in plants. Volume II. Growth, reproduction, and maintenance* (2nd ed.). Oxford: Clarendon Press.

Pfeifer, J., Mielewczik, M., Friedli, M., Kirchgessner, N. & Walter, A. (2018). Non-destructive measurement of soybean leaf thickness via X-ray computed tomography allows the study of diel leaf growth rhythms in the third dimension. *Journal of Plant Research*, *131*(1), 111–124. doi:10. 1007/s10265-017-0967-8

Poire, R., Wiese-Klinkenberg, A., Parent, B., Mielewczik, M., Schurr, U., Tardieu, F. & Walter, A. (2010). Diel time-courses of leaf growth in monocot and dicot species: Endogenous rhythms and temperature ef-

fects. *Journal of Experimental Botany*, *61*(6), 1751–1759. doi:10.1093/jxb/erq049

Poorter, H., Niinemets, U., Walter, A., Fiorani, F. & Schurr, U. (2010). A method to construct dose-response curves for a wide range of environmental factors and plant traits by means of a meta-analysis of phenotypic data. *Journal of Experimental Botany*, *61*(8), 2043–2055. doi:10.1093/jxb/erp358

Poorter, H., Niinemets, U., Poorter, L., Wright, I. J. & Villar, R. (2009). Causes and consequences of variation in leaf mass per area (LMA): A meta-analysis. *New Phytologist*, *182*(3), 565–588. doi:10.1111/j.1469-8137.2009.02830.x

Poorter, H., Niklas, K. J., Reich, P. B., Oleksyn, J., Poot, P. & Mommer, L. (2012). Biomass allocation to leaves, stems and roots: Meta-analyses of interspecific variation and environmental control. *New Phytologist*, *193*(1), 30–50. doi:10.1111/j.1469-8137.2011.03952.x

Pound, M. P., Atkinson, J. A., Townsend, A. J., Wilson, M. H., Griffiths, M., Jackson, A. S., ... French, A. P. (2017). Deep machine learning provides state-of-the-art performance in image-based plant phenotyping. *GigaScience*, *6*(10), 1–10. doi:10.1093/gigascience/gix083

Pound, M. P., French, A. P., Fozard, J. A., Murchie, E. H. & Pridmore, T. P. (2016). A patch-based approach to 3D plant shoot phenotyping. *Machine Vision and Applications*, *27*(5), 767–779. doi:10.1007/s00138-016-0756-8

Price, T. V. & Osborne, C. F. (1990). Computer imaging and its application to some problems in agriculture and plant science. *Critical Reviews in Plant Sciences*, *9*(3), 235–266. doi:10.1080/07352689009382289

Proseus, T. E. & Boyer, J. S. (2008). Calcium pectate chemistry causes growth to be stored in *Chara corallina*: A test of the pectate cycle. *Plant, Cell & Environment*, *31*(8), 1147–1155. doi:10.1111/j.1365-3040.2008.01829.x

Proseus, T. E., Ortega, J. K. E. & Boyer, J. S. (1999). Separating growth from elastic deformation during cell enlargement. *Plant Physiology*, *119*(2), 775–784. doi:10.1104/pp.119.2.775

R Core Team. (2017). *R: A language and environment for statistical computing*. Vienna, Austria.

Raich, J. & Nadelhoffer, K. (1989). Belowground carbon allocation in forest ecosystems: Global trends. *Ecology*, *70*(5), 1346–1354.

Raumonen, P., Kaasalainen, M., Åkerblom, M., Kaasalainen, S., Kaartinen, H., Vastaranta, M., . . . Lewis, P. (2013). Fast automatic precision tree models from terrestrial laser scanner data. *Remote Sensing*, *5*(2), 491–520. doi:10.3390/rs5020491

Remmler, L. & Rolland-Lagan, A.-G. (2012). Computational method for quantifying growth patterns at the adaxial leaf surface in three dimensions. *Plant Physiology*, *159*(1), 27–39. doi:10.1104/pp.112.194662

Repola, J. (2009). Biomass equations for Scots pine and Norway spruce in Finland. *Silva Fennica*, *43*(4), 625–647. doi:10.14214/sf.184

Richardson, A. D., Jenkins, J. P., Braswell, B. H., Hollinger, D. Y., Ollinger, S. V. & Smith, M. L. (2007). Use of digital webcam images to track spring green-up in a deciduous broadleaf forest. *Oecologia*, *152*(2), 323–334. doi:10.1007/s00442-006-0657-z

Rolland-Lagan, A.-G., Bangham, J. A. & Coen, E. (2003). Growth dynamics underlying petal shape and asymmetry. *Nature*, *422*(6928), 161–163. doi:10.1038/nature01443

Rose, J. C., Paulus, S. & Kuhlmann, H. (2015). Accuracy analysis of a multi-view stereo approach for phenotyping of tomato plants at the organ level. *Sensors*, *15*(5), 9651–9665. doi:10.3390/s150509651

Rozema, J., Arp, W., Diggelen, J. V., Kok, E. & Letschert, J. (1987). An eco-physiological comparison of measurements of the diurnal rhythm of the leaf elongation and changes of the leaf thickness of salt-resistant

dicotyledonae and monocotyledonae. *Journal of Experimental Botany*, *38*(3), 442–453. doi:10.1093/jxb/38.3.442

Ruge, U., Whaley, W. G. & Ziegler, H. (1961). Methoden der Wachstumsmessung. In H. Burström (Ed.), *Growth and growth substances / Wachstum und Wuchsstoffe* (pp. 47–173). Berlin, Germany: Springer. doi:10.1007/978-3-642-48934-1_3

Runions, A., Tsiantis, M. & Prusinkiewicz, P. (2017). A common developmental program can produce diverse leaf shapes. *New Phytologist*, *216*(2), 401–418. doi:10.1111/nph.14449

Rusu, R. B. & Cousins, S. (2011). 3D is here: Point Cloud Library (PCL). In *2011 IEEE International Conference on Robotics and Automation* (pp. 1–4). Institute of Electrical and Electronics Engineers (IEEE). doi:10.1109/ICRA.2011.5980567

Ruts, T., Matsubara, S. & Walter, A. (2013). Synchronous high-resolution phenotyping of leaf and root growth in *Nicotiana tabacum* over 24-h periods with GROWMAP-plant. *Plant Methods*, *9*, 2. doi:10.1186/1746-4811-9-2

Ruts, T., Matsubara, S., Wiese-Klinkenberg, A. & Walter, A. (2012). Diel patterns of leaf and root growth: Endogenous rhythmicity or environmental response? *Journal of Experimental Botany*, *63*(9), 3339–3351. doi:10.1093/jxb/err334

Sadok, W., Naudin, P., Boussuge, B., Muller, B., Welcker, C. & Tardieu, F. (2007). Leaf growth rate per unit thermal time follows QTL-dependent daily patterns in hundreds of maize lines under naturally fluctuating conditions. *Plant, Cell & Environment*, *30*(2), 135–146. doi:10.1111/j.1365-3040.2006.01611.x

Scharlemann, J. P., Tanner, E. V., Hiederer, R. & Kapos, V. (2014). Global soil carbon: Understanding and managing the largest terrestrial carbon pool. *Carbon Management*, *5*(1), 81–91. doi:10.4155/cmt.13.77

Scharr, H., Minervini, M., French, A., Klukas, C., Kramer, D., Liu, X., . . . Tsaftaris, S. (2015). Leaf segmentation in plant phenotyping: A collation study. *Machine Vision and Applications*, *27*(4), 585–606. doi:10.1007/s00138-015-0737-3

Schima, R., Mollenhauer, H., Grenzdörffer, G., Merbach, I., Lausch, A., Dietrich, P. & Bumberger, J. (2016). Imagine all the plants: Evaluation of a light-field camera for on-site crop growth monitoring. *Remote Sensing*, *8*(10), 823. doi:10.3390/rs8100823

Schimel, D. S. (1995). Terrestrial ecosystems and the carbon cycle. *Global Change Biology*, *1*(1), 77–91. doi:10.1111/j.1365-2486.1995.tb00008.x

Schmundt, D., Stitt, M., Jahne, B. & Schurr, U. (1998). Quantitative analysis of the local rates of growth of dicot leaves at a high temporal and spatial resolution, using image sequence analysis. *Plant Journal*, *16*(4), 505–514. doi:10.1046/j.1365-313x.1998.00314.x

Schwartz, H. (1890). Sur une définition erronée de l'aire surface courte. In H. Schwartz (Ed.), *Gesammelte Mathematische Abhandlungen* (Vol. 2, pp. 309–311). Berlin, Germany: Springer.

Serrano-Mislata, A., Schiessl, K. & Sablowski, R. (2015). Active control of cell size generates spatial detail during plant organogenesis. *Current Biology*, *25*(22), 2991–2996. doi:0.1016/j.cub.2015.10.008

Shipley, B. & Vu, T. (2002). Dry matter content as a measure of dry matter concentration in plants and their parts. *New Phytologist*, *153*(2), 359–364. doi:10.1046/j.0028-646X.2001.00320.x

Silk, W. K. & Bogeat-Triboulot, M.-B. (2014). Deposition rates in growing tissue: Implications for physiology, molecular biology, and response to environmental variation. *Plant and Soil*, *374*(1), 1–17. doi:10.1007/s11104-013-1726-9

Silk, W. K. & Erickson, R. O. (1979). Kinematics of plant growth. *Journal of Theoretical Biology*, *76*(4), 481–501. doi:10.1016/0022-5193(79)90014-6

Skirycz, A., Claeys, H., De Bodt, S., Oikawa, A., Shinoda, S., Andriankaja, M., ... Inze, D. (2011). Pause-and-stop: The effects of osmotic stress on cell proliferation during early leaf development in *Arabidopsis* and a role for ethylene signaling in cell cycle arrest. *Plant Cell*, *23*(5), 1876–1888. doi:10.1105/tpc.111.084160

Skirycz, A., De Bodt, S., Obata, T., De Clercq, I., Claeys, H., De Rycke, R., ... Inzé, D. (2010). Developmental stage specificity and the role of mitochondrial metabolism in the response of *Arabidopsis* leaves to prolonged mild osmotic stress. *Plant Physiology*, *152*(1), 226–244. doi:10.1104/pp.109.148965

Sklansky, J. (1982). Finding the convex hull of a simple polygon. *Pattern Recognition Letters*, *1*(2), 79–83. doi:10.1016/0167-8655(82)90016-2

Smith, L. N., Zhang, W., Hansen, M. F., Hales, I. J. & Smith, M. L. (2018). Innovative 3D and 2D machine vision methods for analysis of plants and crops in the field. *Computers in Industry*, *97*, 122–131. doi:10.1016/j.compind.2018.02.002

Snavely, N., Seitz, S. M. & Szeliski, R. (2008). Modeling the world from internet photo collections. *International Journal of Computer Vision*, *80*(2), 189–210. doi:10.1007/s11263-007-0107-3

Song, Y., Glasbey, C. A., Polder, G. & van der Heijden, G. (2014). Nondestructive automatic leaf area measurements by combining stereo and time-of-flight images. *IET Computer Vision*, *8*(5), 391–403. doi:10.1049/iet-cvi.2013.0056

Sonnentag, O., Hufkens, K., Teshera-Sterne, C., Young, A. M., Friedl, M., Braswell, B. H., ... Richardson, A. D. (2012). Digital repeat photography for phenological research in forest ecosystems. *Agricultural and Forest Meteorology*, *152*, 159–177. doi:10.1016/j.agrformet.2011.09.009

Sonnewald, U. (2013). Physiology of metabolism. In A. Bresinsky, C. Körner, J. W. Kadereit, G. Neuhaus & U. Sonnewald (Eds.), *Strasburger's plant*

sciences: Including prokaryotes and fungi (pp. 239–409). Berlin, Germany: Springer. doi:10.1007/978-3-642-15518-5_5

Sprangers, K., Avramova, V. & Beemster, G. T. S. (2016). Kinematic analysis of cell division and expansion: Quantifying the cellular basis of growth and sampling developmental zones in *Zea mays* leaves. *Journal of Visualized Experiments*, (118), e54887. doi:doi:10.3791/54887

Sprengel, C. (1828). Von den Substanzen der Ackerkrume und des Untergrundes (About the substances in the plow layer and the subsoil). *Journal für Technische und Ökonomische Chemie*, 2(4), 423–474.

Steppe, K., De Pauw, D. J. W., Lemeur, R. & Vanrolleghem, P. A. (2006). A mathematical model linking tree sap flow dynamics to daily stem diameter fluctuations and radial stem growth. *Tree Physiology*, 26(3), 257–273. doi:10.1093/treephys/26.3.257

Stitt, M. & Zeeman, S. C. (2012). Starch turnover: Pathways, regulation and role in growth. *Current Opinion in Plant Biology*, 15(3), 282–292. doi:10.1016/j.pbi.2012.03.016

Sugimoto-Shirasu, K. & Roberts, K. (2003). "Big it up": Endoreduplication and cell-size control in plants. *Current Opinion in Plant Biology*, 6(6), 544–553. doi:10.1016/j.pbi.2003.09.009

Tackenberg, O. (2007). A new method for non-destructive measurement of biomass, growth rates, vertical biomass distribution and dry matter content based on digital image analysis. *Annals of Botany*, 99(4), 777–783. doi:10.1093/aob/mcm009

Tardieu, F., Cabrera-Bosquet, L., Pridmore, T. & Bennett, M. (2017). Plant phenomics, from sensors to knowledge. *Current Biology*, 27(15), R770–R783. doi:10.1016/j.cub.2017.05.055

Tardieu, F., Granier, C. & Muller, B. (1999). Modelling leaf expansion in a fluctuating environment: Are changes in specific leaf area a consequence of changes in expansion rate? *New Phytologist*, 143(1), 33–44. doi:10.1046/j.1469-8137.1999.00433.x

Tardieu, F., Parent, B., Caldeira, C. F. & Welcker, C. (2014). Genetic and physiological controls of growth under water deficit. *Plant Physiology*, *164*(4), 1628–1635. doi:10.1104/pp.113.233353

Taylor, G., Tricker, P. J., Zhang, F. Z., Alston, V. J., Miglietta, F. & Kuzminsky, E. (2003). Spatial and temporal effects of free-air CO_2 enrichment (POPFACE) on leaf growth, cell expansion, and cell production in a closed canopy of *Poplar*. *Plant Physiology*, *131*(1), 177–185. doi:10.1104/pp.011296

Tisné, S., Reymond, M., Vile, D., Fabre, J., Dauzat, M., Koornneef, M. & Granier, C. (2008). Combined genetic and modeling approaches reveal that epidermal cell area and number in leaves are controlled by leaf and plant developmental processes in *Arabidopsis*. *Plant Physiology*, *148*(2), 1117–1127. doi:10.1104/pp.108.124271

Tisné, S., Serrand, Y., Bach, L., Gilbault, E., Ben Ameur, R., Balasse, H., … Loudet, O. (2013). Phenoscope: An automated large-scale phenotyping platform offering high spatial homogeneity. *Plant Journal*, *74*(3), 534–544. doi:10.1111/tpj.12131

Tomé, F., Jansseune, K., Saey, B., Grundy, J., Vandenbroucke, K., Hannah, M. A. & Redestig, H. (2017). rosettR: protocol and software for seedling area and growth analysis. *Plant Methods*, *13*(1), 13. doi:10.1186/s13007-017-0163-9

Toomey, M., Friedl, M. A., Frolking, S., Hufkens, K., Klosterman, S., Sonnentag, O., … Richardson, A. D. (2015). Greenness indices from digital cameras predict the timing and seasonal dynamics of canopy-scale photosynthesis. *Ecological Applications*, *25*(1), 99–115. doi:10.1890/14-0005.1

Tran, P., Gritcan, I., Cusens, J., Alfaro, A. C. & Leuzinger, S. (2017). Biomass and nutrient composition of temperate mangroves (*Avicennia marina* var. *australasica*) in New Zealand. *New Zealand Journal of Mar-*

ine and Freshwater Research, *51*(3), 427–442. doi:10.1080/00288330.2016.1260604

Trápani, N. & Hall, A. J. (1996). Effects of leaf position and nitrogen supply on the expansion of leaves of field grown sunflower (*Helianthus annuus* L.) *Plant and Soil*, *184*(2), 331–340. doi:10.1007/BF00010462

Tsaftaris, S. A. & Noutsos, C. (2009). Plant phenotyping with low cost digital cameras and image analytics. In I. N. Athanasiadis, P. A. Mitkas, A. E. Rizzoli & J. M. Gomez (Eds.), *Information Technologies in Environmental Engineering* (pp. 238–251). Environmental Science and Engineering. Berlin, Germany: Springer. doi:10.1007/978-3-540-88351-7_18

Tsukaya, H. (2008). Controlling size in multicellular organs: Focus on the leaf. *PLOS Biology*, *6*(7), e174. doi:10.1371/journal.pbio.0060174

Tucker, C. J. (1979). Red and photographic infrared linear combinations for monitoring vegetation. *Remote Sensing of Environment*, *8*(2), 127–150. doi:10.1016/0034-4257(79)90013-0

Turc, O., Bouteillé, M., Fuad-Hassan, A., Welcker, C. & Tardieu, F. (2016). The growth of vegetative and reproductive structures (leaves and silks) respond similarly to hydraulic cues in maize. *New Phytologist*, *212*(2), 377–388. doi:10.1111/nph.14053

Uchiyama, H., Sakurai, S., Mishima, M., Arita, D., Okayasu, T., Shimada, A. & Taniguchi, R. (2017). An easy-to-setup 3D phenotyping platform for KOMATSUNA dataset. In *2017 IEEE International Conference on Computer Vision Workshops* (pp. 2038–2045). Institute of Electrical and Electronics Engineers (IEEE). doi:10.1109/ICCVW.2017.239

Vadez, V., Kholova, J., Hummel, G., Zhokhavets, U., Gupta, S. K. & Hash, C. T. (2015). LeasyScan: A novel concept combining 3D imaging and lysimetry for high-throughput phenotyping of traits controlling plant water budget. *Journal of Experimental Botany*, *66*(18), 5581–5593. doi:10.1093/jxb/erv251

Vasseur, F., Bresson, J., Wang, G., Schwab, R. & Weigel, D. (2018). Image-based methods for phenotyping growth dynamics and fitness components in *Arabidopsis thaliana*. *Plant Methods*, *14*(1), 63. doi:10.1186/s13007-018-0331-6

Verbančič, J., Lunn, J. E., Stitt, M. & Persson, S. (2018). Carbon supply and the regulation of cell wall synthesis. *Molecular Plant*, *11*(1), 75–94. doi:10.1016/j.molp.2017.10.004

Vit, A. & Shani, G. (2018). Comparing RGB-D sensors for close range outdoor agricultural phenotyping. *Sensors*, *18*(12). doi:10.3390/s18124413

von Liebig, J. (1840). *Die organische Chemie in ihrer Anwendung auf Agricultur und Physiologie*. Braunschweig: Friedrich Vieweg und Sohn.

Vos, J., Putten, P. E. L. v. d. & Birch, C. J. (2005). Effect of nitrogen supply on leaf appearance, leaf growth, leaf nitrogen economy and photosynthetic capacity in maize (*Zea mays* L.) *Field Crops Research*, *93*(1), 64–73. doi:10.1016/j.fcr.2004.09.013

Wahab, A. H. (1971). *Dry matter changes and carbohydrate metabolism of germinating soybeans* (Thesis, Iowa State University, Ames, Iowa, United States of America). doi:10.31274/rtd-180813-4581

Waldron, L. J., Terry, N. & Nemson, J. A. (1985). Diurnal cycles of leaf extension in unsalinized and salinized *Beta vulgaris*. *Plant, Cell & Environment*, *8*(3), 207–211. doi:10.1111/1365-3040.ep11604611

Walter, A., Christ, M. M., Barron-gafford, G. A., Grieve, K. A., Murthy, R. & Rascher, U. (2005). The effect of elevated CO_2 on diel leaf growth cycle, leaf carbohydrate content and canopy growth performance of *Populus deltoides*. *Global Change Biology*, *11*(8), 1207–1219. doi:10.1111/j.1365-2486.2005.00990.x

Walter, A., Feil, R. & Schurr, U. (2002). Restriction of nyctinastic movements and application of tensile forces to leaves affects diurnal patterns of expansion growth. *Functional Plant Biology*, *29*(11), 1247–1258. doi:10.1071/pp01255

Walter, A., Liebisch, F. & Hund, A. (2015). Plant phenotyping: From bean weighing to image analysis. *Plant Methods*, *11*(1), 14. doi:10.1186 / s13007-015-0056-8

Walter, A., Scharr, H., Gilmer, F., Zierer, R., Nagel, K. A., Ernst, M., ... Schurr, U. (2007). Dynamics of seedling growth acclimation towards altered light conditions can be quantified via GROWSCREEN: A setup and procedure designed for rapid optical phenotyping of different plant species. *New Phytologist*, *174*(2), 447–455. doi:10.1111 / j.1469-8137. 2007.02002.x

Walter, A., Silk, W. K. & Schurr, U. (2009). Environmental effects on spatial and temporal patterns of leaf and root growth. *Annual Review of Plant Biology*, *60*, 279–304. doi:10.1146/annurev.arplant.59.032607.092819

Watson, D. J. (1958). The dependence of net assimilation rate on leaf-area index. *Annals of Botany*, *22*(1), 37–54. doi:10.1093/oxfordjournals.aob. a083596

Weber, R. (1891). *Lehrbuch der Forsteinrichtung mit besonderer Berücksichtigung der Zuwachsgesetze der Waldbäume*. Berlin, Germany: Springer.

Weiner, J. (1990). Asymmetric competition in plant populations. *Trends in Ecology & Evolution*, *5*(11), 360–364. doi:10.1016/0169-5347(90)90095-U

Weraduwagel, S. M., Chen, J., Anozie, F. C., Morales, A., Weise, S. E. & Sharkey, T. D. (2015). The relationship between leaf area growth and biomass accumulation in *Arabidopsis thaliana*. *Frontiers in Plant Science*, *6*, 167. doi:10.3389/fpls.2015.00167

West, C., Briggs, G. E. & Kidd, F. (1920). Methods and significant relations in the quantitative analysis of plant growth. *New Phytologist*, *19*(7-8), 200–207. doi:10.1111/j.1469-8137.1920.tb07327.x

Wiese, A., Christ, M. M., Virnich, O., Schurr, U. & Walter, A. (2007). Spatiotemporal leaf growth patterns of *Arabidopsis thaliana* and evidence for sugar control of the diel leaf growth cycle. *New Phytologist*, *174*(4), 752–761. doi:10.1111/j.1469-8137.2007.02053.x

Willis, L., Refahi, Y., Wightman, R., Landrein, B., Teles, J., Huang, K. C., . . . Jönsson, H. (2016). Cell size and growth regulation in the *Arabidopsis thaliana* apical stem cell niche. *Proceedings of the National Academy of Sciences*, *113*(51), E8238–E8246. doi:10.1073/pnas.1616768113

Woodwell, G. M. & Whittaker, R. H. (1968). Primary production in terrestrial ecosystems. *American Zoologist*, *8*(1), 19–30. doi:10.1093/icb/8.1.19

Wright, I. J., Leishman, M. R., Read, C. & Westoby, M. (2006). Gradients of light availability and leaf traits with leaf age and canopy position in 28 Australian shrubs and trees. *Functional Plant Biology*, *33*(5), 407–419. doi:10.1071/FP05319

Wu, J., Wu, Q., Pagès, L., Yuan, Y., Zhang, X., Du, M., . . . Li, Z. (2018). RhizoChamber-Monitor: A robotic platform and software enabling characterization of root growth. *Plant Methods*, *14*(1), 44. doi:10.1186/s13007-018-0316-5

Xia, C., Wang, L., Chung, B.-K. & Lee, J.-M. (2015). In situ 3D segmentation of individual plant leaves using a RGB-D camera for agricultural automation. *Sensors*, *15*(8), 20463–20479. doi:10.3390/s150820463

Xinyou, Y. & Van Laar, H. (2005). *Crop systems dynamics: An ecophysiological simulation model for genotype-by-environment interactions*. Wageningen, Netherlands: Wageningen Academic Publishers.

Xiong, X., Yu, L., Yang, W., Liu, M., Jiang, N., Wu, D., . . . Liu, Q. (2017). A high-throughput stereo-imaging system for quantifying rape leaf traits during the seedling stage. *Plant Methods*, *13*(1), 7. doi:10.1186/s13007-017-0157-7

Yang, Q., Wang, L. & Ahuja, N. (2010). A constant-space belief propagation algorithm for stereo matching. In *2010 IEEE Computer Society Conference on Computer Vision and Pattern Recognition* (pp. 1458–1465). Institute of Electrical and Electronics Engineers (IEEE). doi:10.1109/CVPR.2010.5539797

Yang, W. N., Guo, Z. L., Huang, C. L., Duan, L. F., Chen, G. X., Jiang, N., … Xiong, L. Z. (2014). Combining high-throughput phenotyping and genome-wide association studies to reveal natural genetic variation in rice. *Nature Communications*, *5*, 5087. doi:10.1038/ncomms6087

Yoshida, S., Barbier de Reuille, P., Lane, B., Bassel, G. W., Prusinkiewicz, P., Smith, R. S. & Weijers, D. (2014). Genetic control of plant development by overriding a geometric division rule. *Developmental Cell*, *29*(1), 75–87. doi:10.1016/j.devcel.2014.02.002

Zeng, G., Birchfield, S. T. & Wells, C. E. (2008). Automatic discrimination of fine roots in minirhizotron images. *New Phytologist*, *177*(2), 549–557. doi:10.1111/j.1469-8137.2007.02271.x

Zhang, T. & Suen, C. Y. (1984). A fast parallel algorithm for thinning digital patterns. *Communications of the ACM*, *27*(3), 236–239. doi:10.1145/357994.358023

Zhang, W., Hansen, M. F., Smith, M., Smith, L. & Grieve, B. (2018). Photometric stereo for three-dimensional leaf venation extraction. *Computers in Industry*, *98*, 56–67. doi:10.1016/j.compind.2018.02.006

Zhang, X., Hause, R. J. & Borevitz, J. O. (2012). Natural genetic variation for growth and development revealed by high-throughput phenotyping in *Arabidopsis thaliana*. *G3-Genes Genomes Genetics*, *2*(1), 29–34. doi:10.1534/g3.111.001487

Zhen, J., Tripler, E., Peng, X. & Lazarovitch, N. (2017). A wireless device for continuous frond elongation measurement. *Computers and Electronics in Agriculture*, *140*, 1–7. doi:10.1016/j.compag.2017.05.011

Zheng, X. & Wang, X. (2010). Leaf vein extraction based on gray-scale morphology. *International Journal of Image, Graphics and Signal Processing*, *2*(2), 25. doi:10.5815/ijigsp.2010.02.04

Zhu, J., Ingram, P. A., Benfey, P. N. & Elich, T. (2011). From lab to field, new approaches to phenotyping root system architecture. *Current Opinion in Plant Biology*, *14*(3), 310–317. doi:10.1016/j.pbi.2011.03.020

Zimmermann, D., Reuss, R., Westhoff, M., Geßner, P., Bauer, W., Bamberg, E., ... Zimmermann, U. (2008). A novel, non-invasive, online-monitoring, versatile and easy plant-based probe for measuring leaf water status. *Journal of Experimental Botany*, *59*(11), 3157–3167. doi:10.1093/jxb/ern171

Zweifel, R., Eugster, W., Etzold, S., Dobbertin, M., Buchmann, N. & Häsler, R. (2010). Link between continuous stem radius changes and net ecosystem productivity of a subalpine Norway spruce forest in the Swiss Alps. *New Phytologist*, *187*(3), 819–830. doi:10.1111/j.1469-8137.2010.03301.x

Zweifel, R., Haeni, M., Buchmann, N. & Eugster, W. (2016). Are trees able to grow in periods of stem shrinkage? *New Phytologist*, *211*(3), 839–849. doi:10.1111/nph.13995

Appendix

Tidal Inundation

This Appendix reports the recontruction of the tidal innundation for the field study presented in Chapter 3.

At high tide, the study site is flooded for about two hours and twenty minutes depending on the tide height ($\mu = 143\,\mathrm{min}$, $\sigma = 58\,\mathrm{min}$). Water depth data was acquired in 2014 at the same location using a CTD-5 electrical conductivity, temperature, and depth sensor (Decagon Devices, Inc., Pullman, WA, USA; depth resolution of 1 mm; Donnellan Barraclough et al., 2018). The sensor was located in a tube approximately 270 mm below the ground level. For the study period I reconstructed the high tide times, maximal tide height, and flooding duration correlating these data to water depth measurements in Auckland (36°50′S, 174°47′E) obtained from Land Information New Zealand (2017). Land Information New Zealand operates two water depth sensors in Auckland; in this analysis I included data from both. The recorded sensor data for the water depth measurements in the field were very noisy. Therefore, I manually selected three periods with a clean signal including a total of 73 high tide observations for the analysis. A selection example is shown in Figure 29.

The highest water level at the study site lags behind the high tide at sea. The mean observed time difference between the field and Auckland is 135.6 min ($\sigma = 7.7\,\mathrm{min}$; Figure 30).

There is a linear relation between the water depth at high tide in Auckland and in the field, adjusted $R^2 = 0.889$, $F(1, 71) = 577.7$, $p < 0.001$;
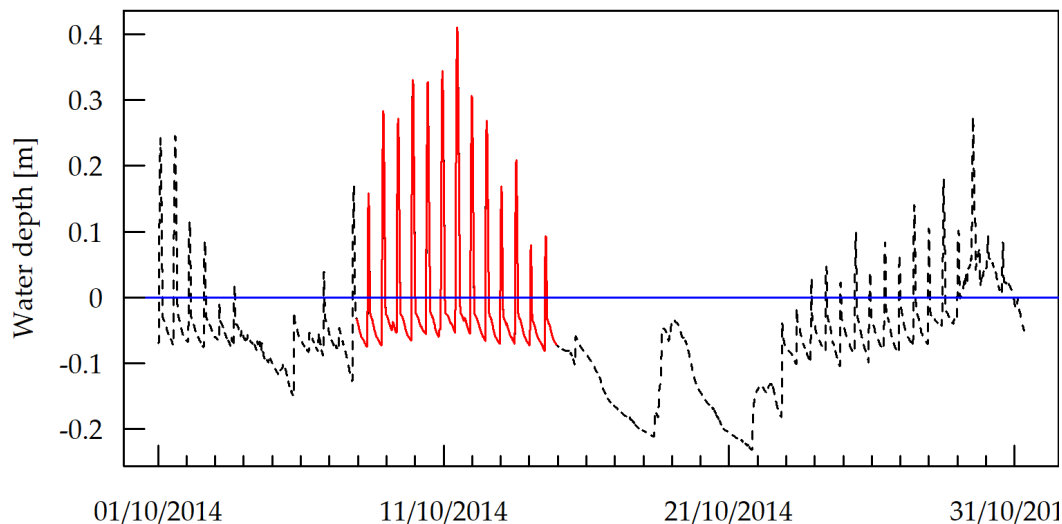
Figure 29. Example of the field water depth sensor data. The period from 8 October to 14 October 2014 (solid red line) was included in the analysis. Negative values occur because the sensor was installed below the ground level.
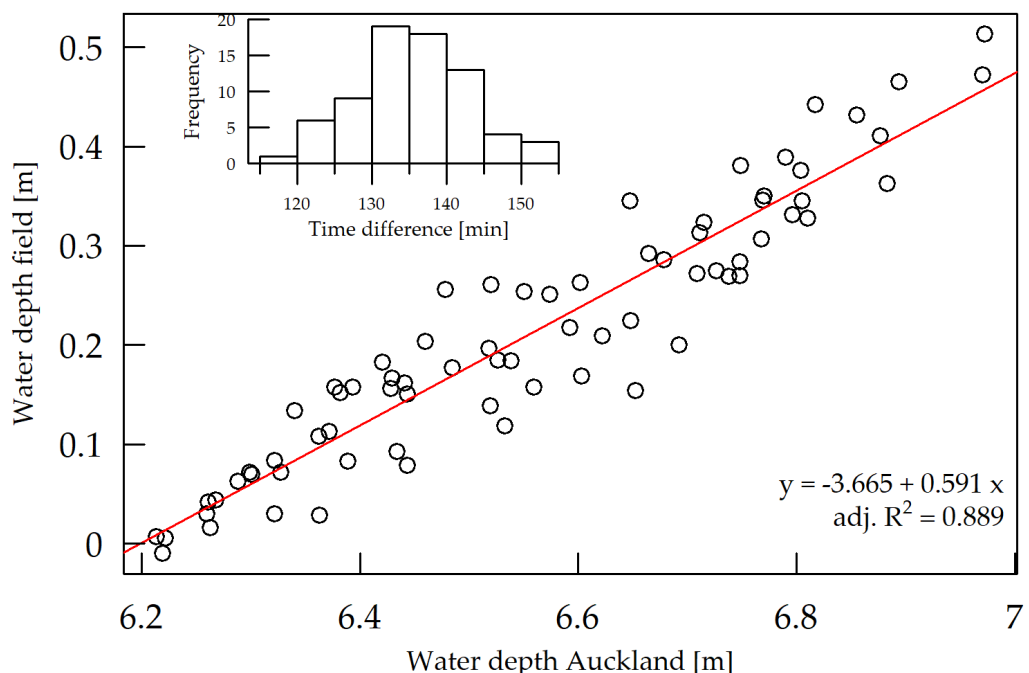

Figure 30. Linear regression between the water depth at high tide in Auckland and in the field. The inset shows the histogram of the time difference of high tide in Auckland and in the field.

see Figure 30 and Eq. (18). The relationship between the flooding duration and the water depth at high tide in the field is linear after square-root-transformation (red curve in Figure 31). An untransformed linear model fits the data quite well too (blue dashed line in Figure 31), but it misrepresents low and high water depth observations. The fact that the linear model predicts a positive intercept, i.e. a positive flooding duration when the water depth is zero, shows that this does not accurately represent reality.

The linear model assumes a constant inflow and outflow speed. The water depth D_i would then simply be a function of the duration t_i:

$$D_i = a \cdot t_i + b \,, \tag{15}$$

with coefficient a in the unit meter per minute and intercept b in the unit meter. Equation 15 can be rewritten like:

$$
\begin{aligned}
t_i &= \frac{1}{a} \cdot D_i - \frac{b}{a} \,, \\
&= c \cdot D_i + d \,,
\end{aligned}
\tag{16}
$$

with coefficient c in the unit minute per meter and intercept d in the unit minute.

However, the flow dynamics of tidal flooding are far more complicated than this linear model. For the purpose of this thesis it is not required to model the flooding depth for any given time point, but it is sufficient to estimate the time point of maximal depth, as well as the inflow and outflow duration. The square-root-transformation leads to a modelled slope coefficient in the unit minutes per square-root of meter, which does not have any physical meaning, but the model represents the observed values very well.

Flooding was defined as water covering the ground (horizontal blue line in Figure 29). For one high tide observation in the sample this was not the case. The tide inflow is significantly faster ($\mu = 58.8\,\text{min}$) than the outflow

($\mu = 83.8\,\mathrm{min}$), $t(71) = -12.94$, $p < 0.001$. Therefore, inflow and outflow time were modelled individually. Both models have a good fit and are highly significant, with adjusted $R^2 = 0.959$, $F(1, 70) = 1659$, $p < 0.001$ for the inflow; see Eq. (19). For the outflow we have adjusted $R^2 = 0.974$, $F(1, 70) = 2695$, $p < 0.001$; see Eq. (20).

Based on these results the tidal inundation was modelled as follows:

$$\boldsymbol{t}_\mathrm{F} = \boldsymbol{t}_\mathrm{A} + a_1 \, , \tag{17}$$

$$D_\mathrm{F} = a_2 \cdot D_\mathrm{A} + b_2 \, , \tag{18}$$

$$t_\mathrm{in} = a_3 \cdot \sqrt{D_\mathrm{F}} + b_3 \, , \tag{19}$$

$$t_\mathrm{out} = a_4 \cdot \sqrt{D_\mathrm{F}} + b_4 \, , \tag{20}$$

with $a_1 = 135.6\,\mathrm{min}$, $a_2 = 0.591$, $b_2 = -3.395\,\mathrm{m}$, $a_3 = 141.3\,\frac{\mathrm{min}}{\sqrt{\mathrm{m}}}$, $b_3 = -3.1\,\mathrm{min}$, and $a_4 = 235.3\,\frac{\mathrm{min}}{\sqrt{\mathrm{m}}}$, $b_4 = -19.2\,\mathrm{min}$. Where $\boldsymbol{t}_\mathrm{A}$ denotes the high tide time in Auckland, $\boldsymbol{t}_\mathrm{F}$ denotes the high tide time in the field, D_A denotes the water depth in meter at high tide in Auckland, D_F denotes the water depth in meter at high tide in the field, t_in and t_out denote the inflow and outflow duration in minutes. The inundation starts at $\boldsymbol{t}_\mathrm{F} - t_\mathrm{in}$ and ends at $\boldsymbol{t}_\mathrm{F} + t_\mathrm{out}$. In cases of no surface flooding ($D_\mathrm{F} < 0\,\mathrm{m}$), t_in and t_out were set to zero.
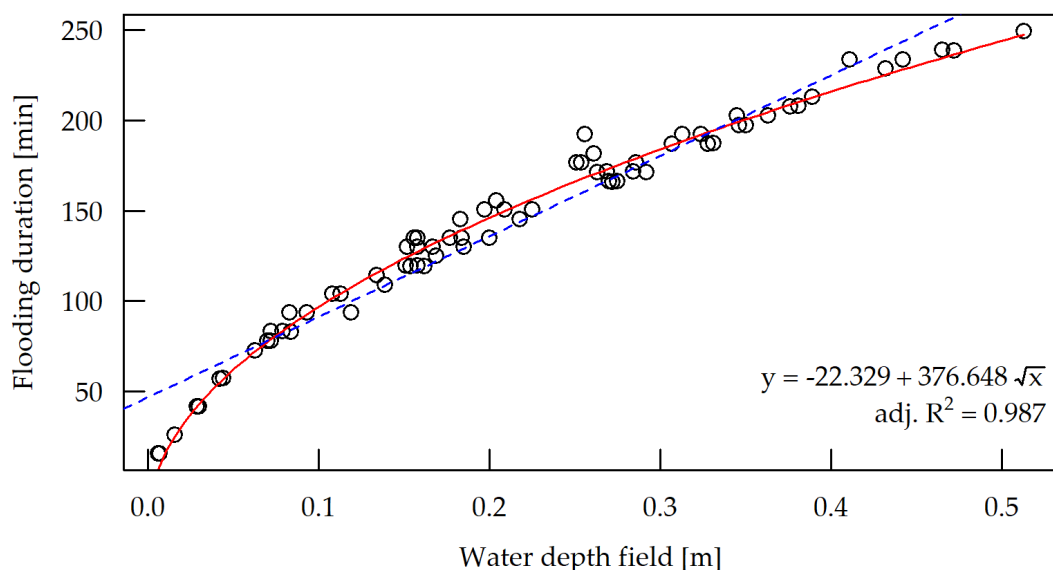
Figure 31. Regression between the water depth at high tide and the flooding duration in the field. Water depth was square-root-transformed for the analysis (red curve). The blue dashed line represents an untransformed linear model.